เซ็นเซอร์ฐานไดฟลูออโรโบรอนเคอร์คิวมินและฐานแอนทราควิโนนอิมิดาโซล เพื่อตรวจวัดนิวคลีโอไทด์

นางสาวศรกฤษณ์ มาบำรุง

วิทยานิพนธ์นี้เป็นส่วนหนึ่งของการศึกษาตามหลักสูตรปริญญาวิทยาศาสตรดุษฎีบัณฑิต
สาขาวิชาเคมี ภาควิชาเคมี
คณะวิทยาศาสตร์ จุฬาลงกรณ์มหาวิทยาลัย
ปีการศึกษา 2554
ลิขสิทธิ์ของจุฬาลงกรณ์มหาวิทยาลัย

BF_2-CURCUMIN-BASED AND ANTHRAQUINONE IMIDAZOLE-BASED SENSORS FOR DETECTION OF NUCLEOTIDES

Miss Sornkrit Marbumrung

A Dissertation Submitted in Partial Fulfillment of the Requirements
for the Degree of Doctor of Philosophy Program in Chemistry
Department of Chemistry
Faculty of Science
Chulalongkorn University
Academic Year 2011

Thesis Title	BF_2-CURCUMIN-BASED AND ANTHRAQUINONE IMIDAZOLE-BASED SENSORS FOR DETECTION OF NUCLEOTIDES
By	Miss Sornkrit Marbumrung
Field of Study	Chemistry
Thesis Advisor	Assistant Professor Boosayarat Tomapatanaget, Ph.D.
Thesis Co-advisor	Gamolwan Tumcharern, Ph.D.

Accepted by the Faculty of Science, Chulalongkorn University in Partial Fulfillment of the Requirements for the Doctoral Degree

……Dean of the Faculty of Science
(Professor Supot Hannongbua, Dr.rer.nat.)

THESIS COMMITTEE

……Chairman
(Assistant Professor Warinthorn Chavasiri, Ph.D.)

……Thesis Advisor
(Assistant Professor Boosayarat Tomapatanaget, Ph.D.)

……Thesis Co-advisor
(Gamolwan Tumcharern, Ph.D.)

……Examiner
(Associate Professor Nongnuj Muangsin, Ph.D.)

……Examiner
(Assistant Professor Sumrit Wacharasindhu, Ph.D.)

……External Examiner
(Nantanit Wanichacheva, Ph.D.)

ศรกฤษณ์ มาบำรุง : เซ็นเซอร์ฐานไดฟลูออโรโบรอนเคอร์คิวมินและฐาน แอนทราควิโนนอิมิดาโซลเพื่อตรวจวัดนิวคลีโอไทด์ . (BF_2-CURCUMIN-BASED AND ANTHRAQUINONE IMIDAZOLE-BASED SENSORS FOR DETECTION OF NUCLEOTIDES) อ. ที่ปรึกษาวิทยานิพนธ์หลัก : ผศ.ดร. บุษยรัตน์ ธรรมพัฒนกิจ , อ. ที่ปรึกษาวิทยานิพนธ์ร่วม : ดร.กมลวรรณ ธรรมเจริญ, 152 หน้า.

ได้สังเคราะห์ฟลูออเรสเซนต์เซ็นเซอร์ที่มีไดฟลูออโรเคอร์คิวมินและไดพิโคลิวเอมีนเป็นองค์ประกอบ จากนั้นศึกษาการเกิดสารประกอบเชิงซ้อนของเซ็นเซอร์ L1 ด้วยเทคนิคยูวีวิสิเบิลและฟลูออเรสเซนต์ โดยพบว่าเกิดสารประกอบเชิงซ้อน ของเซ็นเซอร์ต่อโลหะสังกะสีและทองแดงในอัตราส่วน 1:2 และให้ค่าการดูดกลืนแสงสูงสุดที่ 472 นาโนเมตร ผลของสังกะสีทำให้เกิดการเคลื่อนของค่าการดูดกลืนแสงสูงสุดไปที่ความยาวคลื่นต่ำลง และเซ็นเซอร์ให้ค่าสเปกตรัมการเปล่งแสงสูงสุดที่ 587 นาโนเมตร โดยสังกะสีและทองแดงส่งผลให้ความเข้มของสเปกตรัมการคายแสงลดลง แต่สารประกอบเชิงซ้อนกับสังกะสีของเซ็นเซอร์นี้ไม่สามารถใช้ในการตรวจจับนิวคลีโอไทด์ในน้ำได้ เนื่องจากเมื่ออยู่ในน้ำสังกะสีหลุด ออกจากสารประกอบเชิงซ้อน ดังนั้นจึงสังเคราะห์เซ็นเซอร์ตชนิดใหม่ที่ประกอบด้วยไพรีนและสารประกอบเชิงซ้อนไดพิโคลิวเอมีนที่จับกับสังกะสีเพื่อตรวจวัดนิวคลีโอไทด์ในน้ำ พบว่าเซ็นเซอร์ L2•Zn มีความจำเพาะเจาะจงกับไพโรฟอสเฟตในน้ำ แต่ ในระบบตัวทำละลายอินทรีย์ DMSO:HEPES (0.01 M, pH 7.4 90:10 v/v) พบว่า สามารถจับกับนิวคลีโอไทด์ที่มีหมู่ฟอสเฟต 3 หมู่ได้ดี ได้แก่ เอทีพี (ATP) และยูทีพี (UTP) โดยนิวคลีโอไทด์ส่งผลให้ความเข้มของสเปกตรัมการคายแสงเพิ่มขึ้น เมื่อนำการวิเคราะห์องค์ประกอบหลัก (Principal Component Analysis) มาใช้ในการแยกความสามารถในการจับกับนิวคลีโอไทด์ทั้ง 10 ชนิด ในตัวทำละลายทั้งสองระบบ วิธีการนี้สามารถแยกสารตัวอย่างได้ด้วยความแม่นยำ 88 เปอร์เซ็นต์ นอกจากนี้ ยังสามารถประยุกต์ใช้ในการหาอัตราส่วนระหว่างไพโรฟอสเฟตกับเอทีพีในกระบวนการเอทีพีไฮโดรไลซิส (ATP hydrolysis) ได้อีกด้วย

ภาควิชา.....เคมี..... ลายมือชื่อนิสิต.....

สาขาวิชา.....เคมี..... ลายมือชื่อ อ.ที่ปรึกษาวิทยานิพนธ์หลัก.....

ปีการศึกษา .....2554..... ลายมือชื่อ อ.ที่ปรึกษาวิทยานิพนธ์ร่วม.....

5073880323 : MAJOR CHEMISTRY
KEYWORDS : NUCLEOTIDE / SINGLE FLUORESCENCE SENSOR / SOLVENT-DEPENDENT / PRINCIPAL COMPONENT ANALYSIS / BF_2-CURCUMIN

SORNKRIT MARBUMRUNG : BF_2-CURCUMIN-BASED AND ANTHRAQUINONE IMIDAZOLE-BASED SENSORS FOR DETECTION OF NUCLEOTIDES. ADVISOR : ASST. PROF. BOOSAYARAT TOMAPATANAGET, Ph. D., CO-ADVISOR : GAMOLWAN TUMCHARERN, Ph. D., 152 pp.

A new fluorescence sensor (**L1**), based on BF_2-Curcumin and dpa (bis (2-pyridylmethyl)amine) for detection of $Zn^{2+}$and Cu^{2+} ions was synthesized. The sensor demonstrates the blue-shifted absorption band from 472 nm to 421 nm and the fluorescence quenching at 587 nm in acetonitrile after adding both metal ions. The dpa-Zn complex was expected to be used as chemosensor for detecting biological nucleoside polyphosphates in aqueous solution. Unfortunately, in aqueous system two Zn^{2+} ions upon dpa-Zn complex were released by water. Therefore, we developed the chemosensor containing pyrene and dpa-Zn complex (**L2•Zn**) for detection of nucleotide in aqueous solution. This sensor has a high selectivity for PPi in aqueous solution. In contrast for the case of DMSO:HEPES (0.01 M, pH 7.4 90:10 v/v), **L2•Zn** selectively bind to nucleoside polyphosphates such as ATP and UTP with a large fluorescence enhancement. The Principal Component Analysis (PCA) was used to discriminate between 10 nucleotides by two solvent systems. This approach was found to identify 10 analytes with 88% accuracy. To illustrate the utility of this approach for ATP hydrolysis application, the ratio between the product of reaction (PPi) and the reactant (ATP) can be used in quantitative identification of the PPi and ATP ratios.

Department : CHEMISTRY Student's Signature .....
Field of Study : CHEMISTRY Advisor's Signature .....
Academic Year : 2011 Co-advisor's Signature .....

ACKNOWLEDGEMENTS

The accomplishment of this thesis could not occur without the kindness, personal friendship, encouragement, suggestions, assistance and the extensive supports throughout my doctoral degree career from my thesis advisor, Assist. Prof. Dr. Boosayarat Tomapatanaget. Particular thanks are given to my thesis co-advisor, Dr. Gamolwan Tumcharern for suggestions, assistance and personal friendship. In addition, I would like to thank Assist. Prof. Dr. Warinthorn Chavasiri, Assoc. Prof. Dr. Nongnuj Muangsin, Assist. Prof. Dr. Sumrit Wacharasindhu and Dr. Nantanit Wanichacheva for their input, interest, valuable suggestions and comments as committee members and thesis examiners.

This thesis would not be successful without kindness and helps of a number of people. I am grateful to Dr. Kanet Wongravee and Mr. Anusak Chaicham for MATLAB program and PCA calculation. I am grateful to Assoc. Prof. Dr. Vithaya Ruangpornvisuti for computer simulation data. Special thank is due to Dr. Matinee Jamkratoke for her helpful. In addition, I would like to express my appreciation to former and the current staffs in the Supramolecular Chemistry Research Unit.

Financial supported by Thailand Graduate Institute of Science and Technology (TGIST), The Thailand Research fund (RMU5380003 and RTA5380003), and The 90th Anniversary of Chulalongkorn University Fund (Ratchadaphisek Somphot Endowment Fund). I also thank Center of Excellence on Petrochemical and Materials Technology (NCE-PPAM) and Chulalonkorn University for research support.

Finally, I would like to express my deepest gratitude to my family for their love, care, kindness, encouragement and other assistance throughout my life.

CONTENTS

Page

Page

LIST OF TABLES

LIST OF FIGURES

LIST OF SCHEMES

LIST OF ABBREVIATIONS

Abs.	Absorbance
ADP	Adenosine diphosphate
AMP	Adenosine monophosphate
ATP	Adenosine triphosphate
Ar	Aryl group
^{o}C	Degree Celsius
CH_2Cl_2	Dichloromethane
CH_3CN	Acetonitrile
CMP	Cytidine monophosphate
^{13}C-NMR	Carbon nuclear magnetic resonance
d	Deuterated
DMF	N, N-dimethylformamide
dpa	Dipicolylamine
equiv.	Equivalent
g	Gram
GDP	Guanosine diphosphate
GTP	Guanosine triiphosphate
Hz	Hertz
^{1}H-NMR	Proton nuclear magnetic resonance
I^{o}_{F}	the fluorescence intensity of the solutions containing free ligand
I_F	the fluorescence intensity of the ligand complexed with guest
J	Coupling constant
LDA	Linear Discrimination Analysis
mg	Milligram
mmol	Millimol
mL	Milliliter
M	Molar

M^{-1}	Per molar
PC	Principal Component
PCA	Principal Component Analysis
PPi	Pyrophosphate
ppm	Part per million
s, d, t, m	Splitting patterns of ^{1}H-NMR (singlet, doublet, triplet, multiplet)
THF	Tetrahydrofuran
UDP	Uridine diphosphate
UMP	Uridine monophosphate
UTP	Uridine triphosphate
$\subset$	complexation
μ	micro
δ	Chemical shift

CHAPTER I

INTRODUCTION

1.1 The importance of metal cations and anions

Metal cations play essential roles in chemical and biological process. [1] Although trace amount of transition metal ions are required for living systems, they are indispensable components of important enzymes. Zinc is one of key cation that plays significant roles in various biological processes; such as, enzymes regulation, metalloproteins function, neural signal transmission, and gene expression. [2] It is also known that a disorder of zinc metabolism is closely associated with many severe neurological diseases; such as, Alzheimer's disease (AD), amyotrophic lateral sclerosis (ALS) and Parkinson's disease. [3, 4] Anions especially phosphate, pyrophosphate and nucleotides are crucial in this regard. Nucleotides play pivotal roles in not only physiological events but also cellular communication based on enzymatic processes and signal transduction. For example, ATP is an universal energy source for various cell functions including DNA replication and transcription in all living organism.[5, 6] In addition to these fundamental intracellular function, nucleoside polyphosphates play role as extracellular anion in signal transducers.[7] In particular, pyrophosphate is the product of ATP hydrolysis under cellular conditions.[8] In order to study or monitor biological function, the molecular probe for zinc ion and nucleotide is actively investigated. The structure of nucleotide depicts in Figure 1.1.

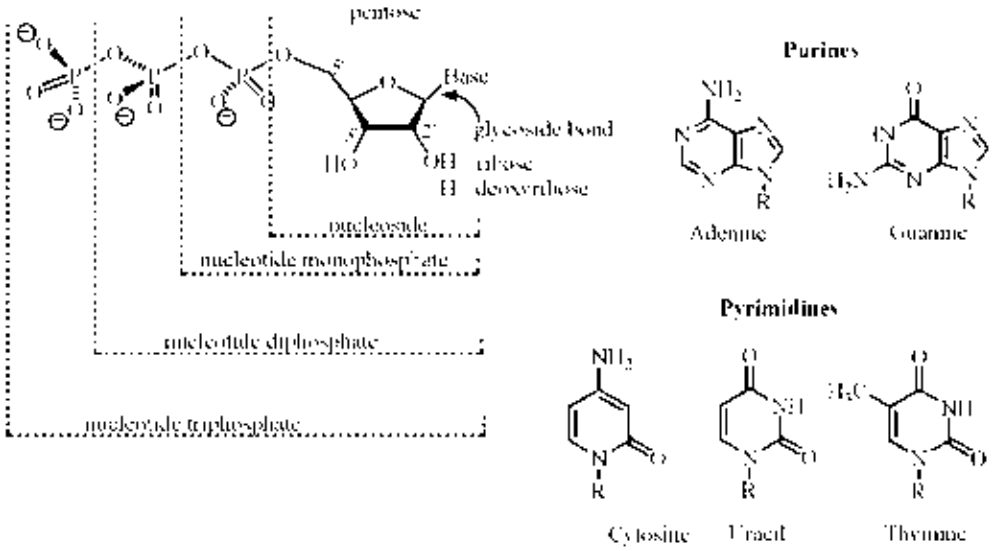

Figure 1.1 Structural elements of the most common nucleotides.

1.2 Concept of supramolecular chemistry

Supramolecular chemistry becomes one of the most rapidly expanding fields in modern chemistry.[9] The knowledge from this enchanting topic can be applied to enormous diversities of chemical system especially the production of molecular devices and artificial biological systems. The definition of supramolecular chemistry may be expressed in many terms as ‘chemistry of molecular assemblies and of the intermolecular bond’ or ‘chemistry of the non-covalent bond’. Supermolecules consist of two or more species held together by weak intermolecular forces (non-covalent intermolecular bond) such as hydrogen bonding, van der Waals interaction, electrostatic interaction, dipole-dipole interaction or π-π interaction.[10] Construction of any supermolecules are lead to the three important functions: molecular recognition, translocation and transformation.[11] Indeed, molecular recognition has become characteristics of the language of supramolecular chemistry and has been studied more widely than the others.

1.3 Molecular recognition and molecular receptors

As mentioned above, molecular recognition is defined by the energy and the information involved in the binding and selection of many analytes by a given receptor molecule. It can be implied as a (molecular) storage and a (supramolecular) read out of molecular information. The design of a molecular receptor for selective recognition, sensing and high stability between receptors and analytes is affected by several factors as follows:

a.) steric complementarity: depending on shapes and sizes of receptors and analytes;

b.) interactional complementarities, i.e. presence of complementary binding sites in the suitable disposition on an analyte and a receptor;

c.) large contact area between molecules of a receptor and an analyte;

d.) multiple interaction sites due to weak intermolecular interactions;

e.) strong overall bindings;[9]

Studies of molecular recognition require suitable molecular receptors to specifically interact with many analytes. Molecular receptors are clearly defined as organic structures held by covalent bonds that are able to bind ionic or molecular analytes by means of intermolecular interactions, leading to an assembly of two or more species. Excellent molecular receptor is one that can bind a particular analyte with high selectivity, high stability and high flexibility.[10] Receptors are divided into two types according to the number of binding site.

1.3.1 Single binding site receptor

1.3.1.1 Cation receptors are constructed based on the chemistry of crown ethers, azacrown ether and cryptands. [12]

1.3.1.2 Anion receptors are interacted with anion by electrostatic interaction, hydrogen bonds, and/or Lewis acid metal ligand interaction. The binding efficiency of anions depends on the characteristic of anion; such as, charge, size, pH, solvation and geometry.

1.3.2 Ditopic receptor

1.3.2.1 Cascade approach: a receptor is able to bind more than one cation. Then, the metal ions interact with an anionic guest. This co-binding occurs within the recognition cavity.

1.3.2.2 Binding zwitterions: the recognition units have the correct spatial arrangement to bind both positive and negative charge of single molecule; for example, amino acids, which contain acidic and basic groups.

1.3.2.3 Binding ion pairs: receptors containing two individual recognition units, one for cation and another for anion.

The design of new multi-site nucleotide receptors that contain Zn(II) complex as binding site for phosphate anions is a new area of coordination chemistry. In order to serve as a potential selective reagent for nucleotides, metal ion has been incorporated into ligand by the aid of strong electrostatic interaction with nucleotide in the part of phosphate ion.

1.4 Chemical sensors (chemosensors)

A chemosensor can be defined as a molecule which is able to bind selectively and reversibly toward analyte of interest with a concomitant change in the property of the system, such as a redox potential, and absorption or luminescence spectra. To obtain the detection of the target analyte, two different procures are needed: molecular recognition and signal transduction. Therefore, chemosensors usually consists of two molecular units: a receptor or an ionophore (able to selectively interact with the analyte), and an active unit or a signaling unit (changing one or more of its properties upon analyte complexation) (Figure 1.2).

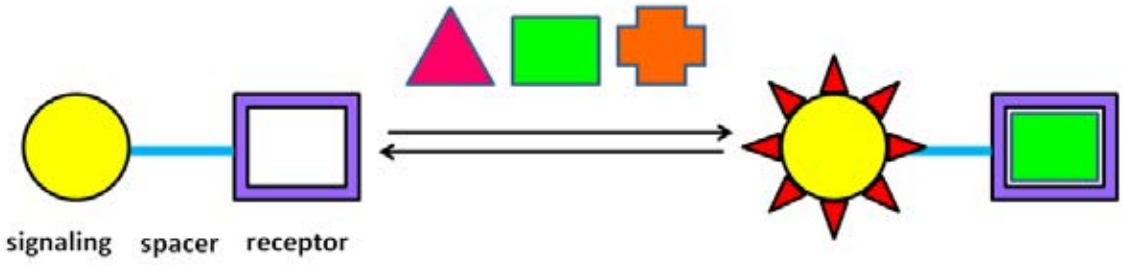

Figure 1.2 A general concept of chemosensors.[13]

1.5 Chromoionophores and fluoroionophores

A number of direct sensing schemes have been described using colorimetric and fluorescent chemosensor whose optical properties change upon direct binding of the guest (*chromoionophores* and *fluoroionophores*).

1.5.1 Chromoionophores

Color transition is popular criteria for the identification and quantitative determination of substances.

In metal-ionophore complexation, ion dipole force influence electronic properties. In case that heteroatoms are constituent of chromoionophores, the electronic disturbance propagates the whole (n+π) system. Difference cation may result in variation of absorption spectra due to the transition of ground and photoexcited states. Similarly, anion can induce a change of absorption properties of receptor. Basically, the change of color of chromoionophores occurs through two mechanisms. [14-15]

1.5.1.1 hypsochromic shifts (blue shift)

Chromoionophore containing an electron donor group (often an amino group) conjugated to aromatic ring (electron acceptor) serves as ionophore as well as chromophore. The nitrogen atoms of the chromoionophore are positively polarized, while

the excited states of cation are stronger destabilization than the ground state, resulting in hypsochromic shifts.

The chromophores are influenced by these ion-dipole forces, depending on the size and direction of the dipole moment. The more the dipole moment alters during the excitation, the more the absorption band shifts.

1.5.1.2 bathochromic shifts (red shift)

Chromoionophore containing an electron acceptor unit also shows color transition upon complexation. The donor atom is surely be polarized positively in the ground state; while, the excited states are more strongly stabilization by binding of guest at the acceptor site, causing bathochromic band shifts. The hydrogen-bond interaction between anion and the electron donor of receptor increased the electron density in the donor group (thiourea group). Increase in charge density results in the red shift of absorption.[16]

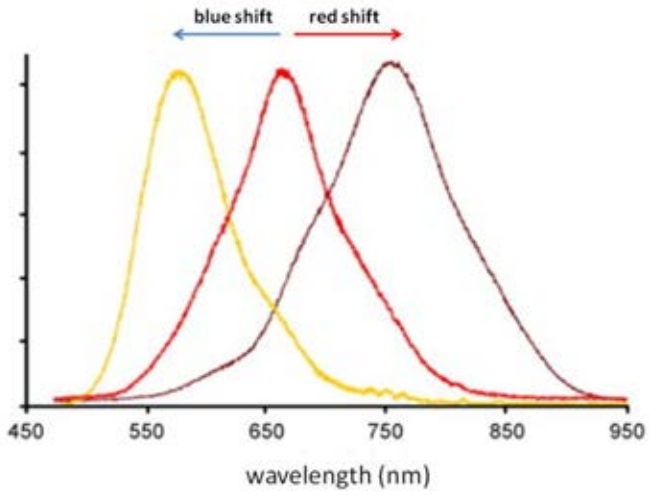

Figure 1.3 General spectrum of hypsochromic and bathochromic shift.

1.5.2 Fluoroionophores

Fluoroionophores or fluorosensors are generally multi-component systems comprising of a signaling moiety (fluorophore) and a guest-binding site (receptor). Spacer group is often used to separate between two units. The components are chosen such that the communication between the receptor and the fluorophore results in "switching off" or "quenching" of fluorescence signal. The presence of a guest molecule leads to the communication between the receptor and fluorophore, resulting in "switching on" or "recovery". [17-19]

Generally, the change of fluorescence behavior of fluoroionophores exhibits through two mechanisms.

1. *Fluorescence PET (Photoinduced Electron Transfer)*; For PET mechanism, the receptor serves as an electron donor (e.g.amino-containing group), and the fluorophore acts as an electron acceptor. In the analyte-free form, upon excitation by photons the electron of the highest occupied molecular orbital (HOMO) of the fluorophore is promoted to the local lowest unoccupied molecular orbital (LUMO). Subsequently, the electron vacancy on the HOMO of the donor transfers to the HOMO of the fluorophore synergistically, which causes fluorescence quenching.[20]

Upon binding to a target analyte, HOMO energy level of excited fluorophore is higher. Electron transfer from HOMO bound receptor cannot transfer to one of excited fluorophore. Fluorescence signal is recovery due to electron transfer from unoccupied to occupied orbital in excited fluorophore. (Figure 1.4).

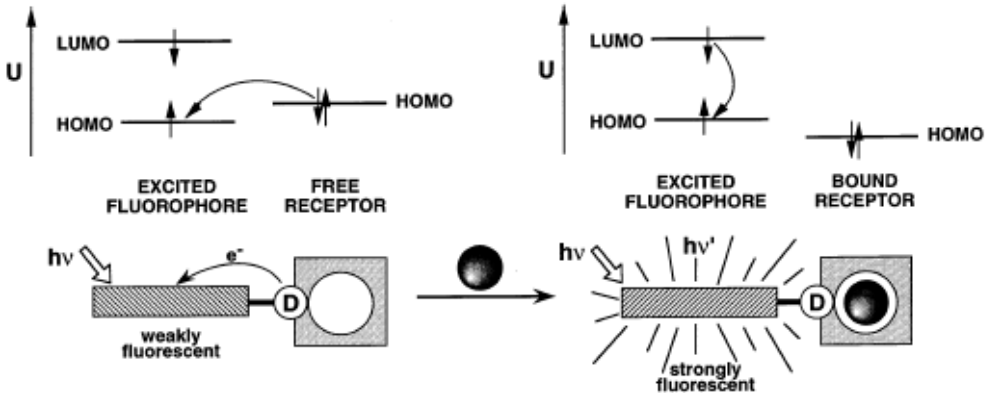

Figure 1.4 Principle of the fluorescence PET mechanism. [17]

Excimer-monomer PET mechanism is a special design for fluorophore which can form an excited-dimer. Eximer is constructed when an excited molecule come close to another during the lifetime of excited state. Consequently, dual fluorescence is observed with monomer band at shorter wavelength and excimer broad band at longer wavelength. Upon cation binding, fluorophore proximity and excimer formation are altered. Therefore, the monomer/excimer fluorescence intensity ratio is observed.

2. *Fluorescence PCT (Photoinduced charge transfer)*. For PCT mechanism, the fluorophore is composed of an electrondonating group (usually an amino group) conjugated to an electron-withdrawing group. Internal charge transfer (ICT) undergoes from the donor to the acceptor. [21] The consequent change of the dipole moment leads to a Stokes' shift, which is influenced by the microenvironment of the fluorophore. The excited state is more strongly destabilized than the ground state by the analyte interaction at the donor group, leading to a blue shift of the absorption and emission spectra. Conversely, the excited state is more stabilized than the ground state by the analyte interaction at the acceptor group resulting in a red shift of the absorption and emission spectra.

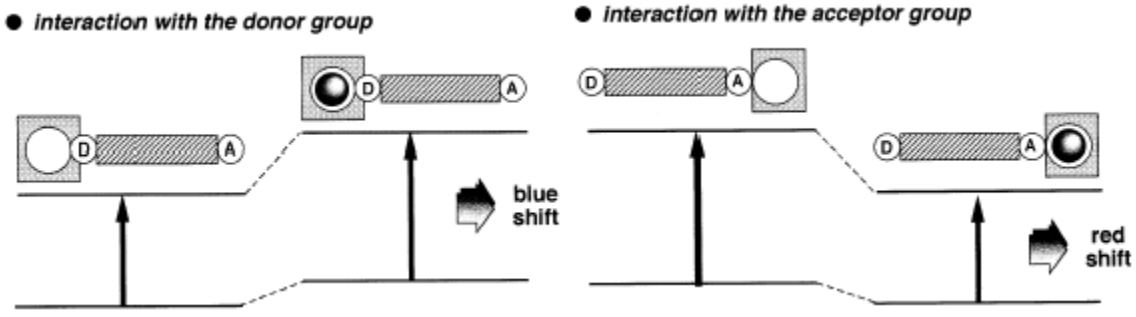

Figure 1.5 Principle of the fluorescence PCT mechanism.

1.6 Determination of the stoichiometry of a complex by the method of continuous variations (Job's method) [22]

The chemical reaction stoichiometry of complex was obtained from a simple and effective approach called the method of continuous variation. To deliberate a complex M_mL_l formed according to the equilibrium

$$mM + lL \rightleftharpoons M_mL_l \qquad 1.1$$

with

$$\beta_{ml} = \frac{[M_mL_l]}{[M]^m[L]^l} \qquad 1.2$$

The method is based on the following fact: the fluorescence intensity Y is measured for a series of solutions containing of the ligand and a serial dilution of the cation. The total molar concentration (C) of ligand (C_L) and metal (C_M) is held constant, but their mole fractions are varied from large to small.

$$C_L + C_M = C = \text{constant}$$

Since the maximum change will occur when the mole fraction of the reactants is closest to the actual stoichiometric mole ratio. The product formula structure and reactant stoichiometry can be determined using this approach.

The maximum at the initially-unknown value of Y is then related to the ration *m/l*. The complex product is equal to Y and the value of Y_0 is related to no cation added (x=0). When plotting the variations in fluorescence intensity versus mole fraction, it is convenient to subtract the fluorescence intensity that would be measured in the absence of cation at each concentration.

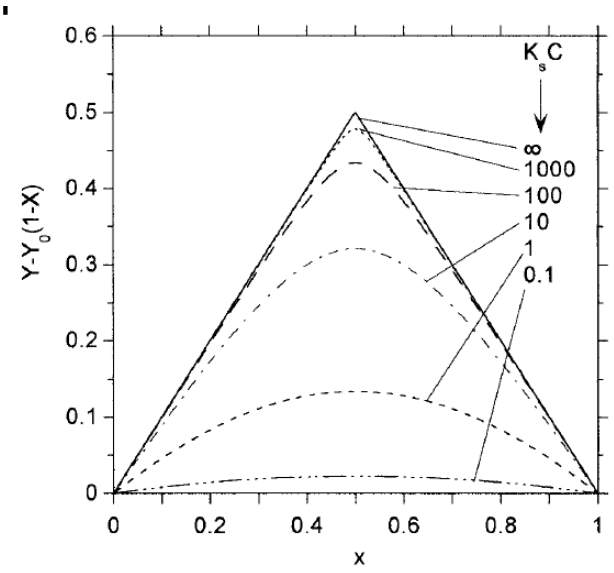

Figure 1.6 Job's plots for a 1:1 complex.

1.7 Limit of detection [23]

A limit of detection (LOD) generally defined as the lowest concentration of analyte that can be detected with reasonable certainty for a given analytical method. The LOD would be able to distinct from the blank or background signal. This definition of the limit of detection is quite arbitrary and entirely open to an analyst to provide an alternative definition for a particular purpose. However, it is required to provide the definition whenever a detection limit is cited in a paper or a report.

This is an alternative definition that determines the detection limit as the smallest measure, x_L. The value of x_L is given by the equation

$$x_L = x_{bi} + 3s_{bi} \qquad 1.3$$

where x_{bi} is the mean of the blank signal, s_{bi} is the standard deviation of the blank.

To convert from measurement units (x_L) to concentration (c_L), sensitivity or slope (S= △concentration/△intensity) is applied. That is,

$$c_L = c_{bi} + 3s_{bi}\,S \qquad 1.4$$

The concentration of the blank is zero, then

$$c_L = 3s_{bi}\,S \text{ or } c_L = 3s_{bi}/\text{slope} \qquad 1.5$$

1.8 Selectivity

A selectivity of a receptor is a preference of that host toward a guest. This is customarily estimated from a magnitude of a thermodynamic *stability constant* of a receptor-guest or, in more general terms, a ligand-metal complex. For fluoroionophore, the method of obtaining a binding constant is through fluorimetric titration-a measurement of fluorescence intensity at different metal-ligand ratios.[24-26]

The complexation of a metal ion M by a ligand L in solution can be represented by the equilibrium

$$M + L \leftrightarrow ML$$

which is controlled by the stability constant

$$K_s = \frac{[ML]}{[L][M]}$$

where the bracket denotes the concentration of each species in mole per liter.

In fluorimetric titration, the fluorescence intensity of the solutions containing free ligand L (I_F^0) and ligand complexed with metal ion ML (I_F) at the chosen emission wavelength are measured and are related to the initial concentration of the ligand (C_0) by

$$I_F^0 = kaC_0 \qquad 1.6$$

I_F depends directly on [L] and [ML]

$$I_F = \text{ka[L]} + \text{kb[ML]} \qquad 1.7$$

Where k, a and b is a constant

Since $[ML] = C_0 - [L]$

Therefore $$I_F - I_F^0 = \text{k(b-a)}(C_0 - [L]) \qquad 1.8$$

After rearrangement

$$\frac{I_F^0}{I_F - I_F^0} = \left(\frac{a}{b-a}\right)\left(\frac{1}{K_s[M]} + 1\right) \qquad 1.9$$

Equation 1.9 shows that a plot of I_F^0 / (I_F - I_F^0) against 1/ [M] would be a straight line in which stability constant K_s can be calculated.

1.9 Principal Component Analysis (PCA) [27]

Principal Component Analysis (PCA) is an unsupervised method utilized to reduce the dimensionality of the data set into a new coordinate system with a minimum loss of information. This is achieved by calculating orthogonal eigenvectors in terms of Principal Components (PCs). The first component (PC1) always represents the highest degree of variance and the second greatest variance is projected to the second component (PC2) and so on. In its simplest form, the transformation of the original data (***X***) using PCA can be expressed by

$$\boldsymbol{X} = \boldsymbol{T}^{\bullet}\boldsymbol{P} + \boldsymbol{E}$$

Where ***T*** is the scores and ***P*** is the loading matrix.

The graphical representation of the decomposition of a data matrix (***X***) into a score matrix (***T***) and loading matrix (***P***) with ***A*** principal components is illustrated in Figure 1.7.

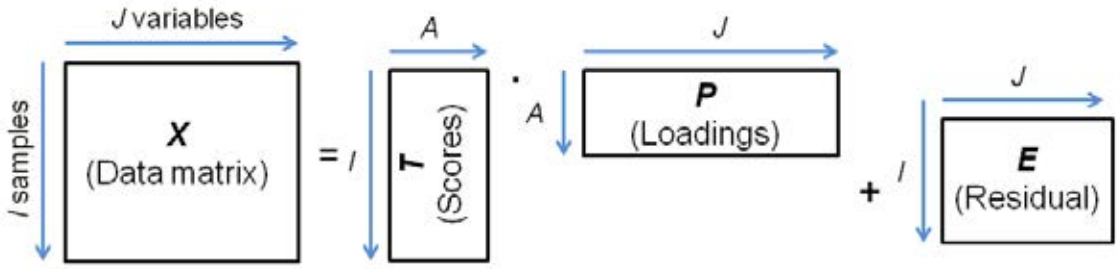

Figure 1.7 Principal components analysis.

The coordinates of the sample relative to the PC axes are termed scores and can be used as an indicator of correlation between analytes.

To describe the PCA approach as mention above, Figure 1.8 exhibits a form of variable reduction of PCA. It represents the reduction of the original variables to a number of significant principal components (PCs). PCA method reduces the large original dataset to a smaller data set lead to simplified interpretation.

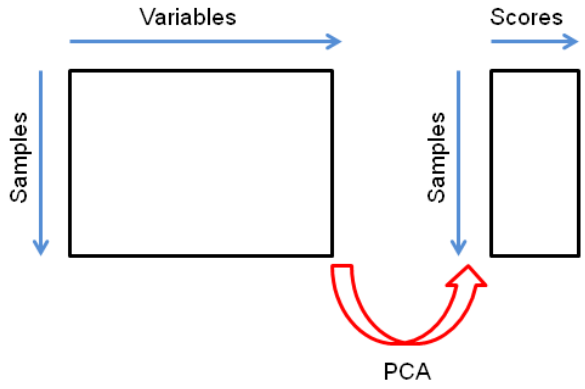

Figure 1.8 PCA as a form of variable reduction.

CHAPTER II

LITERATURE REVIEWS

2.1 Literature reviews

2.1.1 Chemosensors for detection of zinc ion

In the last decade, varieties of chemosensors for Zn^{2+} ions implicated in important cellular roles have been reported. The binding unit of these sensors is mostly composed of nitrogen atoms, which can bind with Zn^{2+} ion using the lone pair electron.[28-30] 2-Dipicolylamine (dpa) is often chosen as cation binding site due to its chelation-enhanced fluorescent property in the presence of Zn^{2+} ion.

In 2002, Nagano and coworkers [31] synthesized two new fluorescent probes for Zn^{2+} ion based on benzofuran derivatives. Sensor **S2** compared to sensor **S1**, was suitable for biological application since it was water-soluble with a high fluorescence quantum yield. Interestingly, the complexation of sensor **S2** toward Zn^{2+} ion illustrated the blue shift from 365 to 335 nm. Hence, concentration of Zn^{2+} was calculated from the fluorescent intensity ratio between 335 and 365 nm. Tight binding between sensor and Zn^{2+} ion with an apparent dissociation constant was reported in the nanomolar range, 0.79 and 2.8 nM for sensor **S1** and **S2**, respectively. Thus, these sensors had enough sensitivity for mammalian cell applications. In order to determine the cell permeability of sensor **S2**, the ethyl ester derivative was prepared. The results found that it could permeate into the cell by esterase in the cytosol. RAW 264.7 cells were stained using 10 μM **S2** derivatives at incubation temperature 37 °C for 1.0 h. The fluorescence emission ratio (340 nm/380 nm) was increased immediately by the addition of Zn^{2+} and 2-mercaptopyridine *N*-oxide (pyrithione). And the increase was reversed by the addition of TPEN. (Figure 2.1)

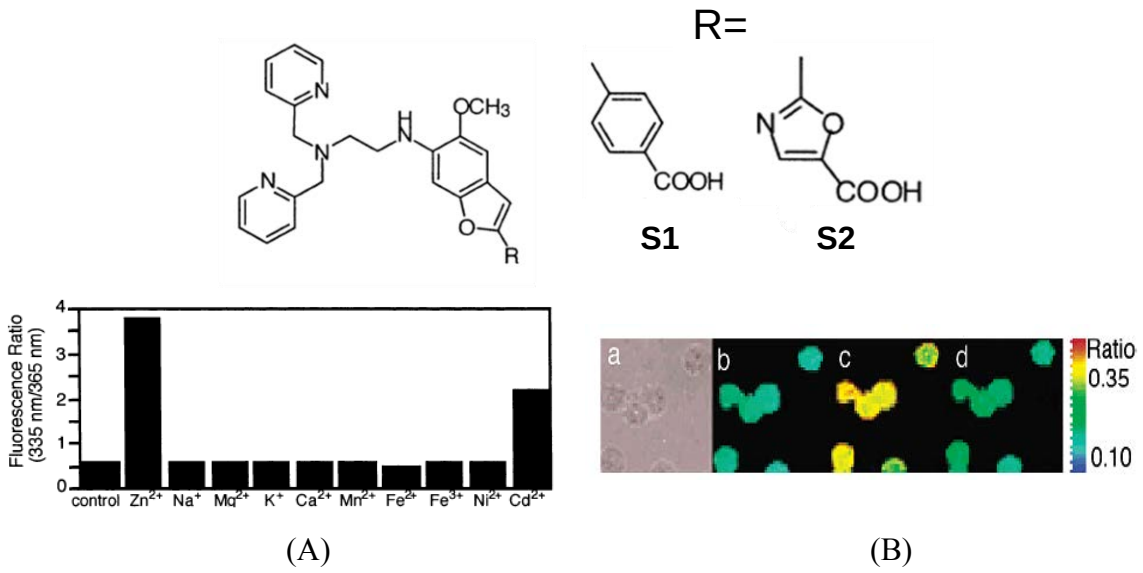

(A) (B)

Figure 2.1 (A) Selectivity of sensor **S2** at pH 7.4 (100 mM HEPES buffer, I = 0.1 ($NaNO_3$)) (B) fluorescence ratiometric images (340 nm/380 nm) of zinc in macrophages (RAW264.7) labeled with ZnAF-R2EE in PBS buffer, pH 7.4. (a) Bright-field transmission image. (b) Ratiometric image of (a). (c) after added 15 μM pyrithion (zinc ionophore) and 150 μM ZnSO4 (d) after added 400 μM TPEN.

In 2006, Qian, Cui and coworkers [32] reported a new mechanism for a ratiometric fluorescent probe for Zn^{2+} based on deprotonation mechanism. The pKa value of sensor **S3** was 3.0. The absorption spectra showed the characteristic peak of sensor **S3** at 451 nm. Upon addition of Zn^{2+} ion, the absorption band at 451 nm decreased, while the new two bands at 309 and 507 nm were developed. For emission titration spectra, the addition of Zn^{2+} solution resulted in a significant fluorescence quenching at 537 nm accompanied with a large red shifted to 593 nm. The apparent binding constant was determined as 6.76 x 10^5. From both results of absorption and emission, they concluded that the capture of Zn^{2+} ion by the receptor leaded to the deprotonation of the secondary amine of **S3**, which caused the ratiometric UV and fluorescence changes. (Figure 2.2)

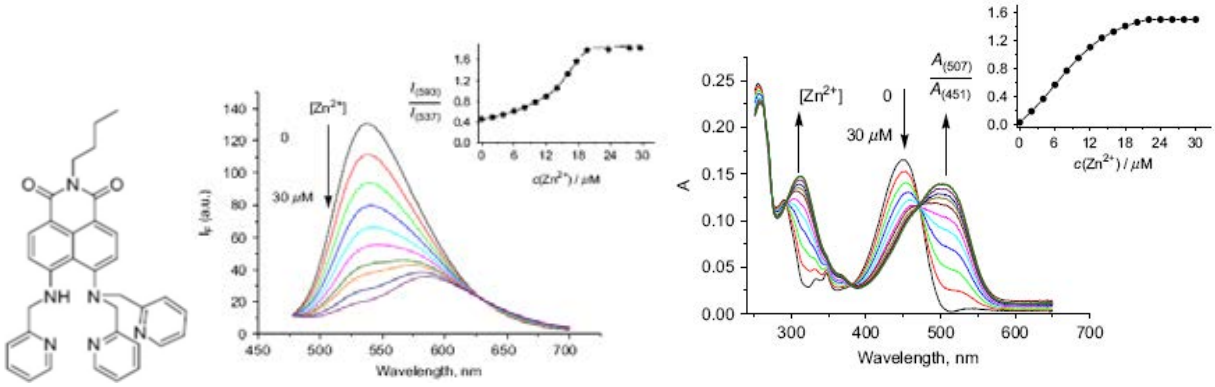

S3 (A) (B)

Figure 2.2 (A) UV–vis absorption spectra (B) fluorescence emission spectra of **S3** in the presence of different concentrations of Zn^{2+} in acetonitrile–water (80:20) solution at pH 7.0 maintained with HEPES buffer (50 mM).

In 2007, Wang and coworkers [33] reported a water-soluble fluorescent sensor **S4** based on the quinoline platform. Sensor **S4** bound extremely tight to Zn^{2+} ion with an apparent dissociation constant in the femtomolar range. Sensor **S4** showed weak fluorescence emission at 425 nm. After complexation with Zn^{2+} ion, the fluorescence intensity of **S4** was increased rapidly with a small red shifted to 438 nm. Moreover, sensor **S4** showed good selectivity for zinc over other physiologically relevant metal ions in the presence of EDTA. (Figure 2.3)

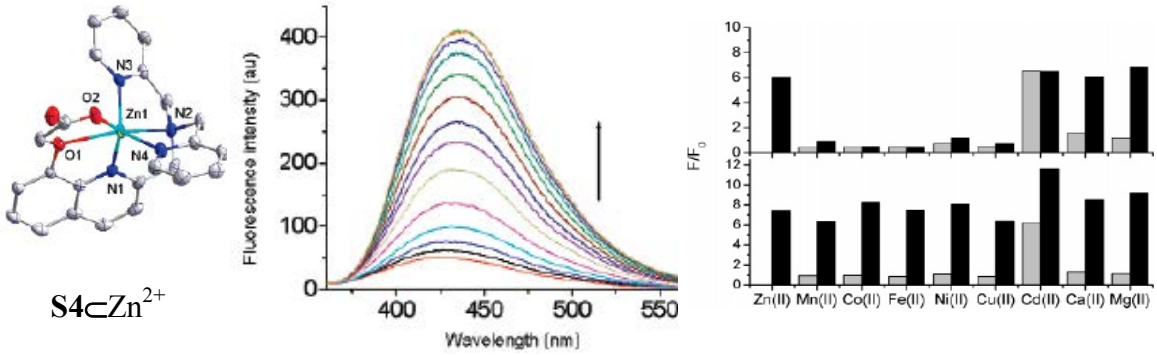

(A) (B)

Figure 2.3 X-ray crystal structure of the zinc complex of **S4** (A) Fluorescence emission spectra of **S4** in the presence of zinc(II)-TPEN buffer solutions (B) metal ion selectivity profiles of **S4** in the absence (top) and the presence of 2 equiv of EDTA (bottom). The ratio of relative integrated emission of 1 + 1 equiv indicated metal ions to that of apoligand (gray bar) and the ratio of relative integrated emission of 1 + 1 equiv indicated metal ions, followed by 1 equiv of Zn^{2+} to that of apoligand (black bar).

In 2008, Akkaya and coworkers [34] reported a novel water-soluble fluorescent sensor **S5** based on distyryl-substituted boradiazaindacene (bodipy). The emission spectrum of sensor **S5** displayed at 726 nm in 5:95 ethanol-aqueous buffer solutions. Upon gradual addition of Zn^{2+} ion, fluorescence enhancement with a concomitant of a blue shift to 625nm was observed. Sensor **S5** bound to Zn^{2+} ion with an apparent dissociation constant of 2.0×10^{-5} M. The fluorescence emission of free chemosensor was extended to near IR region, therefore it is barely visible. After Zn^{2+} addition, complex was bright red in color. It was worth to mention that sensor **S5** shows good selectivity for Zn^{2+} over other biologically relevant metal ions (Figure 2.4).

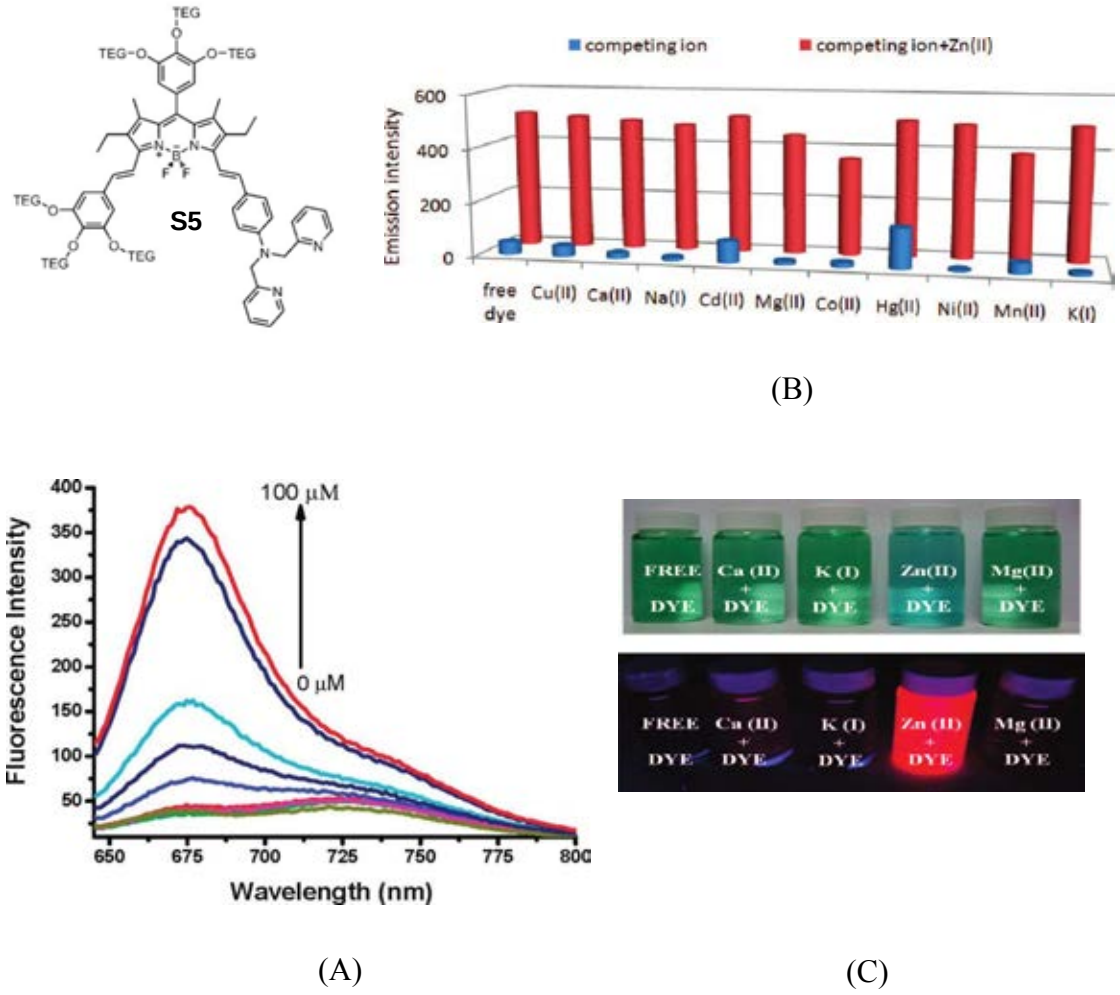

Figure 2.4 (A) emission spectra of **S5** increasing amount of Zn(II) in an ethanol-aqueous buffer mixture (5% in ethanol, HEPES 0.1 M, pH 7.2) (B) the competition experiments between Zn(II) selected metal ions and (C) Digital photographs of the chemosensor solutions (5.0 μM) in the presence of different metal ions at 100 μM concentration. The upper plate is taken under ambient light, and the bottom one under UV illumination at 360 nm.

2.1.2 Chemosensors for detection of pyrophosphate (PPi)

In recent years, the development of sensor for anions is a major research focus. In particular, the selective detection of anion pyrophosphate in aqueous solution needs two requirements. One is a strong affinity for PPi in water, and the other is the ability to convert anion recognition into a signal. An alternative approach for efficient binding of PPi in aqueous media stemmed from metal coordination interactions. Therefore, Zn^{2+} ion has commonly been incorporated into sensor due to the strong hydration effects of anions.

In 2005, Yoon and coworkers [8] reported the fluorescence complex of dpa-2Zn^{2+} attached to fluorescein fluorophore. The complex **S6·Zn^{2+}** showed a unique change in the emission spectrum only with pyrophosphate (PPi) in 100% aqueous solution. The absorption titration spectra exhibited the red shift upon the addition of PPi. Similarly, the emission respond of complex **S6·Zn^{2+}** showed the fluorescence enhancement with a concomitant of gradually red shifted from 523 to 534 nm after addition of PPi. From fluorescence titration, the association constant of complex **S6·Zn^{2+}** was calculated to be 9.84 x 10^{-4} M^{-1}. Consequently, this complex acted as a ratiometric fluorescent sensor for PPi in an aqueous solution. (Figure 2.5)

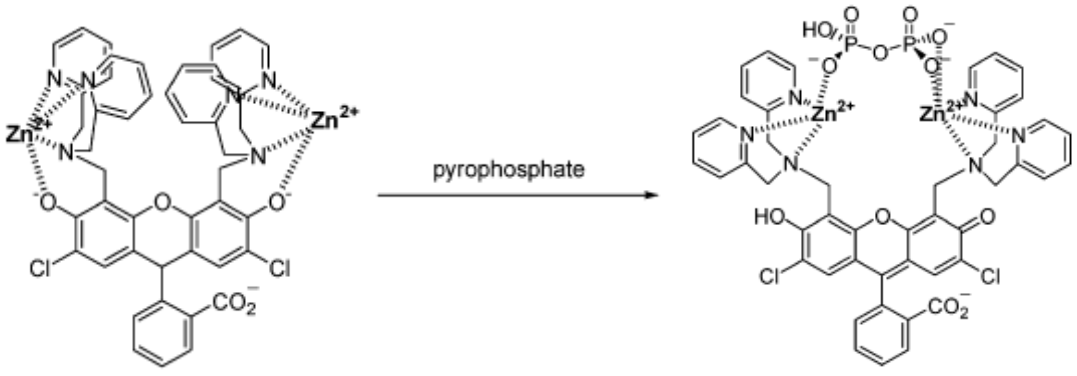

S6•Zn^{2+} **S6•Zn^{2+}⊂ PPi**

Figure 2.5 Proposed mechanism for the Binding mode of complex **S6·Zn^{2+}** with pyrophosphate.

In 2005, Hong and coworkers [35] synthesized a new fluorescent sensor **S7·Zn^{2+}** containing pyrene and Zn^{2+}–dpa. The absorption spectrum of sensor **S7·Zn^{2+}** displayed five well shaped between 260 and 350 nm in an aqueous solution. When PPi or ATP was added, the absorption spectra of **S7·Zn^{2+}** showed a red shift. For fluorescence emission spectrum, sensor **S7·Zn^{2+}** illustrated the emission band at 360-450 nm which was corresponded to the pyrene monomer emission. Upon the addition of PPi, the new emission band at 475 nm was observed while the monomer emission was decreased. The addition of ATP showed the similar result but much less intensity. This result also revealed that **S7·Zn^{2+}** had a higher selectivity for PPi over ATP by the formation of eximer. Moreover, Job's plot suggested a 2:1 stoichiometry between **S7·Zn^{2+}** and PPi. (Figure 2.6)

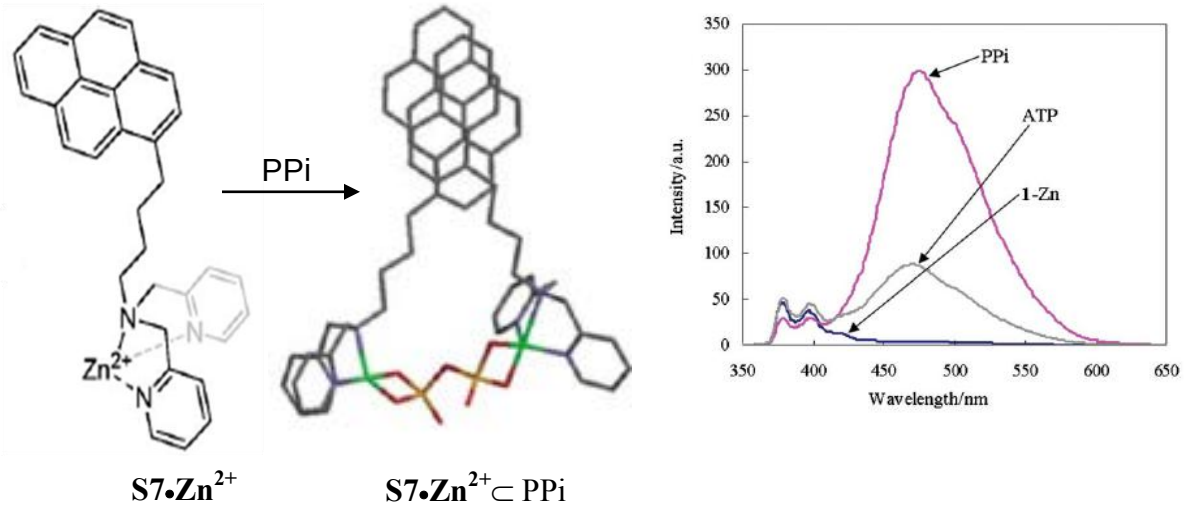

Figure 2.6 (A) Energy-minimized structure of the complex between **7·Zn^{2+}** and PPi (B) fluorescence spectra of **7·Zn^{2+}** (0.02 mM) in aqueous solvent of 10 mM HEPES buffer (pH = 7.4) in the presence of anions (0.4 equiv).

In 2007, Yoon and coworkers [36] reported a new acridine dpa-Zn(II) complex that exhibited a different fluorescence response to PPi and Pi in aqueous solution. The sensor **S8·2Zn^{2+}** displayed a large chelation enhanced fluorescence quenching (CHEQ) effect with a bathochromic shift (~20 nm) upon the addition of PPi. On the contrary, the addition of Pi induced a large chelation enhanced fluorescence (CHEF) effect (~300%) with a gradually shifted from 462 to 444 nm. The association constant for PPi and Pi were observed to be 4.85 x 10^7 and 9.36 x 10^4 M^{-1}, respectively. The large CHEF effect with Pi was ascribed to the hydrogen bonding between the hydrogen of OH in Pi and nitrogen on the acridine moiety. (Figure 2.7)

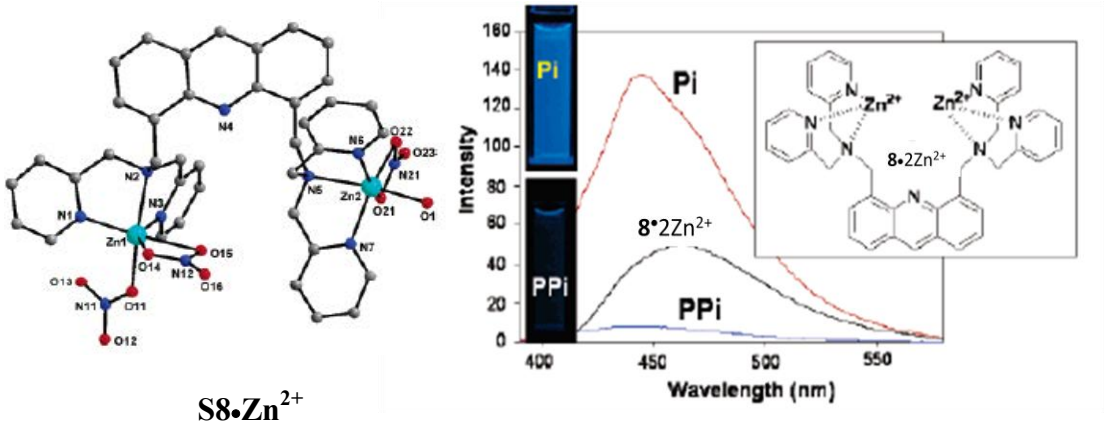

(A) (B)

Figure 2.7 (A) Fluorescence spectral change of sensor **S8·2Zn^{2+}** upon the addition of Pi and PPi at pH 7.4 (10 mM HEPES) (B) the crystal structure of complex **S8·Zn^{2+}**.

In 2010, Chan and coworkers [37] reported a new spiropyran-based fluorescent probe for PPi in aqueous solution. Free sensor **S9** exhibited a dramatic change with Zn^{2+} ion in both absorption and fluorescence spectra. Therefore, the complex **S9·Zn^{2+}** prepared to examine the binding affinity with PPi. The fluorescence response of **S9·Zn^{2+}** with PPi showed a significant increase of fluorescence intensity at 560 nm and a remarkably decrease at 620 nm. The fluorescence intensity ratio of F_{560}/F_{620} as a function of PPi concentration demonstrated a linear range from 1.0 x 10^{-6} to 1.0 x 10^{-4} M (R^2= 0.9963).

The detection limit was found to be 4.0 x 10^{-7} M. This approach is potentially appropriate for quantification in biological process. (Figure 2.8)

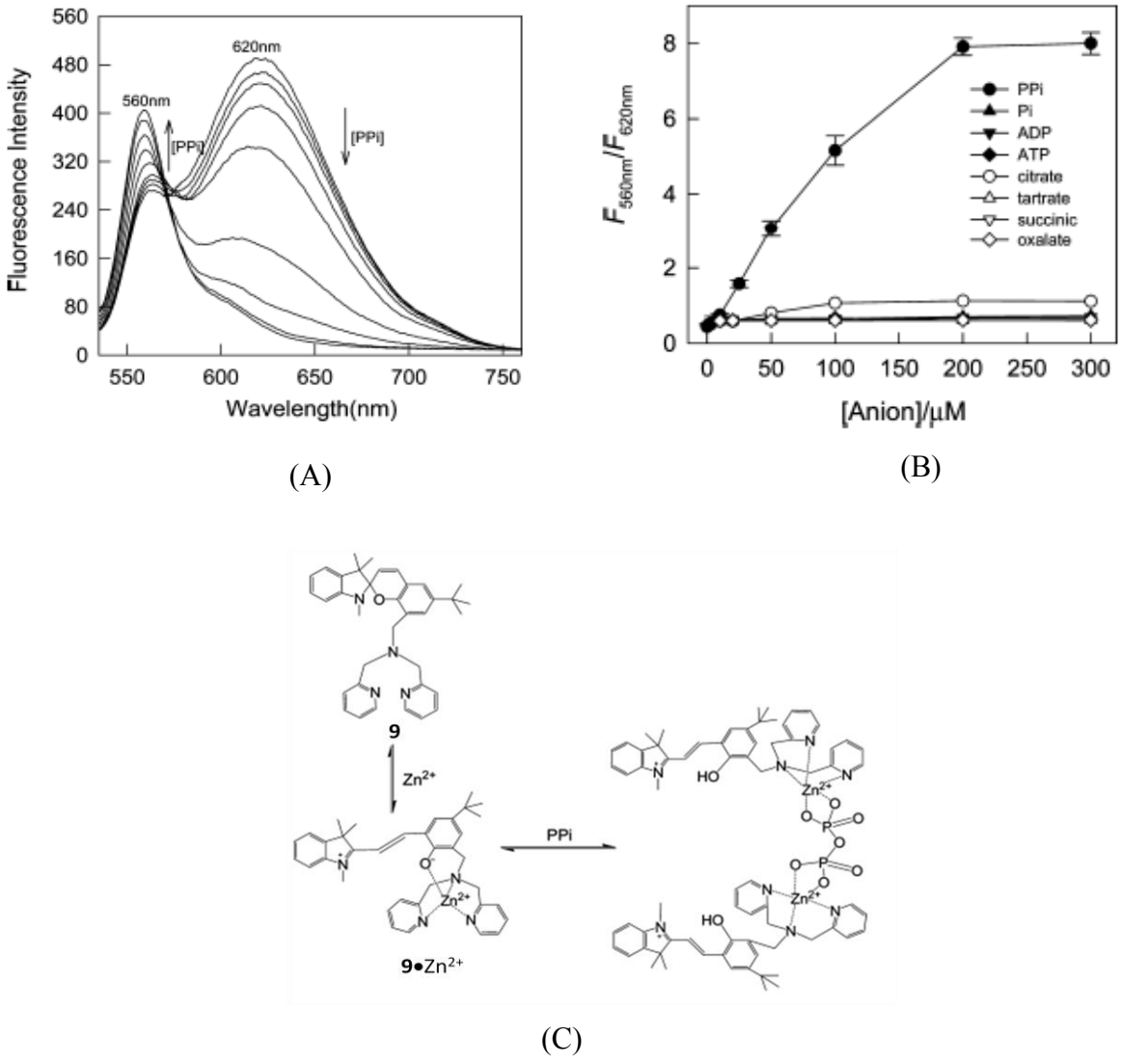

(A) (B)

(C)

Figure 2.8 (A) Fluorescent changes of sensor **S9·Zn^{2+}** upon the addition of PPi (B) changes in the fluorescence intensity of **S9·Zn^{2+}** at 560 nm with respect to that at 620 nm upon addition of different concentrations of anions in the ethanol aqueous solution at pH 7.4 (C) proposed structures of **S9·Zn^{2+}** and **S9·Zn^{2+}**⊂ PPi.

In 2011, Kim and coworkers [38] reported a new Zn^{2+} complex with 1,8-naphthalimide for recognition of pyrophosphate. The fluorescence spectra of sensor **S10** exhibited the fluorescence enhancements with a red shift for 29 nm upon addition of Zn^{2+}. Upon addition of various anions, PPi demonstrated obvious fluorescence quenching with a blue shifted from 505 to 481 nm. Limit of detection for PPi determination is 1.5 μM. It is worth to note that complex **S10·Zn^{2+}** is successfully applied in biological system in C2Cl2 cell. (Figure 2.9)

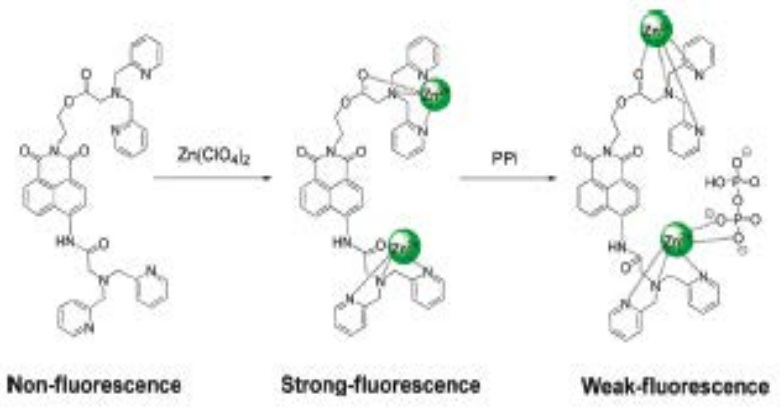

(A)

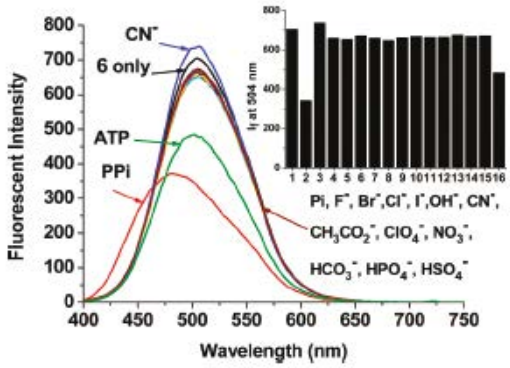

(B)

Figure 2.9 (A) Proposed binding modes of **S10** and S**10·Zn^{2+}** with PPi (B) fluorescence responses of **S10·Zn^{2+}** complex to 10 equiv of various anions in CH_3CN-HEPES buffer (20 mM, pH 7.4) (5:95, v/v).

2.1.3 Chemosensors for detection of adenosine triphosphate (ATP)

Nucleotide is well known to play several important roles in the biological cell. Especially, ATP is a key factor for the energy production and storage in all living systems. Many recognition units such as, imidazolium, amide, guanidinium, and metal complex have been developed for detection of ATP. [39-42] Among the others, the metal complex was preferred to use as binding site for ATP because of its strong electrostatic interaction with phosphate anion groups.

In 2002, Hamachi and coworkers [43] synthesized a new fluorescent sensor containing Zn-dpa and anthracene. From the fluorescence results, sensor **S11·2Zn^{2+}** has a high selectivity for ATP under the natural aqueous solution. The addition of ATP to **S11·2Zn^{2+}** resulted in the enhancement of fluorescence intensity. The binding constant of 2.2 x 10^6 M^{-1} for ATP complexation was determined. Moreover, the binding mode of **S11·2Zn^{2+}** and ATP was also investigated by ^{31}P NMR. The result clearly showed that only β- and γ-phosphate of ATP shifted to the downfield upon the addition of 1 equiv. of **S11·2Zn^{2+}**. This data suggested that sensor **S11·2Zn^{2+}** preferred to bind to β- and γ-phosphate of ATP, which did not associate with α-phosphate. Thus, the coordination of a Zn-dpa to γ -phosphate was the major key of the binding ability. (Figure 2.10)

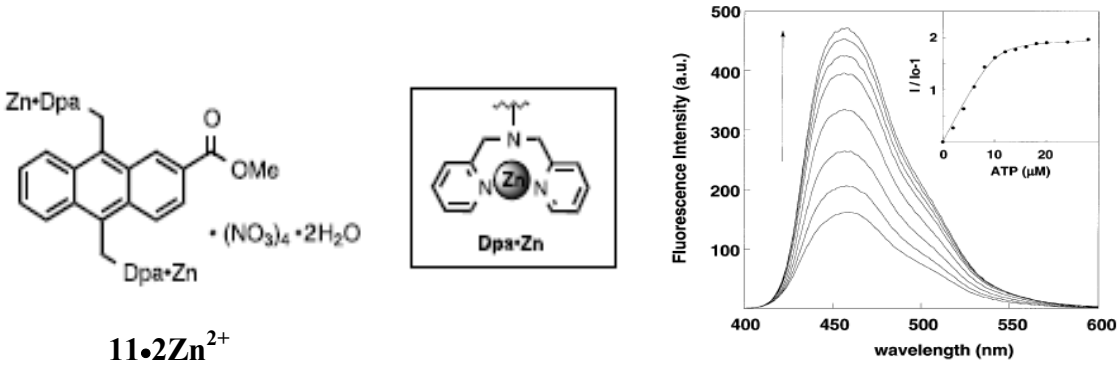

11•2Zn^{2+}

Figure 2.10 Fluorescence spectral changes of **S11·2Zn^{2+}** (10 μM) upon the addition of ATP in 10 mM HEPES buffer (pH 7.2) at 20°C. (Inset) Fluorescent titration curve of **S11·2Zn^{2+}** with ATP.

In 2009, Moro and coworkers [44] reported an ATP fluorescent sensor based on Zn(II)-dpa complex. The fluorescence emission band of sensor **S12·Zn^{2+}** in aqueous solution displayed at 535 nm. After addition of ATP, a significant fluorescence enhancement at 535 nm was observed. Considering, the fluorescence spectral change of **S12·Zn^{2+}** toward various anions presented high sensitivity in ATP and ADP in the low concentration range. (Figure 2.11)

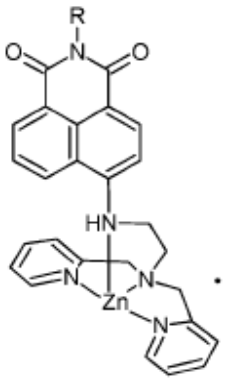

S12•Zn^{2+}

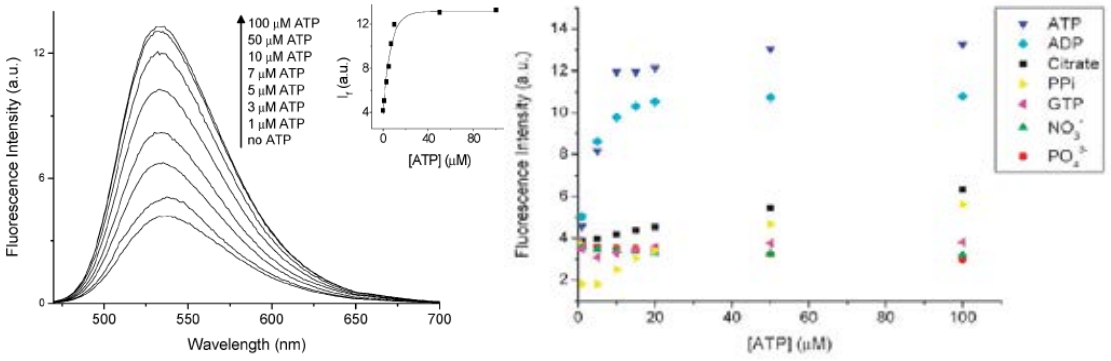

(A) (B)

Figure 2.11 (A) Fluorescence spectral changes of **S12·Zn^{2+}** (10 μM) upon the addition of ATP (B) fluorescence spectral changes of **S12·Zn^{2+}** (5 mM) upon exposure to different concentrations of anionic analytes in 0.1 M HEPES buffer (pH 7.2) at 20°C.

In 2010, Ojida and coworkers [45] reported two fluorescent sensors for ATP based on FRET mechanism. The fluorescent sensor composed of coumarine unit as a FRET donor and xanthene moiety as a FRET acceptor. The fluorescence results demonstrated that both sensors including sensor **S13·2Zn**$^{2+}$ and **S14·2Zn**$^{2+}$ showed a large fluorescence increase at 525 nm of xanthene ring but performed a decrease of the coumarin fluorescence, upon addition of ATP, at 454 and 477 nm for **S13·2Zn**$^{2+}$ and **S14·2Zn**$^{2+}$, respectively. Hence, the binding of sensor to ATP underwent FRET via a turn-on fluorescence sensing mechanism. However, the binding affinity of the chemosensors toward various polyphosphate anions is the same as ATP. Both sensors can then be used as ratiometric chemosensors for polyphosphate anions. These sensors were applied to image the ATP level and used for the indicator of cellular energy inside the cells. Best of all, they utilized for a precise monitoring of various enzymatic reactions in vitro. (Figure 2.12)

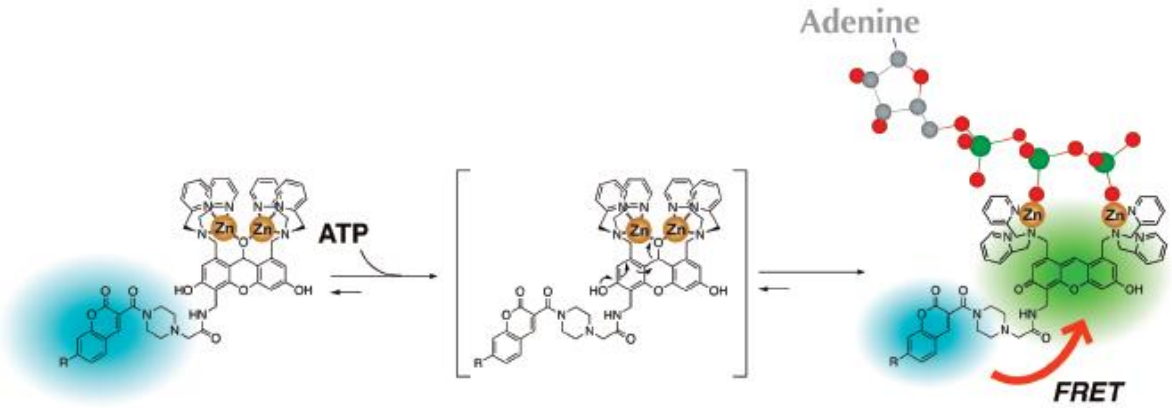

S13·2Zn^{2+} R= OH **S14·2Zn**$^{2+}$ R=NEt_3

Figure 2.12 Schematic illustration of the dual-emission sensing of ATP with the chemosensors. The chemosensors undergo FRET via a turn-on fluorescence sensing mechanism.

In 2011, Jang and coworker [46] reported a chemosensor for detecting ATP by a simple indicator displacement assay (IDA). The chemosensor **S15·2Zn^{2+}** assembling with fluorescein defined as assembly **S16**. The utility of assembly **S16** as a bioanalytical molecular tool has also been demonstrated in IDA. The result of IDA experiment of assembly **16** with various analytes illustrated the binding affinity in the order of ATP > ADP > AMP. To gain support the binding mode of assembly **S16** with ATP, ^{1}H-NMR titration was examined. The ^{1}H-NMR spectra showed a significant downfield shifted of aromatic moiety without splitting upon addition of 1.0 equiv. of ATP. This result confirmed that the coordination environments around the two metal centers are unchanged. (Figure 2.13)

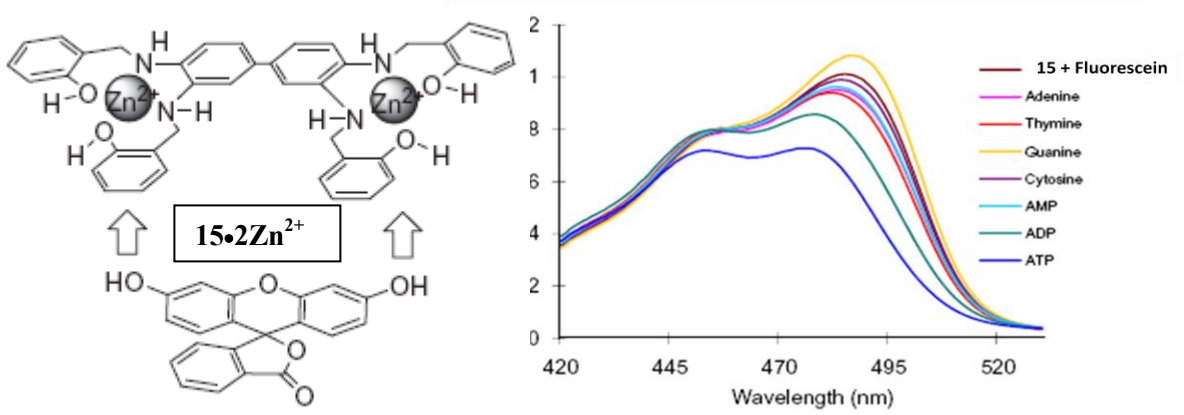

(A) Assembly **S16** (B)

Figure 2.13 (A) structure of assembly **S16** (B) changes in absorbance of the IDA complex (1.0 μM) upon addition of 1.0 equiv of guest substrate in a DMSO/H_2O (1:9, v/v) solvent system.

2.1.4 Principal Component Analysis (PCA)

PCA is a mathematical method that can discriminate the similar analytes on the basic of structure. In the analysis of the differential approach, the pattern recognition often yields impractical and overlapping iterative data. Therefore, PCA is used to reduce the multidimensional of the data set to a single score on two or three principal components (PCs). In the last decade, many publications focus on the utility of PCA for statistical evaluation of the array responses rather than single sensor. [47-49]

In 2003, Anslyn and coworkers [50] reported an excellent combinatorial library of sensors and indicator displacement assay (IDA) to discriminate between ATP, GTP and AMP in aqueous solutions. The sensor composed of guanidinium groups as recognition units for nucleotide triphosphates and it was attached to the tripeptide arms for differential selectivity on resin bead. The anionic fluorescein chromophore was inserted into the array, which consisted of the different peptide sequence of the sensor. Moreover, cationic receptor was also added as an indicator. The red, green and blue (RGB) intensity values performed for each bead in IDA. The PCA score plot can differentiate ATP, GTP and AMP. (Figure 2.14)

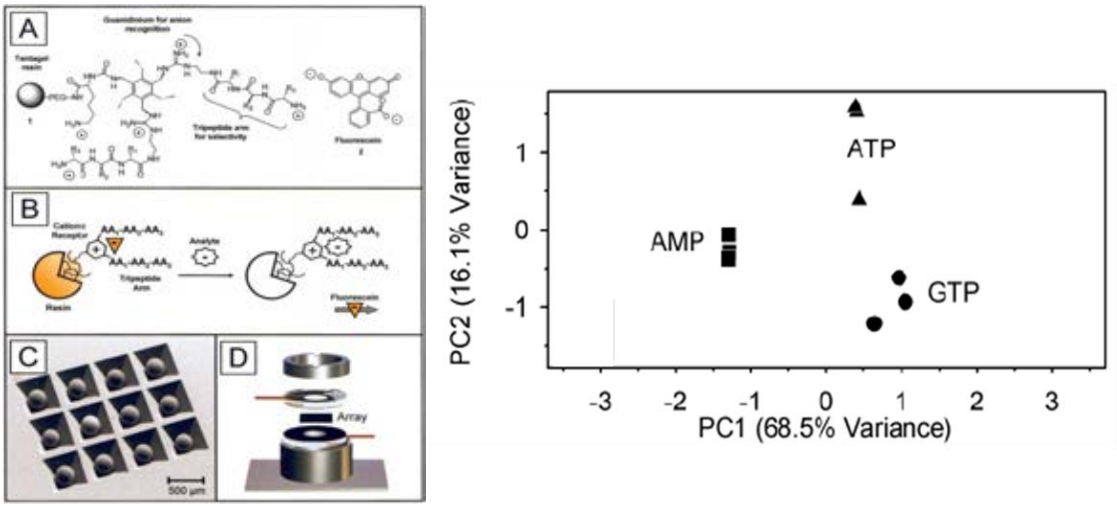

(a) (b)

Figure 2.14 (a) A microscopic to macroscopic representation of the sensing protocol (b) PCA score plot of the three trials for each nucleotide phosphate samples.

In 2006, Anslyn and coworkers [51] reported an enantioselective differential array for amino acid on the basic of indicator displacement assays (IDAs). The differential sensor array consisted of three optical sensors and three chromophores. In the IDAs, the Cu(II) complexes of bidentate N-donor ligands **S17-S19** refered to receptors. The catechol and salicylate-derived chromophores including pyrocatechol violet (**PCV**), chromoxane cyanin R (**CCR**), and chrome azurole S (**CAS**) acted as indicators. Based on the IDAs results, the chemoselectivity is reported in the order of Trp > Phe > Leu ~Val > Tle. The PCA score plot illustrated a good differentiation of each amino acid. The key factor along PC1 is a structure of amino acid in term of aliphatic and aromatic amino acids. The aliphatic amino acids appeared in positive score, while the aromatic amino acids demonstrated in negative area. The PC2 predominate the chiral information, with negative scores for D amino acids and positive scores for L amino acids. (Figure 2.15)

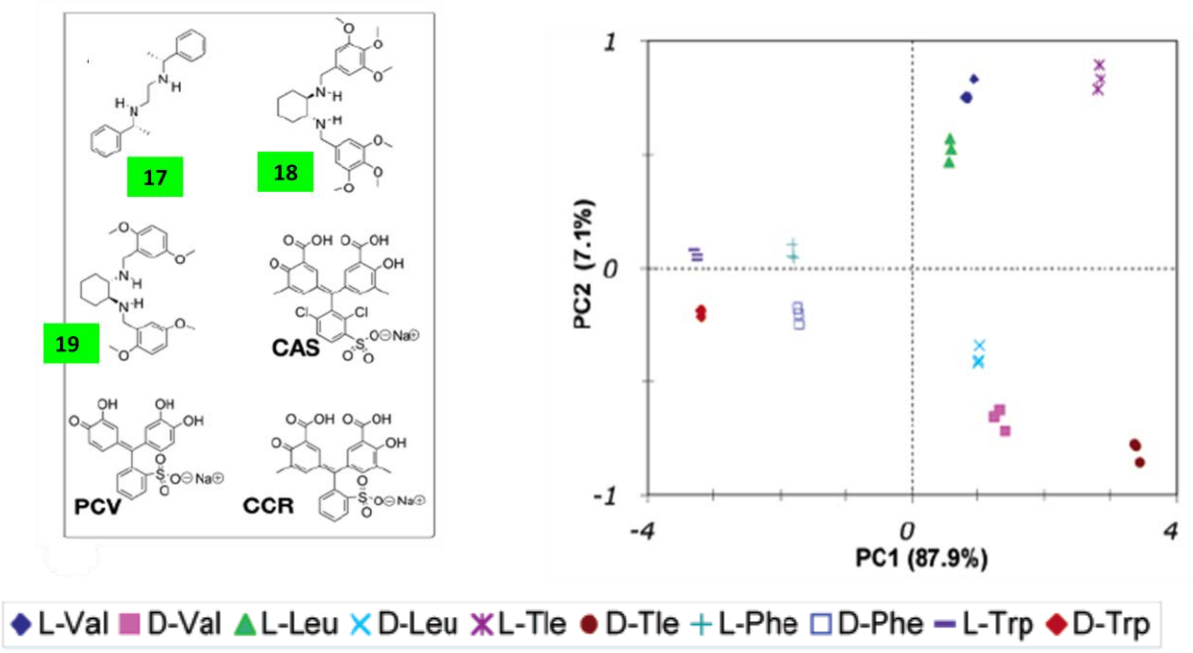

(A) (B)

Figure 2.15 (A) Ligands and indicators used to construct sensor array (B) two-dimensional PCA plots for D and L amino acids prepared from data for all 21 enantioselective indicator displacement assays (IDAs).

In 2008, Singaram and coworkers [52] reported a powerful sensor array, which was able to discriminate biological analytes in aqueous solution at neutral pH. The sensor array comprised of three cationic bis-boronic acids (BBV) receptors and anionic 8-hydroxypyrene-1,3,6-trisulfonic acid trisodium salt (HPTS) fluorescent dye. The binding of anionic diol-containing analytes to the BBVs receptors exhibited stronger fluorescence signals. It implies that this mechanism resulted from a synergistic displacement effect. The recognition pattern was determined by a concentration dependent analysis to present variance. The combination of K_b and F_{max}/F_0 values with three receptors showed a good discrimination at 4.0 x 10^{-3} M as a discrimination limit. (Figure 2.16)

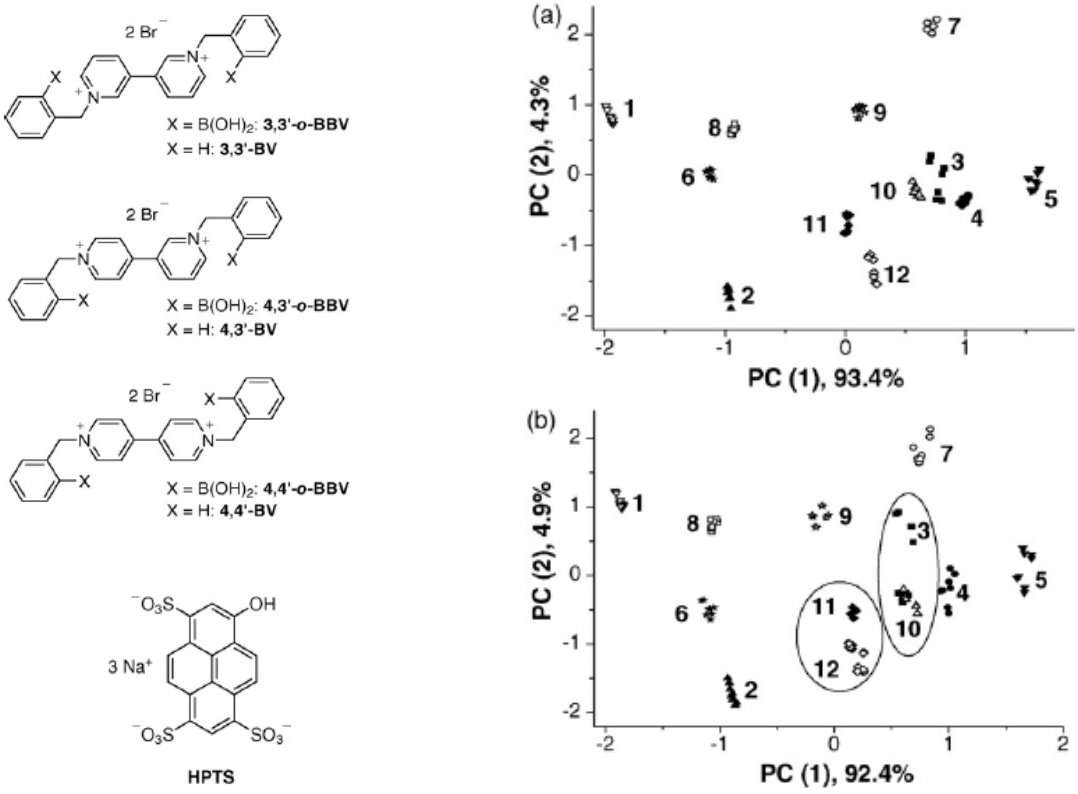

(A) (B)

Figure 2.16 (A) Ligands and indicators used to construct sensor array (B) two-dimensional PCA plots for the identification of phospho sugars and nucleotides at two analyte concentrations (top a) 4.0×10^{-3}M discrimination limit, (bottom b) 2.0×10^{-3} M glucose-1-phosphate (1), glucose-6-phosphate (2), fructose-6-phosphate (3), fructose-1,6-diphosphate (4), ribose-5-phosphate (5) glucose (6), fructose (7), ribose (8), AMP (9), ADP (10), ATP(11), GTP (12).

In 2009, Anslyn and coworkers [53] reported a single squaraine (**SQ**) as both the receptor and the indicator for sensor array. The aim of this experiment was to verify a potential of squaraine sensor for discrimination of various metals and thiols. The combination of **SQ** with five thiols (**PT**, **ACM**, **DMP**, **NT**, **MPA**) could be used to differentiate five metal ions. The combining **SQ** with **ACM** provide a good

discrimination of all five metals. On the contrary, the incorporation of **SQ** with five metals (Hg^{2+}, Pd^{2+}, Cu^{2+}, Fe^{2+}, Ni^{2+}) clearly separated **ACM** and **DMP** from the other thiols. However, this system could be used a single receptor/indicator as a chemometric tool. (Figure 2.17)

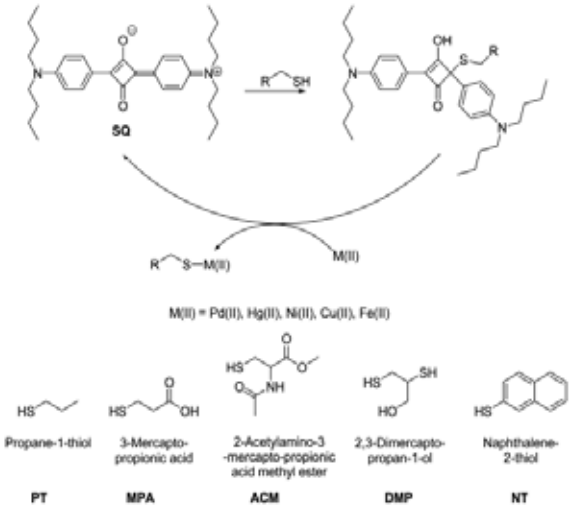

(A)

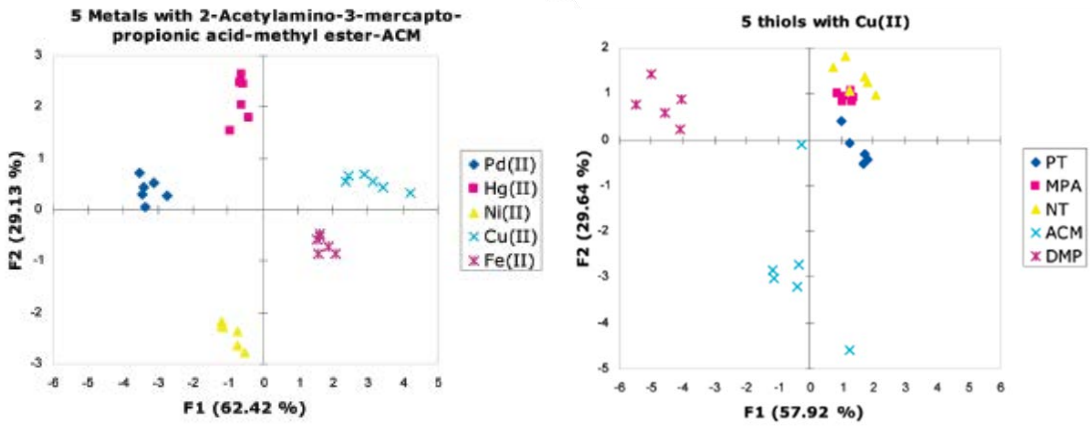

(B)

Figure 2.17 (A) **SQ** and five thiols used to construct sensor array (B) two-dimensional PCA plots (top) pattern-based recognition of five metals with 2-acetylamino- 3-mercaptopropionic acid methyl ester (**ACM**) (bottom) Discrimination of thiols with Cu(II).

In 2010, Suslick and coworkers [54] reported a simple and highly sensitive colorimetic sensor for detection explosive vapor of Triacetone triperoxide (TATP). The TATP vapor was detected by using a solid acid catalyst to pretreat a gas stream. PCA approach was utilized to measure the array response at different concentration of TATP vapor. The result demonstrated a two dimensional of PCA score plot and showed a clear separation of many oxidants at low concentration. Remarkably, the PCA score plot demonstrated that this array could also distinct the TATP from other chemical oxidants. Furthermore, Euclidean distance plot versus increasing TATP vapor concentration performed the linear range from 50 ppb to 10 ppm and gave the low detection of limit of 2 ppb. (Figure 2.18)

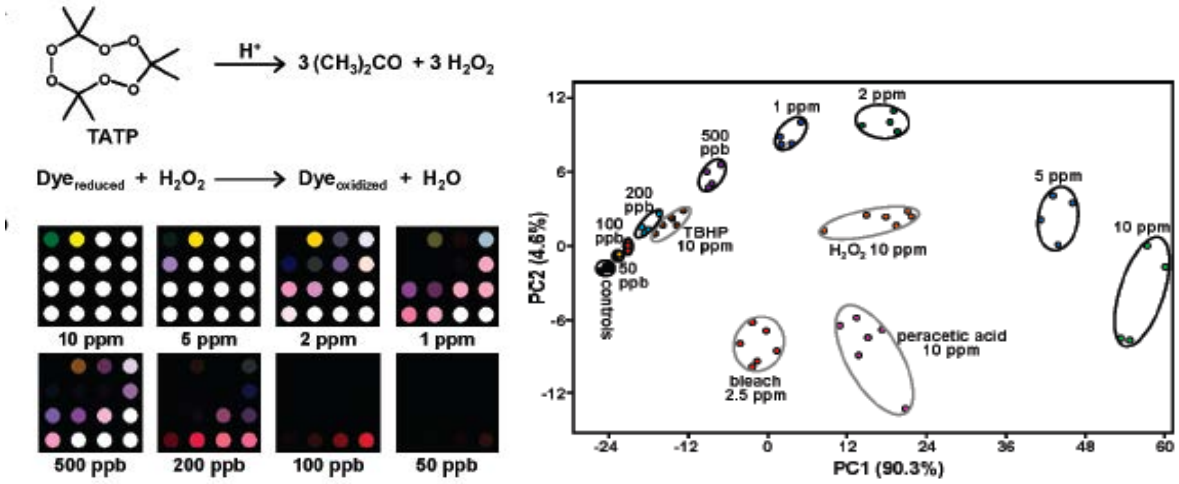

(A) (B)

Figure 2.18 (A) Acid catalyzed decomposition of TATP and color difference maps of TATP vapor (B) two-dimensional PCA plots at different concentrations of TATP vapor and other peroxides.

2.2 Objective and the scope of this research

The objective of this research is to synthesize BF_2-curcumin and pyrene derivatives containing dipicolyl amine (dpa) groups (**L1** and **L2)** as molecular sensor for nucleotides. Complexation studies of ligand **L1** with transition metal ions; such as, Zn^{2+} and Cu^{2+}, are explored by means of absorption and fluorescence titration. To determine the binding affinity of ligand toward various nucleotides, the complexation study of **L2•Zn** with various nucleotides is examined by fluorescence technique. Furthermore, the effect of solvent system to the binding abilities of **L2•Zn** is investigated by Principal Component Analysis (PCA) method. The target molecules were shown in Figure 2.19. The results of this research allow us to understand the relationship between the strength interactions of host and guests. Moreover, the utility of this approach for ATP hydrolysis is applicable. The quantitative identification of the product of reaction (PPi) and the reactant (ATP) can be determined based on ratiometric information.

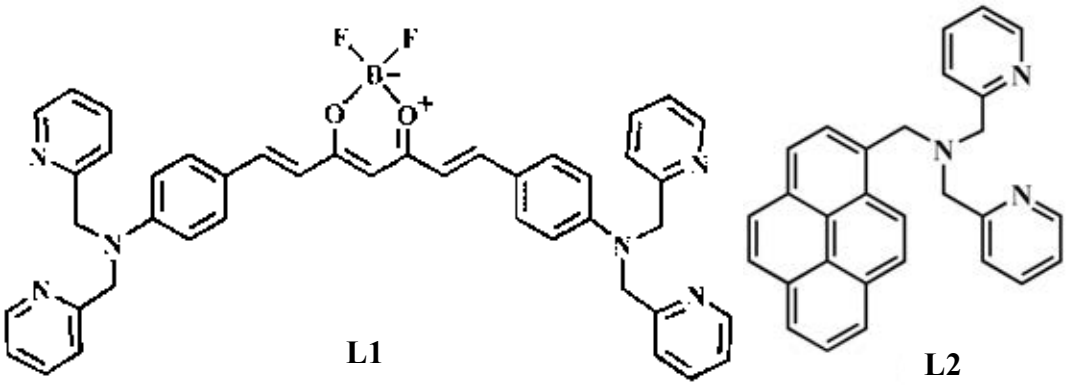

Figure 2.19 The molecular sensors **L1** and **L2**

CHAPTER III

EXPERIMENTAL SECTION

3.1 General procedures

3.1.1 Analytical instrument

Nuclear magnetic resonance (NMR) spectra were recorded on a Varian Mercury Plus 400 NMR spectrometer, ^{13}C-NMR (100 MHz), COSY, HMBC, HMQC spectra were recorded with a Ultrashield^{TM} Plus 400 NMR spectrometer. 2D NOESY spectrum was recorded on a Varian INOVA 500 NMR spectrophotometer. The samples were dissolved in $CDCl_3$, DMSO-d_6, acetonitrile-d_3, and D_2O. The chemical shifts were recorded in part per million (ppm) using a residue proton solvents as internal reference. MALDI-TOF mass spectra were recorded on Bruker Daltonic using doubly recrystallized 2-cyano-4-hydroxy cinnamic acid (CCA) as matrix. ESI-HRS mass spectra were record on Bruker microTOF-QII.

Absorption spectra were measured by a Varian Cary 50 UV-Vis spectrophotometer. Fluorescence spectra were performed on Varian Cary Eclipse spectrofluorometer by personal computer data processing unit. The light source is a pulsed xenon lamp and a detector is a photomultiplier tube. IR spectrum of the sample was recorded on a Nicolet Impact 410 FTIR spectrophotometer at room temperature with the potassium bromide (KBr) disk method. The sample was scanned over a range of 500-4000 cm^{-1} at resolution of 16 cm^{-1} and the number of scan was 32. The measurement was controlled by Omnic software.

3.1.2 Materials

Unless otherwise specified, the solvent and all materials were reagent grades purchased from Fluka, Aldrich, Carlo erba, Merk or Lab scan and used without further purification. Commercial grade solvents such as acetone, dichloromethane,

hexane, methanol and ethyl acetate were purified by distillation before used. Acetonitrile, dimethylformamide and dichloromethane for set up the reaction were dried over calcium hydride and freshly distilled under nitrogen atmosphere prior to use.

Column chromatography was carried out on silica gel (Kieselgel 60, 0.063-0.200 mm, Merk). Thin layer chromatography (TLC) was performed on silica gel plates (Kieselgel 60, F_{254}, 1 mm, Compounds on TLC plates were detected by the UV-light. Acetonitrile spectroscopy grade for fluorescence measurement were obtained from Merk.

All synthesized compounds were characterized by ^{1}H-NMR spectroscopy, mass spectrometry and IR spectroscopy.

3.2 Synthesis

3.2.1 Preparation of BF_2-1,3 pentanedione (1)

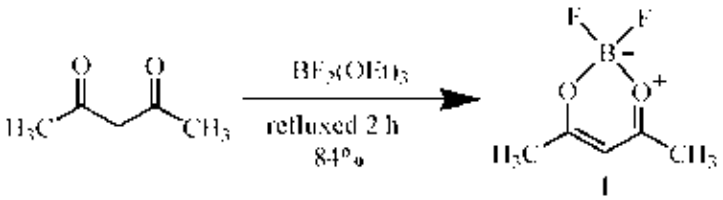

1

In a 25 mL round bottom flask equipped with a magnetic bar, acetylacetone (0.20 g, 2 mmol) and difluoroboron ether (0.43 g, 3 mmol) were refluxed under nitrogen atmosphere for 2 h. The reaction mixture was removed to dryness under the reduced pressure. The product yielded as a yellow solid (0.25 g, 85%).

Characterization data for 1

^{1}H-NMR spectrum (400 MHz, $CDCl_3$): δ (in ppm)

δ 5.99 (s, 1H, C=C*H*), 2.29 (s, 6H, CH_3)

3.2.2 Preparation of Aniline bis(2,2′ dipicolylamine)(2)

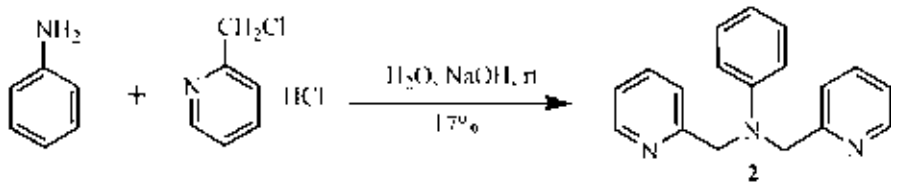

In a 50 mL two-neck round bottom flask equipped with a magnetic bar, a solution of aniline (0.50 g, 5 mmol), sodium hydroxide (05.0 g, 13 mmol) and catalytic amount of tetrabutylammonium iodide in H_2O (10 mL) were stirred under N_2 atmosphere for 1 h. 2-Chloromethylpyridine (159. g, 11 mmol) in H_2O was added into the reaction mixture and the reaction was stirred vigorously for 24 h at room temperature. The mixture was extracted with CH_2Cl_2 and washed with H_2O. The organic layer was dried over Na_2SO_4, and the organic solvent was removed to dryness under the reduced pressure. The resulting solid was purified by column chromatography on silica gel using a gradient of ethyl acetate (20-80%) in dichloromethane as eluent to afford a white solid **2** (0.25 g, 17%).

Characterization data for 2

^{1}H-NMR spectrum (400 MHz, $CDCl_3$): δ (in ppm)

δ 8.59 (d, *J* = 4.4 Hz, 2H, Ar*H*), 7.63 (t, *J* = 8.0 Hz, 2H, Ar*H*), 7.28 (m, 4H, Ar*H*), 7.18 (m, 4H, Ar*H*), 6.71 (m, 3H, Ar*H*), 4.83 (s, 4H, NC*H*$_2$)

3.2.3 Preparation of 4-bis(2,2' dipicolylamine) formaldehyde (3)

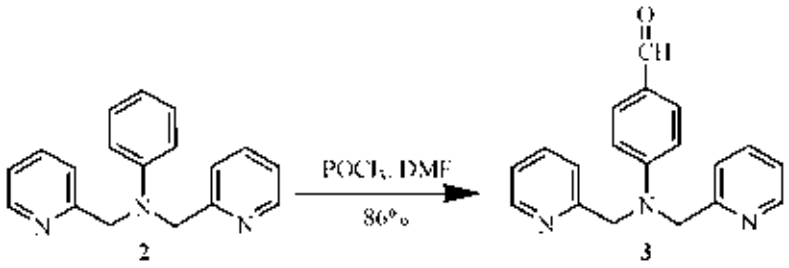

In a 25 mL two-neck round bottom flask equipped with a magnetic bar, $POCl_3$ (0.27 mL, 3 mmol) was added into the solution of DMF (0.34 mL, 2 mmol) in portions in 0.5 h and cooled in an ice bath. The mixture was stirred for 0.5 h. Then compound **2** (0.20 g, 0.7 mmol) in 1 mL of DMF was added in portions in 20 min. The reaction mixture was heated at 90 ºC under N_2 for 3h. The residue was poured into H_2O (5 mL) and neutralized to pH 6-8 with K_2CO_3 along with stirring. The reaction mixture was extracted with CH_2Cl_2 and the organic layer was dried over Na_2SO_4. After evaporation of the solvent, the desired product was obtained as yellow oil (**3) (**0.19g, 86%)

Characterization data for 3

^{1}H NMR spectrum (400 MHz, $CDCl_3$): δ (in ppm)

δ 9.73 (s, 1H, CO*H*), 8.63 (d, *J* = 4.0 Hz, 2H, Ar*H*), 7.70 (m, 4H, Ar*H*), 7.23 (m, 4H, Ar*H*), 6.80 (d, *J* = 9.2 Hz, 2H, Ar*H*), 4.91(s, 4H, CH_2).

3.2.4 Preparation of BF_2-Curbis(dpa)$_2$ (L1)

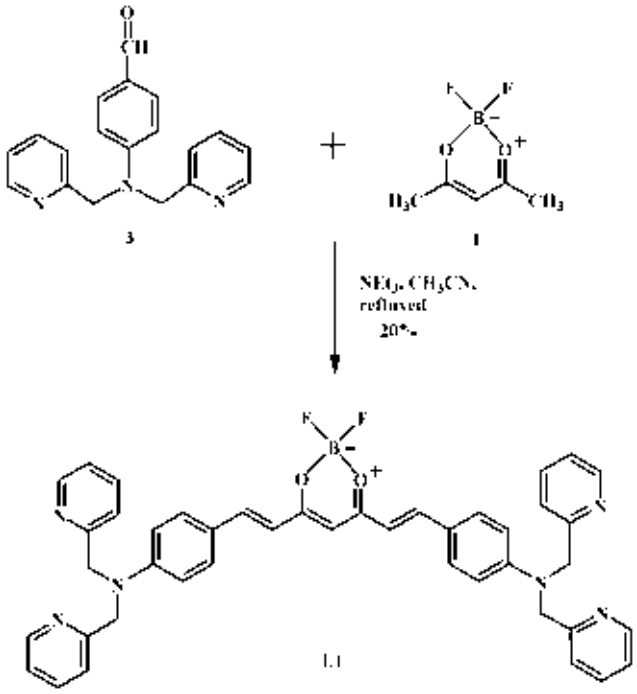

In a 25 mL two-neck round bottom flask equipped with a magnetic bar, compound **1** (0.10 g, 0.67 mmol), triethylamine (0.51 g, 1.68 mmol) and 1 mL acetonitrile were stirred for 1 h under N_2 atmosphere. Then yellow oil **3** (1.59 g, 11 mmol) in 2 mL acetonitrile was added into the reaction mixture. The reaction was heated at 60 ºC for 3 days. The mixture was extracted with CH_2Cl_2 and washed with H_2O. The organic layer was dried over Na_2SO_4. The residue was evaporated and purified by column chromatography on a silica gel with a mixture of 10% methanol in ethyl acetate to obtain a dark purple film. The desired product was purified by precipitation with CH_2Cl_2 and hexane to give solid dark purple (0.01 g, 20%).

Characterization data for L1

^{1}H NMR spectrum (400 MHz, $CDCl_3$) : δ (in ppm)

δ 8.54 (s, *J* = 4.4 Hz, 4H, Ar*H*), 7.58 (t, *J* = 7.6 Hz, 4H, Ar*H*), 7.31 (d, *J* = 8 Hz, 4H, Ar*H*), 7.19 (m, 13H, Ar*H*), 6.71 (m, 4H, Ar*H*), 6.64 (d, *J* = 7.6 Hz, 4H, Ar*H*), 4.80 (s, 8H, CH_2).

HRMS (ESI) mass: calcd for $C_{43}H_{37}BF_2N_6O_2$ m/z [M+H$^+$] 719.3039, found 719.3061

3.2.5 Preparation of BF_2-Curbis(dpa)$_2$⊂2Zn (L1•2Zn)

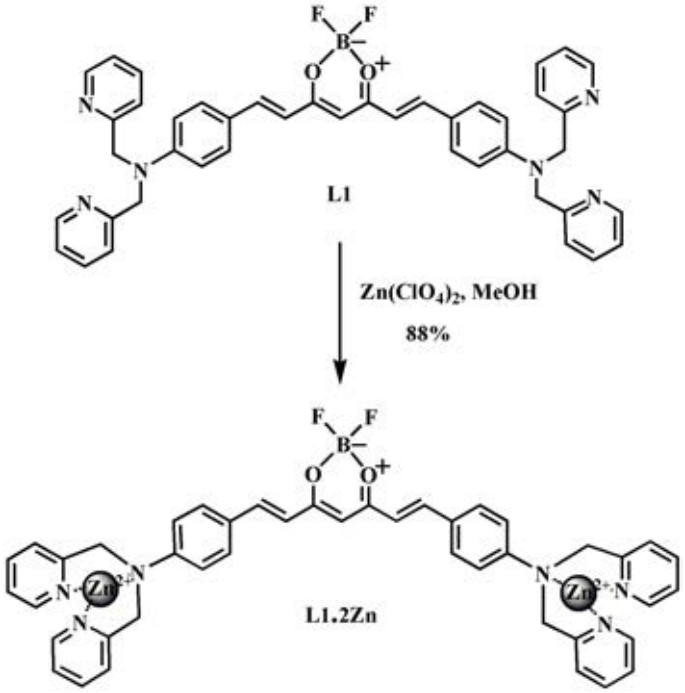

In a 25 mL two-neck round bottom flask equipped with a magnetic bar, a solution of $Zn(ClO_4)_2$ (5.30 mg, 0.0074 mmol) in 2 mL MeOH was added dropwise into a solution of **L1** (5.60 mg, 0.015 mmol) in 5 mL MeOH. After stirring overnight at room temperature, the precipitate was filtered and washed with MeOH to give **L1•2Zn** as an orange powder (0.0050 mg, 88%).

Characterization data for L1•2Zn

^{1}H NMR spectrum (400 MHz, CD_3CN): δ (in ppm)

δ 8.86 (m, 2H), 8.66 (m, 2H), 8.29 (s, 2H), 8.17 (s, 2H), 7.82-7.52 (m, 15H), 7.22 (s, 1H), 7.05 (s, 2H), 6.73 (m, 2H), 6.59(m, 1H), 4.94 (d, *J* = 16 Hz, 4H), 4.50 (d, *J* = 16.8 Hz, 4H).

3.2.6 Preparation of Pyrene-Dpa (L2)

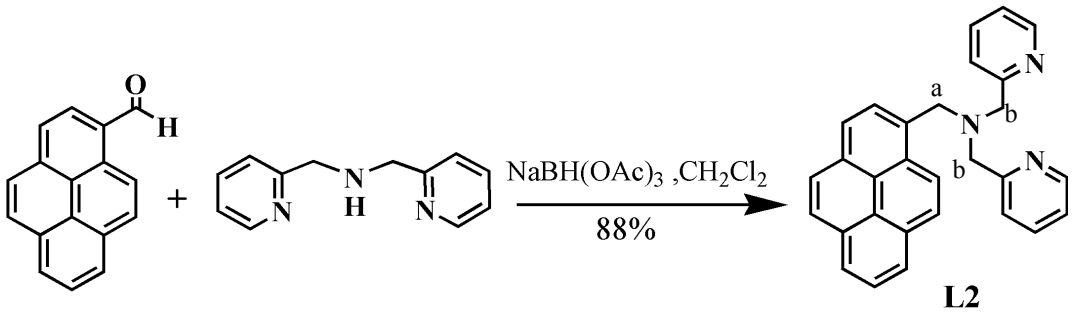

In a 25 mL two-neck round bottom flask equipped with a magnetic bar, sodium tris(acetoxy)borohydride (0.28 g, 1.32 mmol), pyrenecarboxaldehyde (0.23 g, 1 mmol) and dipicolylamine (0.20 g, 1 mmol) in 10 mL CH_2Cl_2 were stirred under N_2 atmosphere at room temperature for 5 h. The reaction mixture was neutralized with sodium hydrogen carbonate and extracted with CH_2Cl_2 and then the solvent was evaporated under vacuum. The residue was purified by column chromatography on silica gel with 5 % MeOH in dichloromethane as eluent to afford a yellow oil which ultimately solidifies when dry (0.36 g, 88%).

Characterization data for L2

^{1}H NMR spectrum (400 MHz, d_6-DMSO): δ (in ppm)

δ 8.50 (d, *J* = 4.0 Hz, 2H, Ar*H*), 8.37 (d, *J* = 8.8 Hz, 1H, Ar*H*), 8.27 (s, 1H, Ar*H*), 8.25-8.01 (m, 7H, Ar*H*), 7.70 (t, *J* = 7.8 Hz, 2H, Ar*H*), 7.48 (d, *J* = 8.0 Hz, 2H, Ar*H*), 7.21 (t, *J* = 10.0 Hz, 2H, Ar*H*), 4.35 (s, 2H, NCH_{2a}), 3.81 (s, 4H, NCH_{2b}).

HRMS (ESI) mass: calcd for $C_{29}H_{23}N_3$ m/z $[M+H]^+$ 414.2048, found 414.2022.

3.2.7 Preparation of Pyrene-Dpa⊂Zn (L2•Zn)

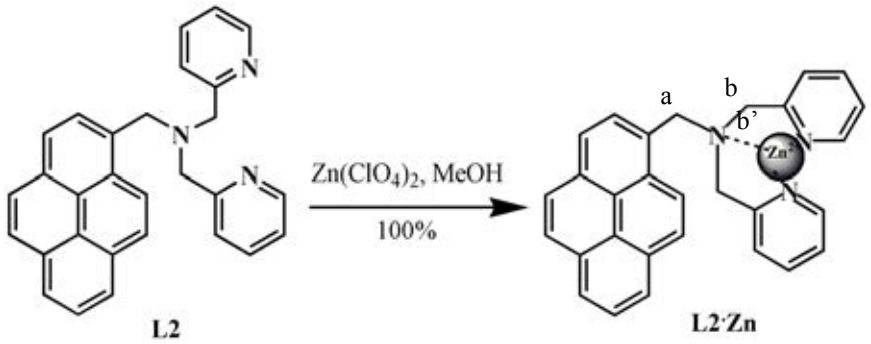

In a 25 mL two-neck round bottom flask equipped with a magnetic bar, a solution of $Zn(ClO_4)_2$ in 5 mL MeOH (0.171 g, 0.47 mmol) was added dropwise into a solution of **L2** (0.112 g, 0.27 mmol) in 5 mL MeOH. Upon stirring overnight at room temperature, the precipitate was filtered and washed with MeOH to give **L2•Zn** (0.21 g, 100%) as a light yellow powder.

Characterization data for L2•Zn

^{1}H NMR spectrum (400 MHz, d_6-DMSO): δ (in ppm)

δ 8.71 (s, 2H, Ar*H*), 8.42 (s, 1H, Ar*H*), 8.37-8.13 (m, 9H, Ar*H*), 7.94 (s, 1H, Ar*H*), 7.68 (s, 2H, Ar*H*), 7.56 (d, *J* = 6.4 Hz, 2H, Ar*H*), 4.55 (s, 2H, NCH_{2a}), 4.35 (d, *J* = 15.2 Hz, 2H, NCH_{2b}), 3.69 (d, *J* = 15.6 Hz, 2H, NC$H_{2b'}$).

HRMS (ESI) mass: calcd for $C_{29}H_{23}N_3Cl_3O_{12}Zn$ m/z $[M+(ClO_4)_3]^-$ 773.9639, found 773.9829.

3.3 Complexation studies of ligand L1

3.3.1 Complexation studies of ligand L1 with zinc perchlorate by ^{1}H-NMR titrations

Typically, a solution of 3.00 x 10^{-3} M of a ligand **L1** (0.00090 g, 1.25 x 10^{-6} mol) in CD_3CN (0.4 mL) was prepared in NMR tube. A solution of 2.40 x 10^{-2} M of Zn^{2+} ion as zinc perchloratehexahydrate in CD_3CN (0.50 mL) was prepared in a vial and added directly to the NMR tube by a microsyringe to have guest:host ratios shown in Table 3.1. ^{1}H-NMR spectra were recorded after each addition.

Table 3.1 Amounts of solutions of Zn^{2+} ion used to prepare various zinc:ligand **L1** ratios

Ratio of Zn^{2+} : ligand	Volume Zn^{2+}	[ligand **L1**] M	[Zn^{2+}] M
0.00 : 1.00	0.00	3.00 x 10^{-3}	0
0.10 : 1.00	5.00	2.96 x 10^{-4}	2.96 x 10^{-4}
0.20 : 1.00	5.00	2.92 x 10^{-4}	5.85 x 10^{-4}
0.30 : 1.00	5.00	2.89 x 10^{-4}	8.67 x 10^{-4}
0.40 : 1.00	5.00	2.86 x 10^{-4}	1.14 x 10^{-3}
0.50 : 1.00	5.00	2.82 x 10^{-4}	1.41 x 10^{-4}
0.60 : 1.00	5.00	2.79 x 10^{-4}	1.67 x 10^{-4}
0.70 : 1.00	5.00	2.76 x 10^{-4}	1.93 x 10^{-4}
0.80 : 1.00	5.00	2.72 x 10^{-4}	2.18 x 10^{-4}
0.90 : 1.00	5.00	2.70 x 10^{-4}	2.43 x 10^{-4}
1.00 : 1.00	5.00	2.66 x 10^{-4}	2.67 x 10^{-4}
1.20 : 1.00	10.00	2.60 x 10^{-4}	3.13 x 10^{-3}
1.40 : 1.00	10.00	2.55 x 10^{-4}	3.57 x 10^{-3}
1.60 : 1.00	10.00	2.50 x 10^{-4}	4.00 x 10^{-3}
1.80 : 1.00	10.00	2.45 x 10^{-4}	4.41 x 10^{-3}
2.00 : 1.00	10.00	2.40 x 10^{-4}	4.80 x 10^{-3}
2.50 : 1.00	25.00	2.28 x 10^{-4}	5.71 x 10^{-3}
3.00 : 1.00	25.00	2.18 x 10^{-4}	6.54 x 10^{-3}
3.50 : 1.00	25.00	2.09 x 10^{-4}	7.38 x 10^{-3}
4.00 : 1.00	25.00	2.00 x 10^{-4}	8.00 x 10^{-3}
5.00 : 1.00	25.00	1.84 x 10^{-4}	9.20 x 10^{-3}

3.3.2 Complexation studies of ligand L1 by UV-vis titrations

3.3.2.1 Complexation studies of Ligand L1 with Zn^{2+} and Cu^{2+} ion

Typically, a solution of 1.8 x 10^{-5} M of a ligand **L1** in dried acetonitrile was prepared. A solution of 3.6 x 10^{-4} M of zinc trifluoromethane sulfonate and 1.0 x 10^{-3} M copper nitrate in dried acetonitrile was prepared in a 10 mL volumetric flask.

Absorption spectra of ligand **L1** and cation complexes were recorded from 200-700 nm at ambient temperature. The solution of cation was added directly to 2.00 mL of 1.8 x 10^{-5} M ligand **L1** in a 1-cm quartz cuvette by micropipette and stirred for 1 minute. Absorption spectra were measured after each addition. Table 3.2 and 3.3 shows a concentration of cation in titration experiments.

Table 3.2 The concentration of Zn^{2+} ion was used in cation complexation studies with ligand **L1** and the final ratios of guest:host

Point	Zn^{2+}/**L1**	[**L1**] mM	[Zn^{2+}] mM	V of Zn^{2+} (mL)	V total (mL)
1	0.00	0.018	0	0	2
2	0.10	0.01791	0.00179	0.01	2.01
3	0.20	0.01782	0.00356	0.02	2.02
4	0.30	0.01773	0.00532	0.03	2.03
5	0.40	0.01765	0.00706	0.04	2.04
6	0.50	0.01756	0.00878	0.05	2.05
7	0.60	0.01748	0.01049	0.06	2.06
8	0.70	0.01739	0.01217	0.07	2.07
9	0.80	0.01731	0.01385	0.08	2.08
10	0.90	0.01722	0.0155	0.09	2.09
11	1.00	0.01714	0.01714	0.1	2.1
12	1.20	0.01698	0.02038	0.12	2.12
13	1.40	0.01682	0.02355	0.14	2.14
14	1.60	0.01667	0.02667	0.16	2.16
15	1.80	0.01651	0.02972	0.18	2.18
16	2.00	0.01636	0.03273	0.2	2.2
17	2.50	0.016	0.04	0.25	2.25
18	3.00	0.01565	0.04696	0.3	2.3
19	3.50	0.01532	0.05362	0.35	2.35
20	4.00	0.015	0.06	0.4	2.4
21	4.50	0.01469	0.06612	0.45	2.45
22	5.00	0.0144	0.072	0.5	2.5

Point	Zn^{2+}/**L1**	[**L1**] mM	[Zn^{2+}] mM	V of Zn^{2+} (mL)	V total (mL)
23	6.00	0.01385	0.08308	0.6	2.6
24	7.00	0.01333	0.09333	0.7	2.7
25	8.00	0.01286	0.10286	0.8	2.8
26	9.00	0.01241	0.11172	0.9	2.9
27	10.00	0.012	0.12	1	3
28	12.00	0.01125	0.135	1.2	3.2
29	14.00	0.01059	0.14824	1.4	3.4
30	16.00	0.01	0.16	1.6	3.6
31	18.00	0.00947	0.17053	1.8	3.8
32	20.00	0.009	0.18	2	4

Table 3.3 The concentration of Cu^{2+} ion was used in cation complexation studies with ligand **L1** and the final ratios of guest:host

Point	Cu^{2+}/**L1**	[**L1**] mM	[Cu^{2+}] mM	V of Cu^{2+} (mL)	V total (mL)
1	0.00	0.02	0	0	2
2	0.05	0.01998	0.001	0.002	2.002
3	0.10	0.01996	0.002	0.004	2.004
4	0.15	0.01994	0.00299	0.006	2.006
5	0.20	0.01992	0.00398	0.008	2.008
6	0.25	0.0199	0.00498	0.01	2.01
7	0.30	0.01988	0.00596	0.012	2.012
8	0.35	0.01986	0.00695	0.014	2.014
9	0.40	0.01984	0.00794	0.016	2.016
10	0.45	0.01982	0.00892	0.018	2.018
11	0.50	0.0198	0.0099	0.02	2.02
12	0.60	0.01976	0.01186	0.024	2.024
13	0.70	0.01972	0.01381	0.028	2.028
14	0.80	0.01969	0.01575	0.032	2.032
15	0.90	0.01965	0.01768	0.036	2.036
16	1.00	0.01961	0.01961	0.04	2.04
17	1.20	0.01953	0.02344	0.048	2.048
18	1.40	0.01946	0.02724	0.056	2.056
19	1.60	0.01938	0.03101	0.064	2.064
20	1.80	0.01931	0.03475	0.072	2.072
21	2.00	0.01923	0.03846	0.08	2.08
22	3.00	0.01887	0.0566	0.12	2.12
23	4.00	0.01852	0.07407	0.16	2.16
24	5.00	0.01818	0.09091	0.2	2.2
25	6.00	0.01786	0.10714	0.24	2.24
26	7.00	0.01754	0.12281	0.28	2.28

3.3.3 Complexation studies of ligand L1 by fluorescent titrations

3.3.3.1 Complexation studies of ligand L1 with Cu^{2+} and Zn^{2+} ion

Typically, a solution of $5.00x10^{-6}$ M of a ligand **L1** in dried acetonitrile was prepared by adding 50 μL of a stock solution of ligand **L1** ($1x10^{-3}$ M) in a 10 mL volumetric flask. A solution of $2.00x10^{-4}$ M of zinc perchlorate hexahydrate and copper nitrate in dried acetonitrile was prepared in a 10 mL volumetric flask.

Fluorescent spectra of ligand **L1** and cation complexes were recorded from 500-800 nm at ambient temperature. The solution of cation was added directly to 2.00 mL of $5.00x10^{-6}$ M ligand **L1** in a 1-cm quartz cuvette by micropipette and stirred for 1 minute. Fluorescent spectra were measured after each addition. Table 3.4 and 3.5 shows a concentration of cation in titration experiments, under the following condition.

Condition for fluorescence spectrophotometry

Excitation wavelength: 488 nm

Slit width of excitation and emission: 5, 5

Smoothing factor: 20

Scan rate and the PMT voltage: medium (600)

Table 3.4 The concentration of Zn^{2+} ion was used in cation complexation studies with ligand **L1** and the final ratios of guest:host

Point	Zn^{2+}/**L1**	[**L1**] mM	[Zn^{2+}] mM	V of Zn^{2+} (mL)	V total (mL)
1	0.00	0.005000	0	0	2
2	0.02	0.004998	0.0001	0.001	2.001
3	0.04	0.004995	0.0002	0.002	2.002
4	0.06	0.004993	0.0003	0.003	2.003
5	0.08	0.004990	0.0004	0.004	2.004
6	0.10	0.004988	0.0005	0.005	2.005
7	0.12	0.004985	0.0006	0.006	2.006
8	0.14	0.004983	0.0007	0.007	2.007
9	0.16	0.004980	0.0008	0.008	2.008
10	0.18	0.004978	0.0009	0.009	2.009

Point	Zn^{2+}/**L1**	[**L1**] mM	[Zn^{2+}] mM	V of Zn^{2+} (mL)	V total (mL)
11	0.20	0.004975	0.001	0.01	2.01
12	0.24	0.004970	0.00119	0.012	2.012
13	0.28	0.004965	0.00139	0.014	2.014
14	0.32	0.004960	0.00159	0.016	2.016
15	0.36	0.004955	0.00178	0.018	2.018
16	0.40	0.004950	0.00198	0.02	2.02
17	0.44	0.004946	0.00218	0.022	2.022
18	0.50	0.004938	0.00247	0.025	2.025
19	0.60	0.004926	0.00296	0.03	2.03
20	0.70	0.004914	0.00344	0.035	2.035
21	0.80	0.004902	0.00392	0.04	2.04
22	0.90	0.004890	0.0044	0.045	2.045
23	1.00	0.004878	0.00488	0.05	2.05
24	1.10	0.004866	0.00535	0.055	2.055
25	1.20	0.004854	0.00583	0.06	2.06
26	1.30	0.004843	0.0063	0.065	2.065
27	1.40	0.004831	0.00676	0.07	2.07
28	1.50	0.004819	0.00723	0.075	2.075
29	1.60	0.004808	0.00769	0.08	2.08
30	1.70	0.004796	0.00815	0.085	2.085
31	1.80	0.004785	0.00861	0.09	2.09
32	1.90	0.004773	0.00907	0.095	2.095
33	2.00	0.004762	0.00952	0.1	2.1
34	2.10	0.004751	0.00998	0.105	2.105
35	2.20	0.004739	0.01043	0.11	2.11
36	2.30	0.004728	0.01087	0.115	2.115
37	2.40	0.004717	0.01132	0.12	2.12
38	2.50	0.004706	0.01176	0.125	2.125
39	2.66	0.004688	0.01247	0.133	2.133
40	2.86	0.004666	0.01335	0.143	2.143
41	3.06	0.004645	0.01421	0.153	2.153
42	3.26	0.004623	0.01507	0.163	2.163
43	3.46	0.004602	0.01592	0.173	2.173
44	3.66	0.004581	0.01677	0.183	2.183
45	4.06	0.004539	0.01843	0.203	2.203
46	4.46	0.004498	0.02006	0.223	2.223
47	4.86	0.004458	0.02167	0.243	2.243
48	5.46	0.004399	0.02402	0.273	2.273
49	6.06	0.004342	0.02631	0.303	2.303
50	7.06	0.004250	0.03	0.353	2.353
51	8.06	0.004161	0.03354	0.403	2.403
52	9.06	0.004077	0.03693	0.453	2.453

Point	Zn^{2+}/**L1**	[**L1**] mM	[Zn^{2+}] mM	V of Zn^{2+} (mL)	V total (mL)
53	11.06	0.003917	0.04332	0.553	2.553
54	13.06	0.003769	0.04923	0.653	2.653
55	17.06	0.003505	0.0598	0.853	2.853
56	23.06	0.003172	0.07314	1.153	3.153
57	29.06	0.002896	0.08416	1.453	3.453

Table 3.5 The concentration of Cu^{2+} ion was used in cation complexation studies with ligand **L1** and the final ratios of guest:host

Point	Cu^{2+} /**L1**	[**L**1] mM	[Cu^{2+}] mM	V of Cu^{2+} (mL)	V total (mL)
1	0.00	0.005	0.00000	0	2
2	0.04	0.005	0.00020	0.002	2.002
3	0.08	0.00499	0.00040	0.004	2.004
4	0.12	0.00499	0.00060	0.006	2.006
5	0.16	0.00498	0.00080	0.008	2.008
6	0.20	0.00498	0.00100	0.01	2.01
7	0.24	0.00497	0.00119	0.012	2.012
8	0.28	0.00497	0.00139	0.014	2.014
9	0.32	0.00496	0.00159	0.016	2.016
10	0.36	0.00496	0.00178	0.018	2.018
11	0.40	0.00495	0.00198	0.02	2.02
12	0.44	0.00495	0.00218	0.022	2.022
13	0.48	0.00494	0.00237	0.024	2.024
14	0.52	0.00494	0.00257	0.026	2.026
15	0.56	0.00493	0.00276	0.028	2.028
16	0.60	0.00493	0.00296	0.03	2.03
17	0.70	0.00491	0.00344	0.035	2.035
18	0.80	0.0049	0.00392	0.04	2.04
19	0.90	0.00489	0.00440	0.045	2.045
20	1.00	0.00488	0.00488	0.05	2.05
21	1.20	0.00485	0.00583	0.06	2.06
22	1.40	0.00483	0.00676	0.07	2.07
23	1.60	0.00481	0.00769	0.08	2.08
24	1.80	0.00478	0.00861	0.09	2.09
25	2.00	0.00476	0.00952	0.1	2.1
26	2.20	0.00474	0.01043	0.11	2.11
27	2.40	0.00472	0.01132	0.12	2.12
28	2.60	0.00469	0.01221	0.13	2.13
29	2.80	0.00467	0.01308	0.14	2.14

Point	Cu^{2+} /**L1**	[**L**1] mM	[Cu^{2+}] mM	V of Cu^{2+} (mL)	V total (mL)
28	3.00	0.00465	0.01395	0.15	2.15
29	3.20	0.00463	0.01481	0.16	2.16
30	0.00	0.005	0.00000	0	2
31	0.04	0.005	0.00020	0.002	2.002

3.3.3.2 Determination of the stoichiometry of the L1 with Zn^{2+} and Cu^{2+} complexes by Job's method

Typically, a solution of 5.00 x 10^{-6} M ligand **L1** and cations (Zn^{2+} and Cu^{2+} ion) in acetonitrile were prepared in a 25 mL volumetric flask. Solution of **L1** and cation were pipetted to a 1-cm quartz cuvette to provide the total volume 2 mL according to Table 3.6. Emission spectrum of each addition was measured after stirred 1 min.

Table 3.6 Amounts of solutions of cations (Zn^{2+} and Cu^{2+}) used to prepare various ligand **L1**:M^{2+} ratios

Point	ratio of **L1**:M^{2+}	volume of **L1** (ml)	volume of M^{2+} (ml)
1	1.00:0.00	2.00	0.00
2	0.90:0.10	1.80	0.20
3	0.80:0.20	1.60	0.40
4	0.70:0.30	1.40	0.60
5	0.60:0.40	1.20	0.80
6	0.50:0.50	1.00	1.00
7	0.40:0.60	0.80	1.20
8	0.30:0.70	0.60	1.40
9	0.20:0.80	0.40	1.60
10	0.10:0.90	0.20	1.80
11	0.00:1.00	0.00	2.00

3.3.3.3 Quantum yield studies of Ligand L1 in various solvents:CH_2Cl_2, THF and CH_3CN

Typically, the initial of samples concentration of ligand **L1** showing the absorbance < 0.1 was prepared in dried acetonitrile. Five concentrations of samples were prepared by the dilution of the initial concentration of **L1**. Absorbance and emission intensity of each concentration of **L1** was recorded by UV-vis and fluorescence spectrophotometer, respectively.

3.3.3.4 Anion interference studies

The competitive samples were prepared by the mixture of 5.00×10^{-6} M ligand **L1** and 5.00×10^{-5} M of Zn^{2+} or Cu^{2+} in 2 mL and 100 equiv. of the competitive cations such as Ag^{+}, Cd^{2+}, Co^{2+}, and Ni^{2+}. The solution mixture between ligand **L1** and these cations was stirred for 1 minute. Fluorescent spectra of samples were measured at the excitation of 488 nm. Table 3.7 shows a concentration of cation (Zn^{2+} and Cu^{2+}) in each experiment under the following condition.

Table 3.7 The mole ratio of cations that used in interference studies with ligand **L1**

interference cations	concentration (M)	**L1**:cations	
		L1:Zn^{2+}:M^{2+}	**L1**:Cu^{2+}:M^{2+}
Zn^{2+}	5.00×10^{-5}	-	1:10:100
Cu^{2+}	5.00×10^{-5}	1:10:100	-
Ag^{+}	5.00×10^{-3}	1:10:100	1:10:100
Cd^{2+}	5.00×10^{-3}	1:10:100	1:10:100
Co^{2+}	5.00×10^{-3}	1:10:100	1:10:100
Ni^{2+}	5.00×10^{-3}	1:10:100	1:10:100

3.3.3.5 Determination of detection limit of L1 by Fluorescence spectrophotometry

Typically, a solution of $5.00x10^{-6}$ M of a ligand **L1** in dried acetonitrile was prepared by adding 50 μL of a stock solution of ligand **L1** ($1x10^{-3}$ M) in a 10 mL volumetric flask. Fluorescence spectra of **L1** were measured for 10 times under the following condition.

Condition for fluorescence spectrophotometry

Excitation wavelength: 488 nm

Slit width of excitation and emission: 5, 5

Smoothing factor: 20

Scan rate and the PMT voltage: medium (600)

3.4 Complexation studies of ligand L2•Zn

3.4.1 Complexation studies of ligand L2•Zn in DMSO:HEPES (0.01 M, pH 7.4, 1:99v/v)

3.4.1.1 Complexation studies of ligand L2•Zn with various nucleotides by Fluorescence Spectrophotometry

Typically, a solution of $1.00x10^{-5}$ M **L2•Zn** in DMSO:HEPES (0.01M, pH 7.4, 1:99 v/v) was prepared. All of nucleotide anions (ATP, ADP, AMP, UTP, UDP, UMP, GDP, GMP, CMP and PPi) were prepared in $1.00x10^{-3}$ M in HEPES buffer 0.01M, pH 7.4.

Fluorescence spectra of **L2•Zn** and anion complexes were recorded from 356-600 nm at ambient temperature. The solution of a stock solution of anion (200 μL) was added directly to 2.00 mL of 1.00 x 10^{-5} M ligand **L2•Zn** in a 1-cm quartz cuvette by micropipette and the mixture was stirred for 5 min. Fluorescence spectra of sample were measured. Table 3.8 shows a concentration of analytes in experiments, under the following condition.

Condition for fluorescence spectrophotometry

Excitation wavelength: 346 nm

Slit width of excitation and emission: 5, 5

Smoothing factor: 10

Scan rate and the PMT voltage: 650

Table 3.8 The concentration of nucleotide anions were used in anion complexation studies with ligand **L2•Zn** and the final ratios of guest:host

anion	[anion] M	Final guest:host ratios
ATP	9.09×10^{-5}	10:1
ADP	9.09×10^{-5}	10:1
anion	[anion] M	Final guest:host ratios
AMP	9.09×10^{-5}	10:1
UTP	9.09×10^{-5}	10:1
UDP	9.09×10^{-5}	10:1
UMP	9.09×10^{-5}	10:1
GDP	9.09×10^{-5}	10:1
GMP	9.09×10^{-5}	10:1
CMP	9.09×10^{-5}	10:1
PPi	9.09×10^{-5}	10:1

3.4.1.2 Complexation studies of ligand L2•Zn with various anions: PPi, ATP and ADP by fluorescent titrations

Typically, a solution of 1.00 x 10^{-5} M ligand **L2•Zn** in DMSO:HEPES (0.01M, pH 7.4, 1:99 v/v) was prepared by adding 0.10 mL of a stock solution of ligand **L2•Zn** (1x10^{-3} M) in a 10 mL volumetric flask. A stock solution of 1.00 x 10^{-3} M anion (PPi, ATP and ADP) in HEPES buffer 0.01M, pH 7.4 was prepared in a 5 mL volumetric flask.

Fluorescent spectra of ligand **L2•Zn** and anion complexes were recorded from 356-600 nm at ambient temperature. The solution of an anion was added directly to 2.00 mL of 1.00 x 10^{-5} M ligand **L2•Zn** in a 1-cm quartz cuvette by micropipette and stirred for 5 min. Fluorescent spectra were measured after each addition. Table 3.9, 3.10 and 3.11 shows a concentration of anions in titration experiments.

Table 3.9 The concentration of PPi ion was used in cation complexation studies with ligand **L2•Zn** and the final ratios of guest:host

Point	PPi / **L2•Zn**	[**L2•Zn**] mM	[PPi] mM	V of PPi (mL)	V total (mL)
1	0.00	$1.00x10^{-5}$	0.00	0	2
2	0.10	$9.99x10^{-6}$	$9.99x10^{-7}$	0.002	2.002
3	0.20	$9.98x10^{-6}$	$2.00x10^{-6}$	0.004	2.004
4	0.30	$9.97x10^{-6}$	$2.99x10^{-6}$	0.006	2.006
5	0.40	$9.96x10^{-6}$	$3.98x10^{-6}$	0.008	2.008
6	0.50	$9.95x10^{-6}$	$4.98x10^{-6}$	0.01	2.01
7	0.60	$9.94x10^{-6}$	$5.96x10^{-6}$	0.012	2.012
8	0.70	$9.93x10^{-6}$	$6.95x10^{-6}$	0.014	2.014
9	0.80	$9.92x10^{-6}$	$7.93x10^{-6}$	0.016	2.016
10	1.00	$9.90x10^{-6}$	$9.90x10^{-6}$	0.02	2.02
11	1.20	$9.88x10^{-6}$	$1.19x10^{-5}$	0.024	2.024
12	1.40	$9.86x10^{-6}$	$1.38x10^{-5}$	0.028	2.028
13	1.60	$9.84x10^{-6}$	$1.57x10^{-5}$	0.032	2.032
14	1.80	$9.82x10^{-6}$	$1.77x10^{-5}$	0.036	2.036
15	2.00	$9.80x10^{-6}$	$1.96x10^{-5}$	0.04	2.04
16	3.00	$9.71x10^{-6}$	$2.91x10^{-5}$	0.06	2.06
17	4.00	$9.61x10^{-6}$	$3.85x10^{-5}$	0.08	2.08
18	5.00	$9.52x10^{-6}$	$4.76x10^{-5}$	0.1	2.1

Point	PPi / **L2•Zn**	[**L2•Zn**] mM	[PPi] mM	V of PPi (mL)	V total (mL)
19	6.00	$9.43x10^{-6}$	$5.66x10^{-5}$	0.12	2.12
20	7.00	$9.35x10^{-6}$	$6.54x10^{-5}$	0.14	2.14
21	8.00	$9.26x10^{-6}$	$7.41x10^{-5}$	0.16	2.16
22	9.00	$9.17x10^{-6}$	$8.26x10^{-5}$	0.18	2.18
23	10.00	$9.09x10^{-6}$	$9.09x10^{-5}$	0.2	2.2
24	11.00	$9.01x10^{-6}$	$9.90x10^{-5}$	0.22	2.22
25	13.00	$8.85x10^{-6}$	$1.15x10^{-4}$	0.26	2.26

Table 3.10 The concentration of ATP ion was used in cation complexation studies with ligand **L2•Zn** and the final ratios of guest:host

Point	ATP / **L2•Zn**	[**L2•Zn**] mM	[ATP] mM	V of ATP (mL)	V total (mL)
1	0.00	$1.00x10^{-5}$	0.00	0	2
2	0.05	$9.99x10^{-6}$	$9.99x10^{-7}$	0.01	2.01
3	0.10	$9.98x10^{-6}$	$2.00x10^{-6}$	0.02	2.02
4	0.15	$9.97x10^{-6}$	$2.99x10^{-6}$	0.03	2.03
5	0.20	$9.96x10^{-6}$	$3.98x10^{-6}$	0.04	2.04
6	0.30	$9.95x10^{-6}$	$4.98x10^{-6}$	0.06	2.06
7	0.40	$9.94x10^{-6}$	$5.96x10^{-6}$	0.08	2.08
8	0.50	$9.93x10^{-6}$	$6.95x10^{-6}$	0.1	2.1
9	0.60	$9.92x10^{-6}$	$7.93x10^{-6}$	0.12	2.12
10	0.70	$9.90x10^{-6}$	$9.90x10^{-6}$	0.14	2.14
11	0.80	$9.88x10^{-6}$	$1.19x10^{-5}$	0.16	2.16
12	0.90	$9.86x10^{-6}$	$1.38x10^{-5}$	0.18	2.18
13	1.00	$9.84x10^{-6}$	$1.57x10^{-5}$	0.2	2.2
14	1.20	$9.82x10^{-6}$	$1.77x10^{-5}$	0.24	2.24
15	1.40	$9.80x10^{-6}$	$1.96x10^{-5}$	0.28	2.28
16	1.70	$9.71x10^{-6}$	$2.91x10^{-5}$	0.34	2.34
17	2.00	$9.61x10^{-6}$	$3.85x10^{-5}$	0.4	2.4
18	2.50	$9.52x10^{-6}$	$4.76x10^{-5}$	0.5	2.5
19	3.00	$9.43x10^{-6}$	$5.66x10^{-5}$	0.6	2.6

Table 3.11 The concentration of ADP ion was used in cation complexation studies with ligand **L2•Zn** and the final ratios of guest:host

Point	ADP / **L2•Zn**	[**L2•Zn**] mM	[ADP] mM	V of ADP (mL)	V total (mL)
1	0.00	1.00×10^{-5}	0.00	0	2
2	0.05	9.95×10^{-6}	4.98×10^{-7}	0.01	2.01
3	0.10	9.90×10^{-6}	9.90×10^{-6}	0.02	2.02
4	0.15	9.85×10^{-6}	1.48×10^{-6}	0.03	2.03
5	0.20	9.80×10^{-6}	1.96×10^{-6}	0.04	2.04
6	0.30	9.71×10^{-6}	2.91×10^{-6}	0.06	2.06
7	0.40	9.61×10^{-6}	3.85×10^{-6}	0.08	2.08
8	0.50	9.52×10^{-6}	4.76×10^{-6}	0.1	2.1
9	0.60	9.43×10^{-6}	5.66×10^{-6}	0.12	2.12
10	0.70	9.35×10^{-6}	6.54×10^{-6}	0.14	2.14
11	0.80	9.26×10^{-6}	7.41×10^{-6}	0.16	2.16
12	0.90	9.17×10^{-6}	8.26×10^{-6}	0.18	2.18
13	1.00	9.09×10^{-6}	9.10×10^{-6}	0.2	2.2
14	1.20	8.93×10^{-6}	1.07×10^{-5}	0.24	2.24
15	1.40	8.77×10^{-6}	1.22×10^{-5}	0.28	2.28
16	1.70	8.55×10^{-6}	1.45×10^{-5}	0.34	2.34
17	2.00	8.33×10^{-6}	1.67×10^{-5}	0.4	2.4
18	2.50	8.00×10^{-6}	2.00×10^{-5}	0.5	2.5
19	3.00	7.69×10^{-6}	2.31×10^{-5}	0.6	2.6
20	4.00	7.14×10^{-6}	2.86×10^{-5}	0.8	2.8

3.4.1.3 Determination of the stoichiometry of the L2•Zn with PPi and ATP complexes by Job's method

Typically, a solution of 1.00 x 10^{-5}M ligand **L2•Zn** and anions in DMSO:HEPES (0.01M, pH 7.4, 1:99 v/v) were prepared in a 25 mL volumetric flask. Solution of **L2•Zn** and anions were pipetted to a 1-cm quartz cuvette to provide the total volume 2 mL according to Table 3.12. Fluorescence spectrum of each addition was measured after stirred 5 min.

Table 3.12 Amounts of solutions of anions used to prepare various ligand **L2•Zn**:anion ratios

Point	ratio of **L2•Zn**:anion	volume of **L2•Zn** (ml)	volume of anion (ml)
1	1.00:00	2.00	0.00
2	0.90:0.10	1.80	0.20
3	0.80:0.20	1.60	0.40
4	0.70:0.30	1.40	0.60
5	0.60:0.40	1.20	0.80
6	0.50:0.50	1.00	1.00
7	0.40:0.60	0.80	1.20
8	0.30:0.70	0.60	1.40
9	0.20:0.80	0.40	1.60
10	0.10:0.90	0.20	1.80
11	0.00:1.00	0.00	2.00

3.4.1.4 Computational method

The structure optimizations of PPi/(**L2•Zn**)$_2$, ATP/(**L2•Zn**)$_2$ complexes and their components were carried out using density functional theory (DFT) method. The DFT computations have been performed with hybrid density functional B3LYP which is the Becke's three–parameter exchange functional with the Lee–Yang–Parr correlation functional combined with the Los Alamos LanL2DZ split–valence basis set called as B3LYP/LANL2DZ level of theory. All computations were performed using GAUSSIAN 03 program.

3.4.2 Complexation studies of ligand L2•Zn in DMSO:HEPES (0.01 M, pH 7.4, 90:10 v/v)

3.4.2.1 Complexation studies of ligand L2•Zn with various nucleotides by Fluorescence Spectrophotometry

Typically, a solution of $1.00x10^{-5}$ M **L2•Zn** in DMSO was prepared. All of nucleotide anions (ATP, ADP, AMP, UTP, UDP, UMP, GDP, GMP, CMP and PPi) were prepared in $1.00x10^{-3}$ M in HEPES buffer 0.01M, pH 7.4.

Fluorescence spectra of **L2•Zn** and anion complexes were recorded from 356-600 nm at ambient temperature. The solution of a stock solution of anion (200 μL) was added directly to 2.00 mL of 1 x 10^{-5} M ligand **L2•Zn** in a 1-cm quartz cuvette by micropipette and the mixture was stirred for 5 min. Fluorescence spectra of sample were measured. Table 3.13 shows a concentration of analytes in experiments, under following condition.

Condition for fluorescence spectrophotometry

Excitation wavelength: 346 nm

Slit width of excitation and emission: 5, 5

Smoothing factor: 10

Scan rate and the PMT voltage: 650

Table 3.13 The concentration of nucleotide anions were used in anion complexation studies with ligand **L2•Zn** and the final ratios of guest:host

anion	[anion] M	Final guest:host ratios
ATP	9.09×10^{-5}	10:1
ADP	9.09×10^{-5}	10:1
AMP	9.09×10^{-5}	10:1
UTP	9.09×10^{-5}	10:1
UDP	9.09×10^{-5}	10:1
UMP	9.09×10^{-5}	10:1
GDP	9.09×10^{-5}	10:1
GMP	9.09×10^{-5}	10:1

anion	[anion] M	Final guest:host ratios
CMP	9.09×10^{-5}	10:1
PPi	9.09×10^{-5}	10:1

3.4.2.2 Complexation studies of ligand L2•Zn with various anions : UTP, UDP, ATP and ADP by fluorescent titrations

Typically, a solution of 1.00×10^{-5} M ligand **L2•Zn** in DMSO was prepared by adding 1.00 mL of a stock solution of ligand **L2•Zn** (1.00×10^{-3} M) in a 100 mL volumetric flask. A stock solution of 1.00×10^{-3} M anion (PPi, ATP and ADP) in HEPES buffer 0.01M, pH 7.4 was prepared in a 5 mL volumetric flask.

Fluorescent spectra of ligand **L2•Zn** and anion complexes were recorded from 356-600 nm at ambient temperature. The solution of an anion was added directly to 2.00 mL of 1.00×10^{-5} M ligand **L2•Zn** in a 1-cm quartz cuvette by micropipette and stirred for 5 min. Fluorescent spectra were measured after each equivalent of anion. Table 3.14, 3.15, 3.16 and 3.17 shows a concentration of anions in titration experiments.

Table 3.14 The concentration of UTP ion was used in cation complexation studies with ligand **L2•Zn** and the final ratios of guest:host

Point	UTP / **L2•Zn**	[**L2•Zn**] mM	[UTP] mM	V of UTP (mL)	V total (mL)
1	0.00	1.00×10^{-5}	0.00	0	2
2	0.10	9.99×10^{-6}	9.99×10^{-7}	0.002	2.002
3	0.20	9.98×10^{-6}	2.00×10^{-6}	0.004	2.004
4	0.30	9.97×10^{-6}	2.99×10^{-6}	0.006	2.006
5	0.40	9.96×10^{-6}	3.98×10^{-6}	0.008	2.008
6	0.50	9.95×10^{-6}	4.98×10^{-6}	0.01	2.01
7	0.60	9.94×10^{-6}	5.96×10^{-6}	0.012	2.012
8	0.70	9.93×10^{-6}	6.95×10^{-6}	0.014	2.014
9	0.80	9.92×10^{-6}	7.94×10^{-6}	0.016	2.016
10	0.90	9.91×10^{-6}	8.92×10^{-6}	0.018	2.018

Point	UTP / **L2•Zn**	[**L2•Zn**] mM	[UTP] mM	V of UTP (mL)	V total (mL)
11	1.00	$9.90x10^{-6}$	$9.90x10^{-6}$	0.02	2.02
12	1.20	$9.88x10^{-6}$	$1.19x10^{-5}$	0.024	2.024
13	1.40	$9.86x10^{-6}$	$1.38x10^{-5}$	0.028	2.028
14	1.60	$9.84x10^{-6}$	$1.57x10^{-5}$	0.032	2.032
15	1.80	$9.82x10^{-6}$	$1.77x10^{-5}$	0.036	2.036
16	2.00	$9.80x10^{-6}$	$1.96x10^{-5}$	0.04	2.04
17	3.00	$9.71x10^{-6}$	$2.91x10^{-5}$	0.06	2.06
18	5.00	$9.52x10^{-6}$	$4.76x10^{-5}$	0.1	2.1
19	10.00	$9.09x10^{-6}$	$9.09x10^{-5}$	0.2	2.2

Table 3.15 The concentration of UDP ion was used in cation complexation studies with ligand **L2•Zn** and the final ratios of guest:host

Point	UDP / **L2•Zn**	[**L2•Zn**] mM	[UDP] mM	V of UDP (mL)	V total (mL)
1	0.00	$1.00x10^{-5}$	0.00	0	2
2	0.20	$9.98x10^{-6}$	$2.00x10^{-6}$	0.004	2.004
3	0.40	$9.96x10^{-6}$	$3.98x10^{-6}$	0.008	2.008
4	0.60	$9.94x10^{-6}$	$5.96x10^{-6}$	0.012	2.012
5	0.80	$9.92x10^{-6}$	$7.94x10^{-6}$	0.016	2.016
6	1.00	$9.90x10^{-6}$	$9.90x10^{-6}$	0.02	2.02
7	1.20	$9.88x10^{-6}$	$1.19x10^{-5}$	0.024	2.024
8	1.40	$9.86x10^{-6}$	$1.38x10^{-6}$	0.028	2.028
9	1.60	$9.84x10^{-6}$	$1.57x10^{-6}$	0.032	2.032
10	1.80	$9.82x10^{-6}$	$1.77x10^{-6}$	0.036	2.036
11	2.00	$9.80x10^{-6}$	$1.96x10^{-6}$	0.04	2.04
12	3.00	$9.71x10^{-6}$	$2.91x10^{-5}$	0.06	2.06
13	4.00	$9.61x10^{-6}$	$3.85x10^{-5}$	0.08	2.08
14	5.00	$9.52x10^{-6}$	$4.76x10^{-5}$	0.1	2.1
15	7.00	$9.35x10^{-6}$	$6.54x10^{-5}$	0.14	2.14
16	9.00	$9.17x10^{-6}$	$8.26x10^{-5}$	0.18	2.18
17	10.00	$9.09x10^{-6}$	$9.09x10^{-5}$	0.2	2.2

Table 3.16 The concentration of ATP ion was used in cation complexation studies with ligand **L2•Zn** and the final ratios of guest:host

Point	ATP / **L2•Zn**	[**L2•Zn**] mM	[ATP] mM	V of ATP (mL)	V total (mL)
1	0.00	1.00×10^{-5}	0.00	0	2
2	0.10	9.99×10^{-6}	9.99×10^{-7}	0.002	2.002
3	0.20	9.98×10^{-6}	2.00×10^{-6}	0.004	2.004
4	0.30	9.97×10^{-6}	2.99×10^{-6}	0.006	2.006
5	0.40	9.96×10^{-6}	3.98×10^{-6}	0.008	2.008
6	0.50	9.95×10^{-6}	4.98×10^{-6}	0.01	2.01
7	0.60	9.94×10^{-6}	5.96×10^{-6}	0.012	2.012
8	0.70	9.93×10^{-6}	6.95×10^{-6}	0.014	2.014
9	0.80	9.92×10^{-6}	7.94×10^{-6}	0.016	2.016
10	0.90	9.91×10^{-6}	8.92×10^{-6}	0.018	2.018
11	1.00	9.90×10^{-6}	9.90×10^{-6}	0.02	2.02
12	1.20	9.88×10^{-6}	1.19×10^{-5}	0.024	2.024
13	1.40	9.86×10^{-6}	1.38×10^{-5}	0.028	2.028
14	1.60	9.84×10^{-6}	1.57×10^{-5}	0.032	2.032
15	1.80	9.82×10^{-6}	1.77×10^{-5}	0.036	2.036
16	2.00	9.80×10^{-6}	1.96×10^{-5}	0.04	2.04
17	3.00	9.71×10^{-6}	2.91×10^{-5}	0.06	2.06
18	5.00	9.52×10^{-6}	4.76×10^{-5}	0.1	2.1
19	10.00	9.09×10^{-6}	9.09×10^{-5}	0.2	2.2

Table 3.17 The concentration of ADP ion was used in cation complexation studies with ligand **L2•Zn** and the final ratios of guest:host

Point	ADP / **L2•Zn**	[**L2•Zn**] mM	[ADP] mM	V of ADP (mL)	V total (mL)
1	0.00	1.00×10^{-5}	0.00	0	2
2	0.10	9.90×10^{-6}	9.90×10^{-7}	0.02	2.02
3	0.20	9.80×10^{-6}	1.96×10^{-6}	0.04	2.04
4	0.30	9.71×10^{-6}	2.91×10^{-6}	0.06	2.06
5	0.40	9.61×10^{-6}	3.84×10^{-6}	0.08	2.08
6	0.50	9.52×10^{-6}	4.76×10^{-6}	0.1	2.1
7	0.60	9.43×10^{-6}	5.66×10^{-6}	0.12	2.12
8	0.70	9.35×10^{-6}	6.54×10^{-6}	0.14	2.14
9	0.80	9.26×10^{-6}	7.41×10^{-6}	0.16	2.16
10	0.90	9.17×10^{-6}	8.26×10^{-6}	0.18	2.18

Point	ADP / **L2•Zn**	[**L2•Zn**] mM	[ADP] mM	V of ADP (mL)	V total (mL)
11	1.00	$9.09x10^{-6}$	$9.09x10^{-6}$	0.2	2.2
12	1.20	$8.93x10^{-6}$	$1.07x10^{-5}$	0.24	2.24
13	1.40	$8.77x10^{-6}$	$1.22x10^{-5}$	0.28	2.28
14	1.60	$8.62x10^{-6}$	$1.38x10^{-5}$	0.32	2.32
15	1.80	$8.48x10^{-6}$	$1.53x10^{-5}$	0.36	2.36
16	2.00	$8.33x10^{-6}$	$1.67x10^{-5}$	0.4	2.4
17	3.00	$7.69x10^{-6}$	$2.31x10^{-5}$	0.6	2.6
18	5.00	$6.67x10^{-6}$	$3.33x10^{-5}$	1	3
19	10.00	$5.00x10^{-6}$	$5.00x10^{-5}$	2	4

3.4.2.3 Complexation studies of ligand L2•Zn with ATP (adenosine triphosphate) by ^{1}H-NMR spectroscopy.

A solution of $4.35x10^{-2}$ M ligand **L2•Zn** (8.37 mg, 1.74×10^{-5} mol), a solution of $4.35x10^{-2}$ M of a ligand **L2•Zn** (8.37 mg, 1.74×10^{-5} mol) containing 1.74×10^{-5} mol (1 equiv) of ATP and a solution of ATP in DMSO-d_6:D_2O (7:1 v/v, 0.4 mL) were prepared in NMR tube. All of samples were measured in ^{1}H-NMR and the complexed solution of **1•Zn** and ATP in DMSO-d_6:D_2O was measured in 2D-NOESY spectroscopy.

3.4.2.4 Principal Component analysis (PCA) method

For PCA analysis, the solution of 200 μL analytes ($1.00x10^{-3}$ M in HEPES buffer 0.10 M, pH 7.4) was added directly to 2.00 mL of 1.00×10^{-5} M **L2•Zn** in a 1-cm quartz cuvette by micropipette and the mixture was stirred for 5 minutes. The fluorescent spectra of **L2•Zn** and each analytes were measured at the excitation of 346 nm. The sample was measured at 5 replicates in each analytes. PCA calculation was evaluated by the responsive fluorescence spectra from 356-600 nm using MATLAB 7.11(version R2011a).

CHAPTER IV

RESULTS AND DISCUSSION

4.1 Design concept

The design and synthesis of chemosensor that was capable to detect cation, anion or nucleotide in aqueous system are attractive approaches. Molecular sensor usually consists of two units: a receptor and a sensory unit. It is well known that dipicolylamine (dpa) is a good receptor unit for binding selectively with Zn^{2+} using lone pair electrons of nitrogen atom.[30] The sensory units (chromophores and fluorophores) can be attached to dpa. Consequently, these systems are an interest of utilization for recognition of analytes in the applications of molecular switches, molecular sensors, molecular gates, and etc.

On the basic of this strategy, we used dipicolylamine moieties for binding transition metals such as Zn^{2+} and Cu^{2+} ion due to their abilities to provide beneficial metal coordination interaction. It was expected for making an electrostatic interaction between cationic Zn^{2+} ion and phosphate species of nucleotides in polar solvents such as water.[55] Actually, the aqueous solvents showed very poor affinity for recognition of anions due to the influence of the strong hydration.[56] Therefore, Zinc(II)-dipicolylamine complexes have been widely used as binding units for phosphate chemosensors.[57-61] Furthermore, BF_2-curcumin and pyrene are expected to be an excellent fluorophore because BF_2-curcumin gives a high quantum yield, while pyrene group is very sensitive to solvent polarity and it has widely used for molecular probes using fluorescence spectrophotometry.

Consequently, the chemosensor **L1•2Zn** and **L2•Zn** were synthesized by using dipicolylamine as binding sites upon the different fluorophores such as BF_2-curcumin and pyrene. The complexation was studied by ^{1}H- NMR, UV-Vis and fluorescent techniques.

The chemosensor **L1** was synthesized in the several bases, solvent systems and different reaction conditions. We attempted to synthesize **L1** in the numerous synthetic pathways as shown in the following scheme.

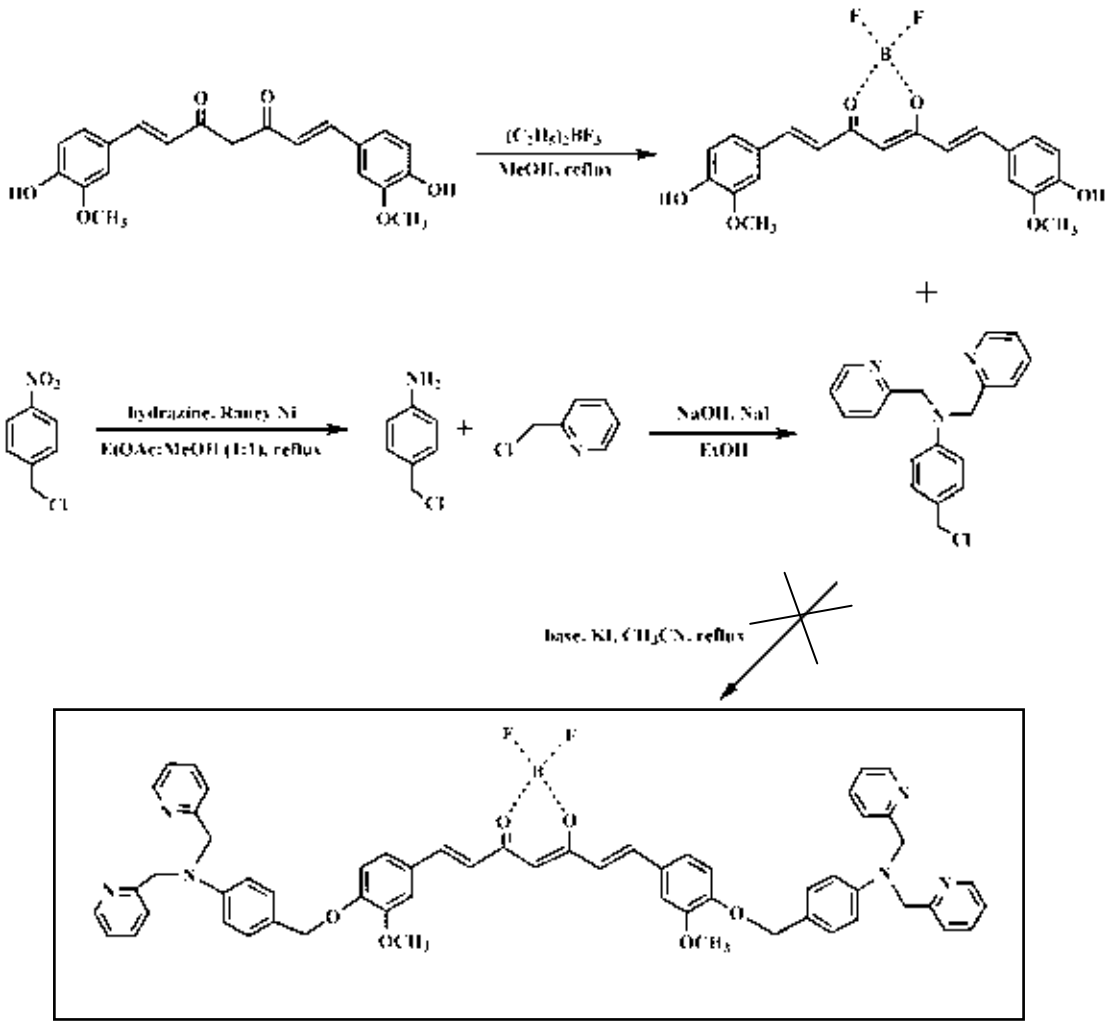

Scheme 4.1 Synthesis pathway 1 of ligand **L1**

The various conditions in the last step for synthesis of ligand **L1** were listed in Table 4.1.

Table 4.1 The different reaction conditions were used in final step of synthetic pathway 1

condition	base	solvent	catalyst	temperature	vacuum line
1	Na_2CO_3	CH_3CN	NaI	reflux	-
2	Na_2CO_3	CH_3CN	NaI	reflux	use
3	$CsCO_3$	CH_3CN	KI	reflux	-
4	NaH	CH_3CN	NaI	reflux	-
6	NaH	THF	KI	reflux	-
7	pyridine	CH_3CN	NaI	rt	-

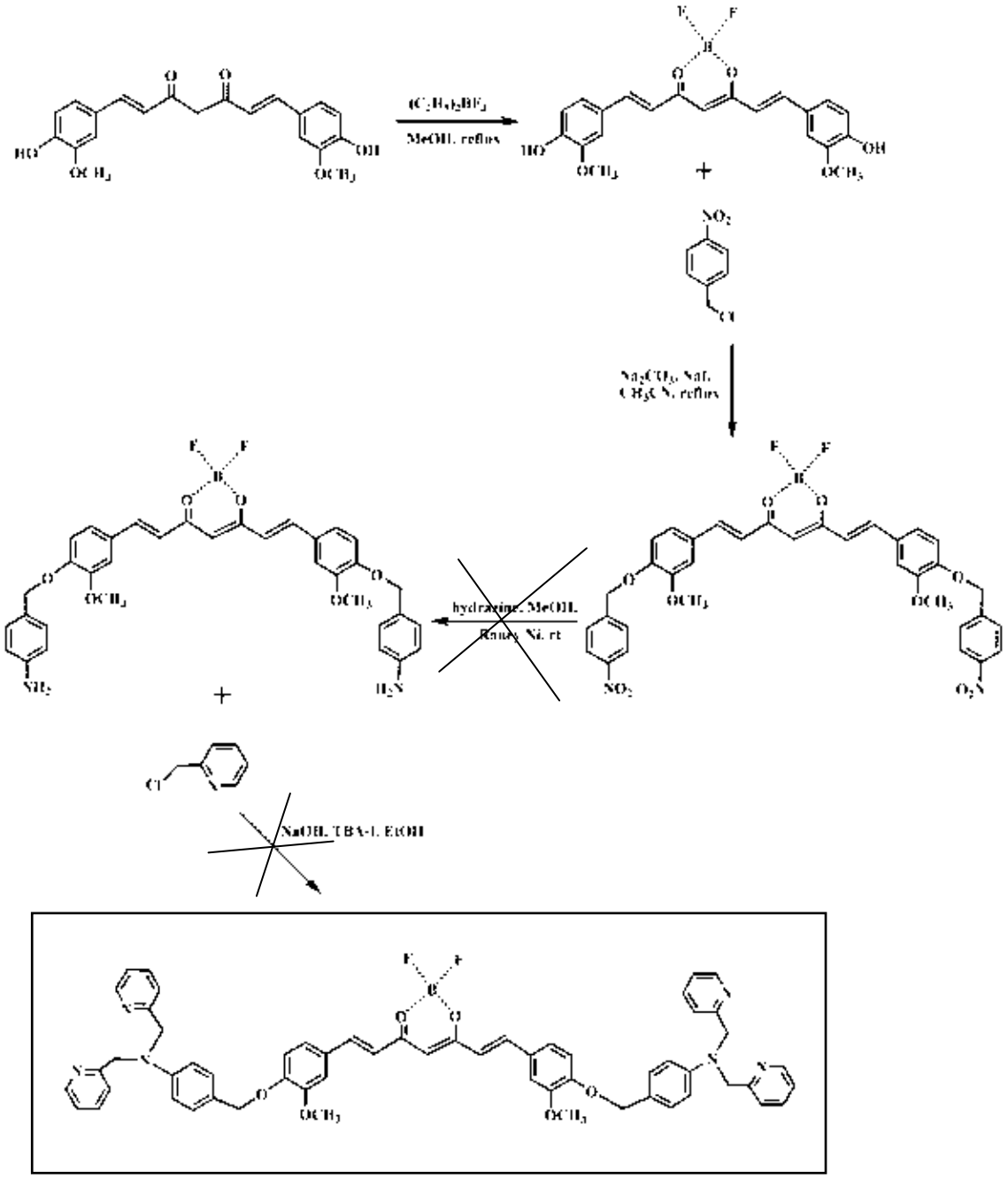

Scheme 4.2 Synthesis pathway 2 of ligand **L1**

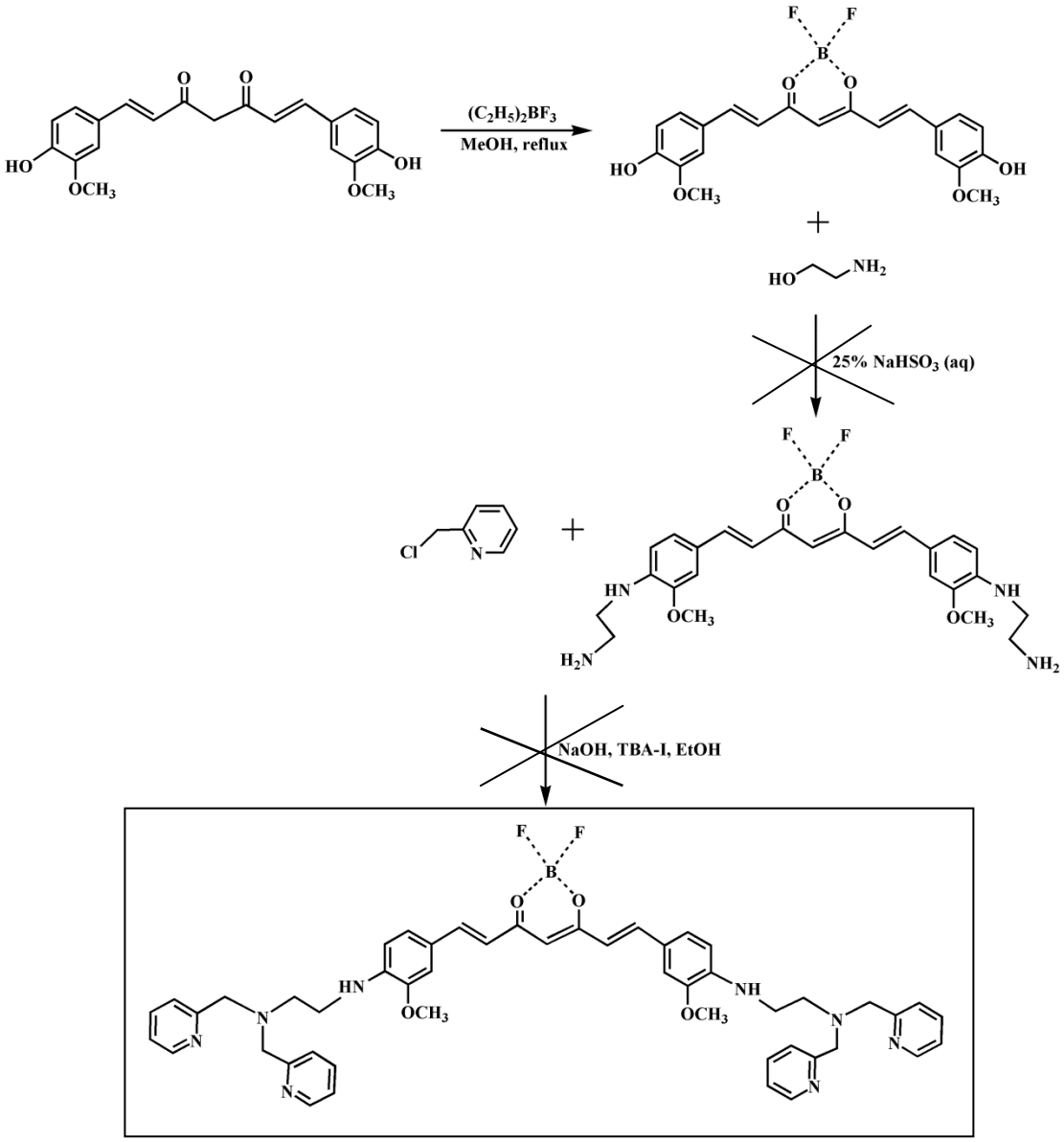

Scheme 4.3 Synthesis pathway 3 of ligand **L1**

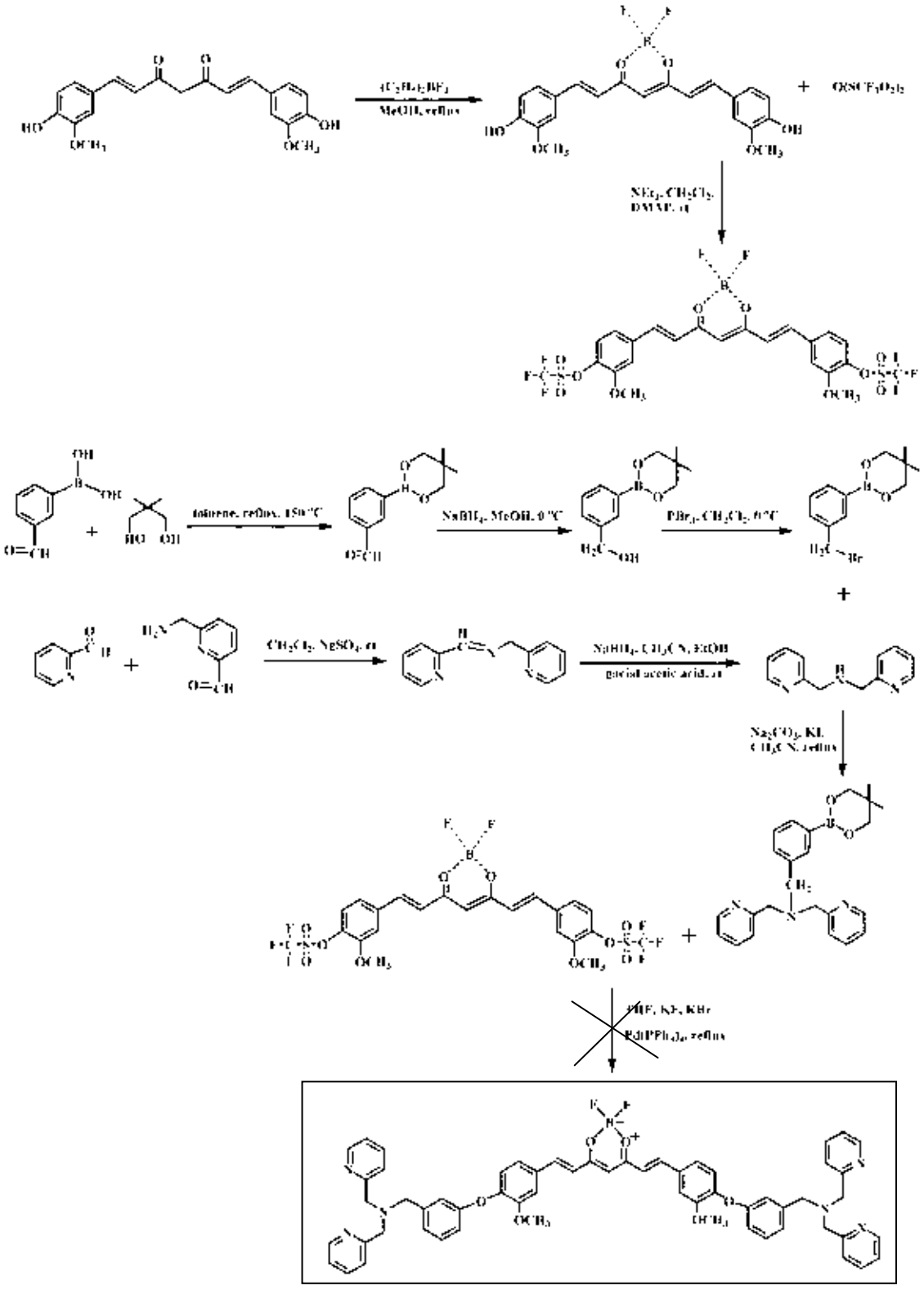

Scheme 4.4 Synthesis pathway 4 of ligand **L1**

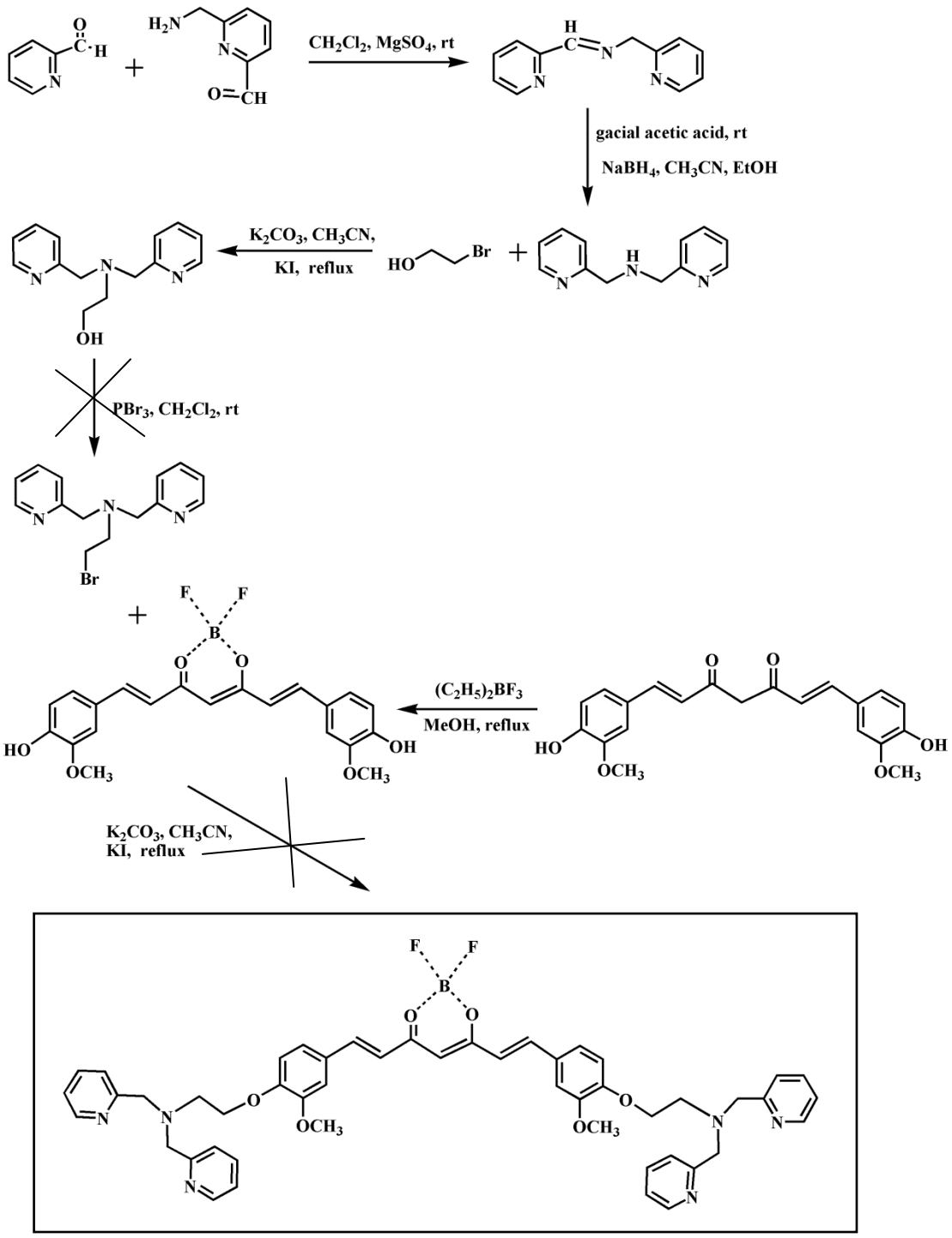

Scheme 4.5 Synthesis pathway 5 of ligand **L1**

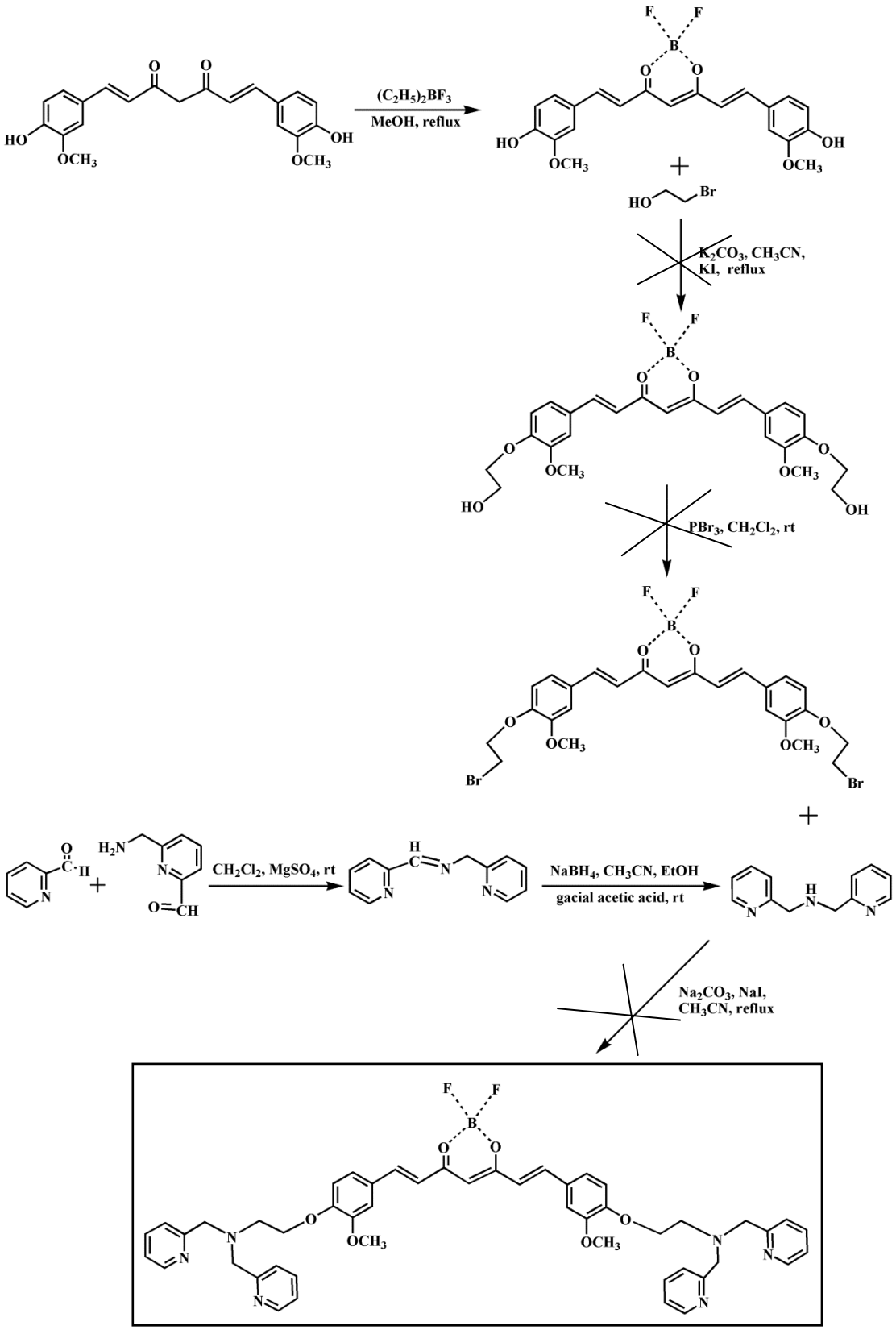

Scheme 4.6 Synthesis pathway 6 of ligand **L1**

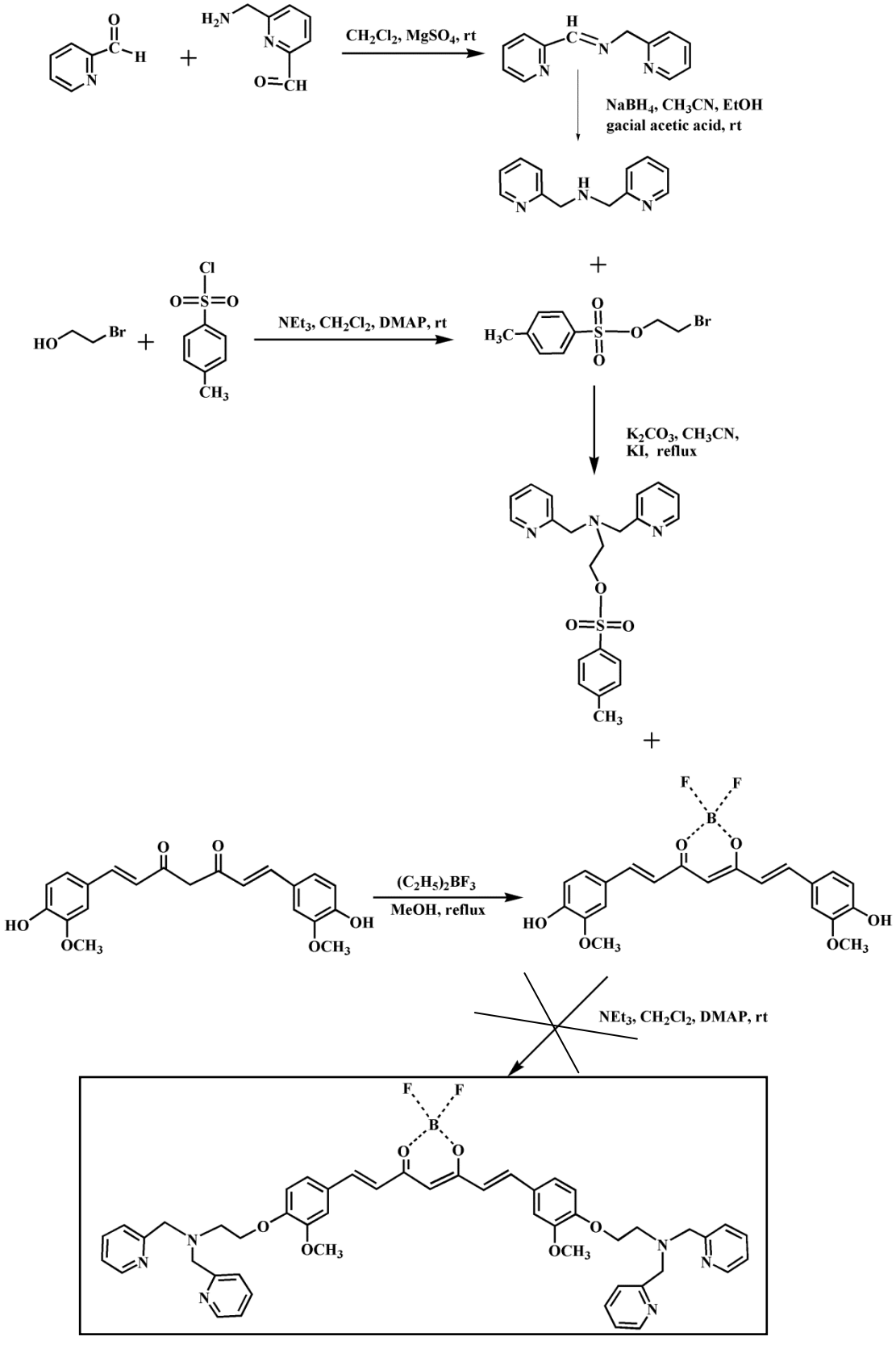

Scheme 4.7 Synthesis pathway 7 of ligand **L1**

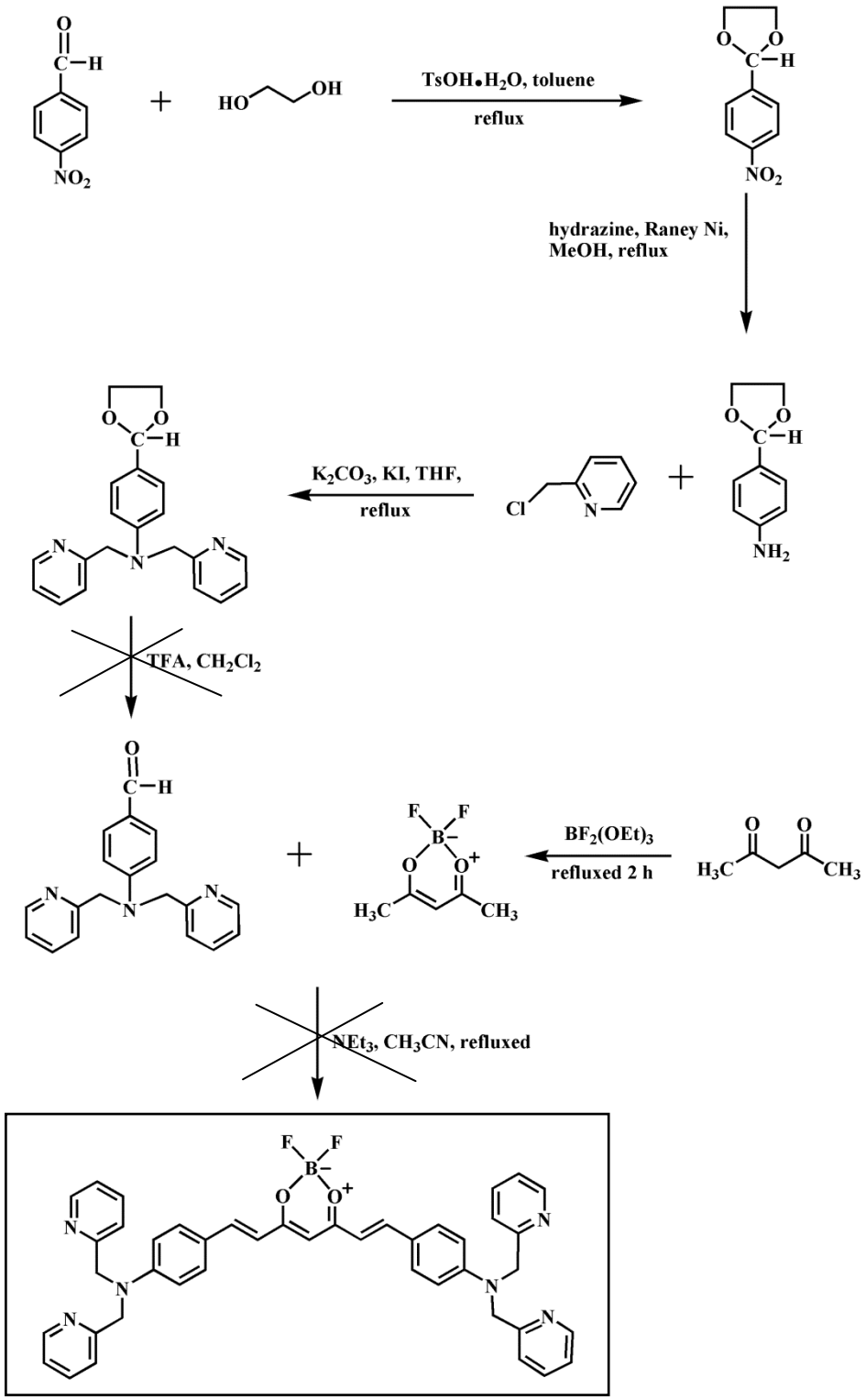

Scheme 4.8 Synthesis pathway 8 of ligand **L1**

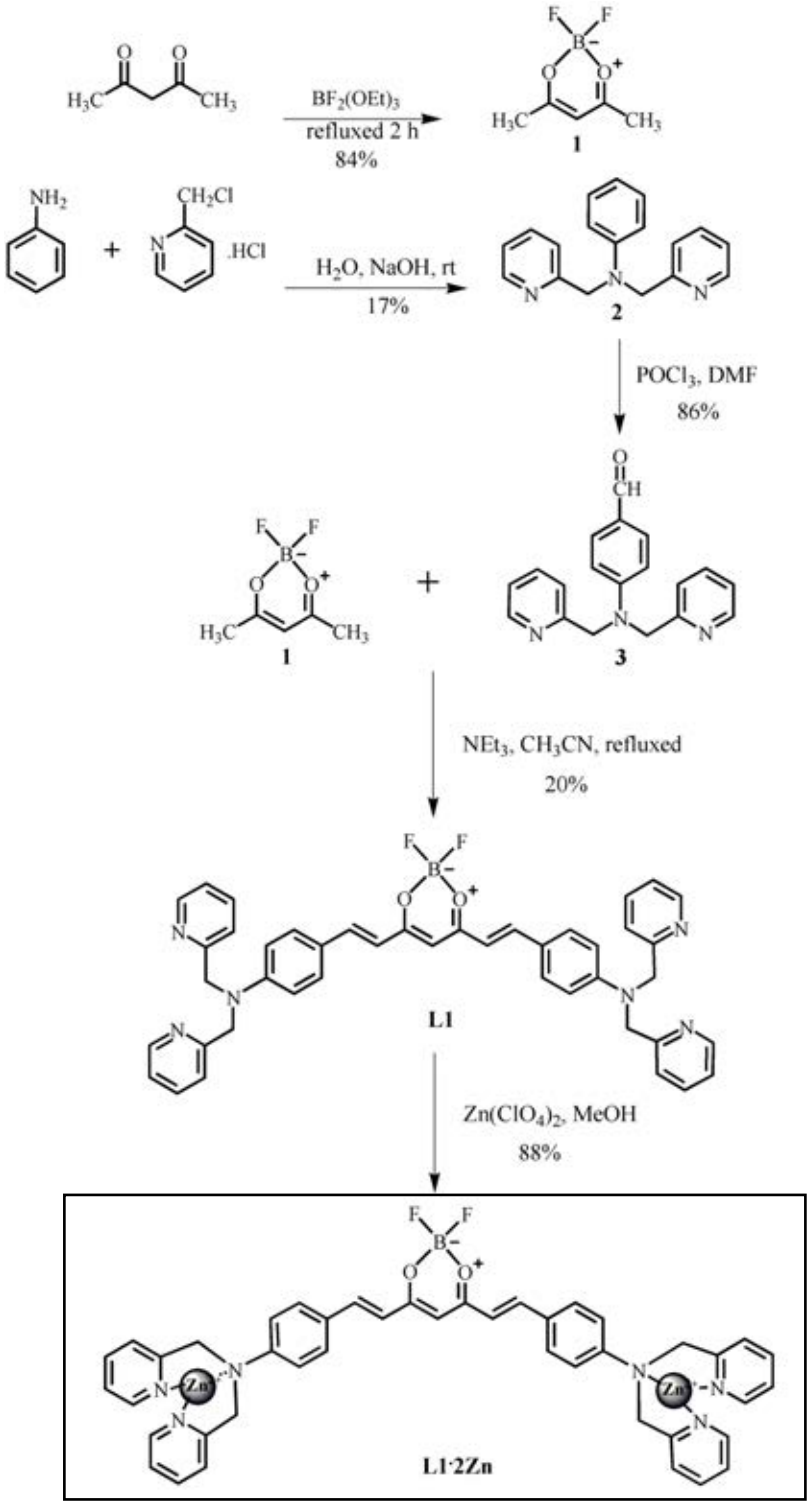

Scheme 4.9 Synthesis pathway 9 of ligand **L1•2Zn**

4.2 Synthesis and characterization of ligand L1•2Zn and L2•Zn

4.2.1 Synthesis and characterization of curcumin derivatives containing dipicolylamine moieties (L1•2Zn)

The curcumin derivative containing dipicolylamine moieties (**L1•2Zn**) have been successfully synthesized under the scheme 4.9. In order to improve the yields of ligand **L1•2Zn**, several bases, solvent systems and different reaction conditions were carried out. The ligand **L1•2Zn** was prepared by the nucleophilic substitution, Vilsmeier-Haack and condensation reaction in various conditions.

The synthetic pathway was started by modification of acetylacetone with difluoroboron ether under refluxing for 2 h. The pale yellow solid was obtained without the purification in 85% yield.[62] The ^{1}H-NMR spectrum showed the characteristic peaks of the modified compound as singlet of the methyl protons at 2.29 ppm. The unsaturated proton (C=C*H*-C) moved to downfield shift from 5.46 to 5.99 ppm.

Nucleophilic substitution of compound **2**[63] was prepared by the reaction between aniline and 2-chloromethyl pyridine in the presence of sodium hydroxide as base, and the tetrabutylammonium iodide as a phase transfer catalyst in H_2O. The desired product was purified by column chromatography using a gradient of ethyl acetate (20-80%) in dichloromethane as eluent, to afford 17% yield as a white solid of **2**. From ^{1}H-NMR data of compound **2**, the range of aromatic protons (7.28-6.71 ppm) assigned to aromatic protons of dipicolylamine showed a significant difference from those of aniline. The doublets and triplets of aromatic protons of dipicolylamine moieties were appeared at 8.59 ppm and 7.63 ppm, respectively. Moreover, the appearance of singlet assignment of Ar-C*H*$_2$ at 4.83 in the spectrum supported the structure of compound **2**.

Compound **3** was synthesized by Vilsmeier-Haack reaction.[63] The reaction of the DMF with $POCl_3$ produces an electrophilic iminium cation. The slow addition of compound **2** into the reaction at 90 ºC caused subsequently electrophilic aromatic substitution to generate an iminium ion intermediate, which is easily hydrolyzed by water. The desired aryl aldehyde **3** was obtained as yellow oil in 86 % yield after

neutralized to pH 6-8 with K_2CO_3 to get rid of residue acid and then was extracted with dichloromethane. The ^{1}H-NMR data of the corresponding **3** displayed the singlet of aldehyde proton at 9.73 ppm. Interestingly, the aromatic protons of compound **3** were assigned by downfield shift to 7.70-6.80 ppm possibly caused by an electron withdrawing group of carbonyl.

Finally, the **BF_2-Curbis(dpa)$_2$ (L1)** was achieved by condensation reaction[64] between compound **1** and compound **3** in the presence of triethylamine as base in acetonitrile. In order to deprotonate the methyl protons of compound **1**, triethylamine was left stirring in acetonitrile for 1 h prior to addition of the solution of compound **3** in acetonitrile. The reaction was heated at 90 ºC under nitrogen atmosphere for 3 days. Obviously, the visual color change of solution was observed from pale yellow to black. The final product (**L1)** was obtained as a dark purple powder in 20% yield after purification by column chromatography using ethyl acetate until 10% methanol as eluent and precipitation with CH_2Cl_2 and hexane. The ^{1}H-NMR spectrum of compound **L1** depicted in Figure 4.1 showed the disappearance of aldehyde proton at 9.73 ppm belonging to compound **3** and that of the chemical shift at 2.99 ppm assigned to methyl group of compound **1**. Furthermore, the aromatic protons shift to upfield at 8.54-6.64 ppm, possibly caused by the influence of an electron donating group of dpa moieties. Interestingly we observed the characteristic signals of the singlet assignment of ArCH_2 at 4.80 and 7.19 ppm in the spectrum which supported the structure of **L1**.

IR spectrum (Figure 4.2) of **L1** exhibited an absorption bands of ketone C=O stretching at 1747.83 cm^{-1}, aromatic C=C stretching at 1591.30 and 1513.04 cm^{-1} and C=C stretching of curcumin at 1382.61, 1173.91 and 1143.99 cm^{-1}. The observation of an intense peak at 718.3061 m/z from ESI-HRMS mass spectrum agreed with the structure of **L1** as shown in the Figure 4.3.

The **L1•2Zn** complex was prepared by mixing **L1** with two equivalents of zinc perchlorate in methanol at room temperature. From the ^{1}H-NMR data as shown in Figure 4.4 of the desired complex, the aliphatic ethylene protons (NCH_2Ar) of complex was splitted into two double peaks at 4.50 ppm. While the singlet peak of this signal (NCH_2Ar) at 4.94 ppm belonging to uncomplexed compound still remained

in the spectrum. Moreover, the downfield-shifted aromatic protons at 8.86-6.80 ppm stemmed from Zn^{2+} complexed **L1** using lone pair electrons of nitrogen atom.

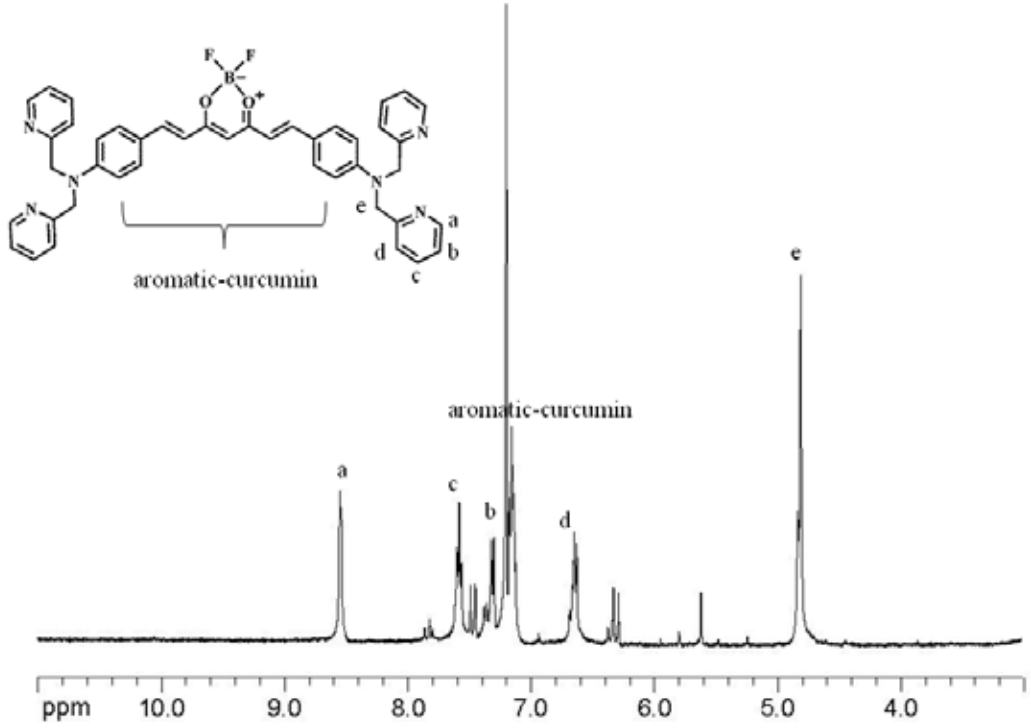

Figure 4.1 The ^{1}H-NMR spectrum of curcumin derivatives containing dipicolylamine moieties (**L1**) in $CDCl_3$ (400 MHz)

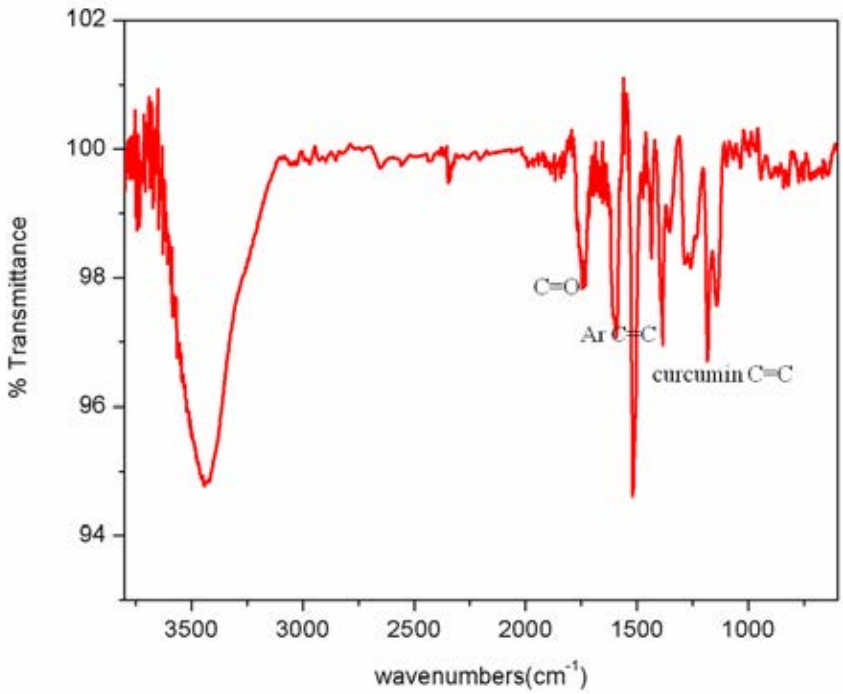

Figure 4.2 IR spectrum of **L1**

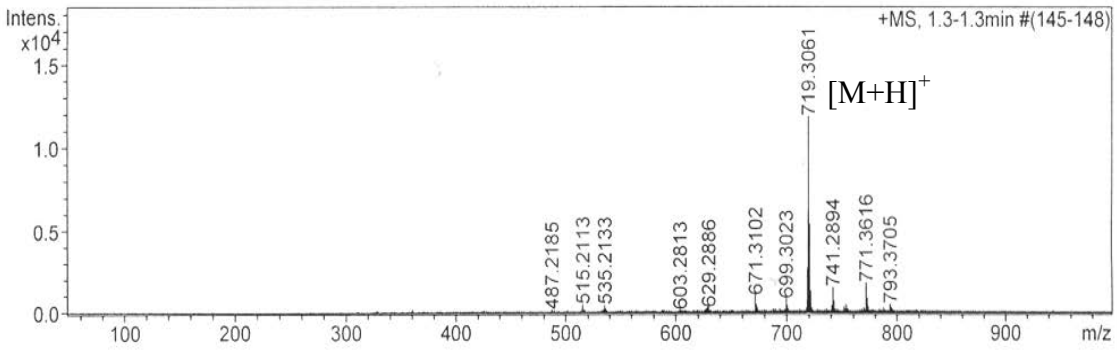

Figure 4.3 ESI-HRMS mass spectrum of **L1**

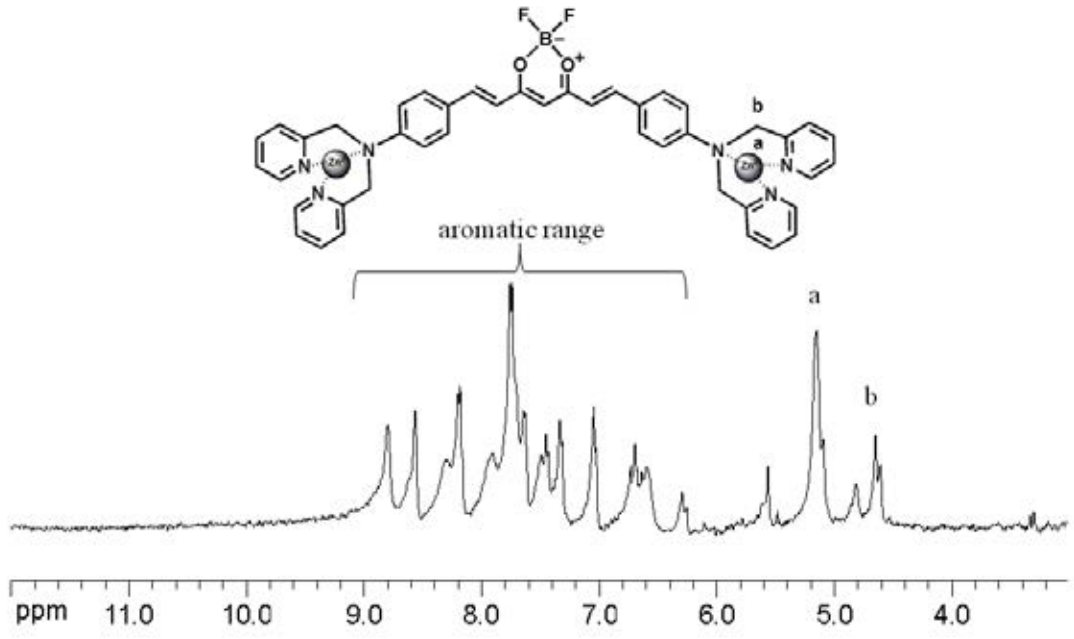

Figure 4.4 The ^{1}H-NMR spectrum of curcumin derivatives complex (**L1•2Zn**) in CD_3CN (400 MHz).

4.2.2 Synthesis and characterization of pyrene derivatives containing dipicolylamine moiety (L2•Zn)

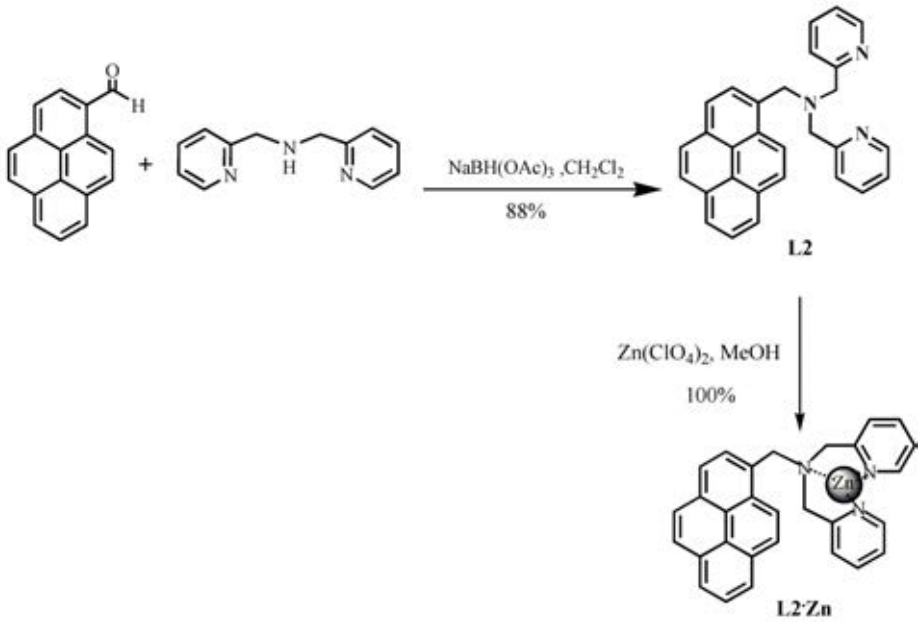

Scheme 4.10 Synthesis pathway of ligand **L2•Zn**

The ligand containing dipicolylamine and pyrene (**L2)** was synthesized following the scheme 4.10. Ligand **L2** was accomplished by the reductive amination coupling between pyrenecarboxaldehyde and dipicolylamine in the presence of sodium tri-acetoxyborohydride as a reducing agent in CH_2Cl_2. The reaction mixture was stirred under N_2 atmosphere at room temperature for 5 h. After purified by column chromatography, **L2** was obtained as yellow oil which ultimately solidifies when dry in 88% yield. From ^{1}H-NMR spectrum, the pyridine aromatic protons of **L2** showed as doublet signal of NCH_a protons at 8.50 ppm, triplet protons of H_c at 7.70 ppm, doublet proton of H_b at 7.48 ppm and triplet proton of H_d at 7.21 ppm. The range of aromatic protons from 8.37 ppm to 8.01 ppm of **L2** showed a significant characteristic peak of pyrene group. Furthermore, ^{1}H-NMR spectrum of **L2** exhibited two signals of methylene protons adjacent to pyrene and pyridine at 4.33 and 3.81

ppm, respectively, as shown in Figure 4.5. Additionally, ESI-HRMS mass spectrum in Figure 4.6 showed the intense peak at m/z 414.2022 corresponding to $[M+H]^+$.

The **L2•Zn** complex was prepared by mixing **L2** and one equivalent of zinc perchlorate in methanol with 100% yield. From ^{1}H-NMR spectrum of **L2•Zn**, the influence of the electron donor of N atom to Zn^{2+} complex caused the downfield shift of the aromatic protons at 8.71, 8.42, 7.94, 7.68 and 7.56 ppm. Moreover, the appearance of two singlet assignment of methylene protons adjacent to pyridine at 4.35 and 3.81 ppm revealed that these methylene protons were in the different environments possibly caused by zinc complexation (Figure 4.7).

IR spectrum (Figure 4.8) of **L2•Zn** exhibited an absorption bands of pyrene C=C stretching at 1612.01, 1056.50, 841.74, 764.43 and 707.16 cm^{-1} and pyridine C=C stretching at 1443.07 cm^{-1}. The intense peak of ESI-HRMS spectrum at 773.9829 m/z corresponding to $[M+Zn^{2+}+3(ClO_4)]^-$ confirmed the structure of **L2•Zn**. (as shown in Figure 4.9)

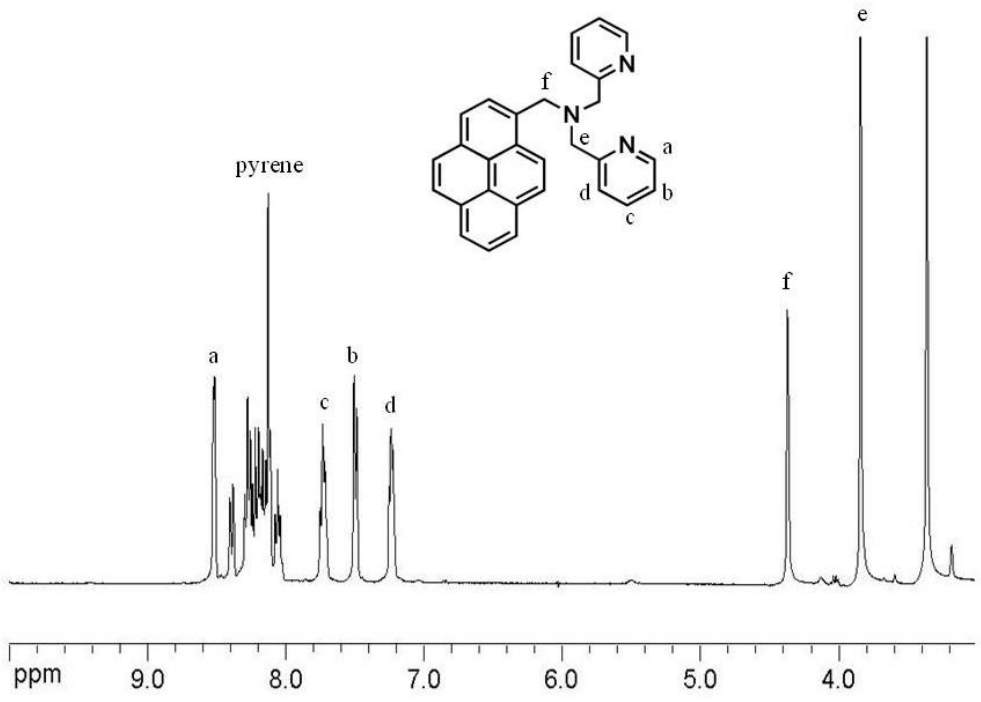

Figure 4.5 The ^{1}H-NMR spectrum of pyrene containing dipicolylamine (**L2**) in DMSO-d_6 (400 MHz).

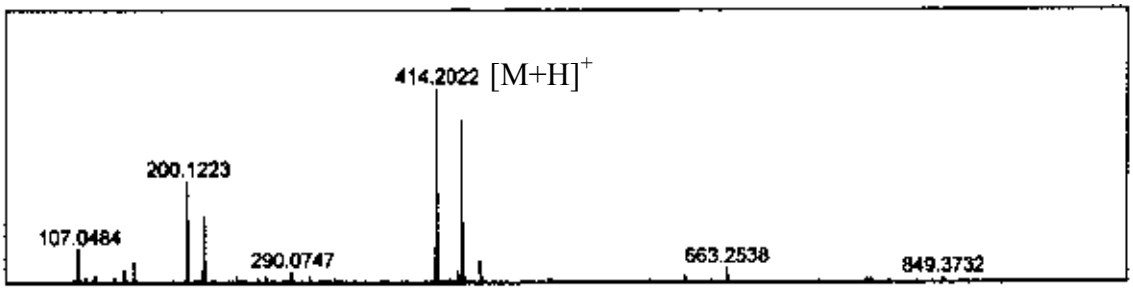

Figure 4.6 ESI-HRMS mass spectrum of **L2**

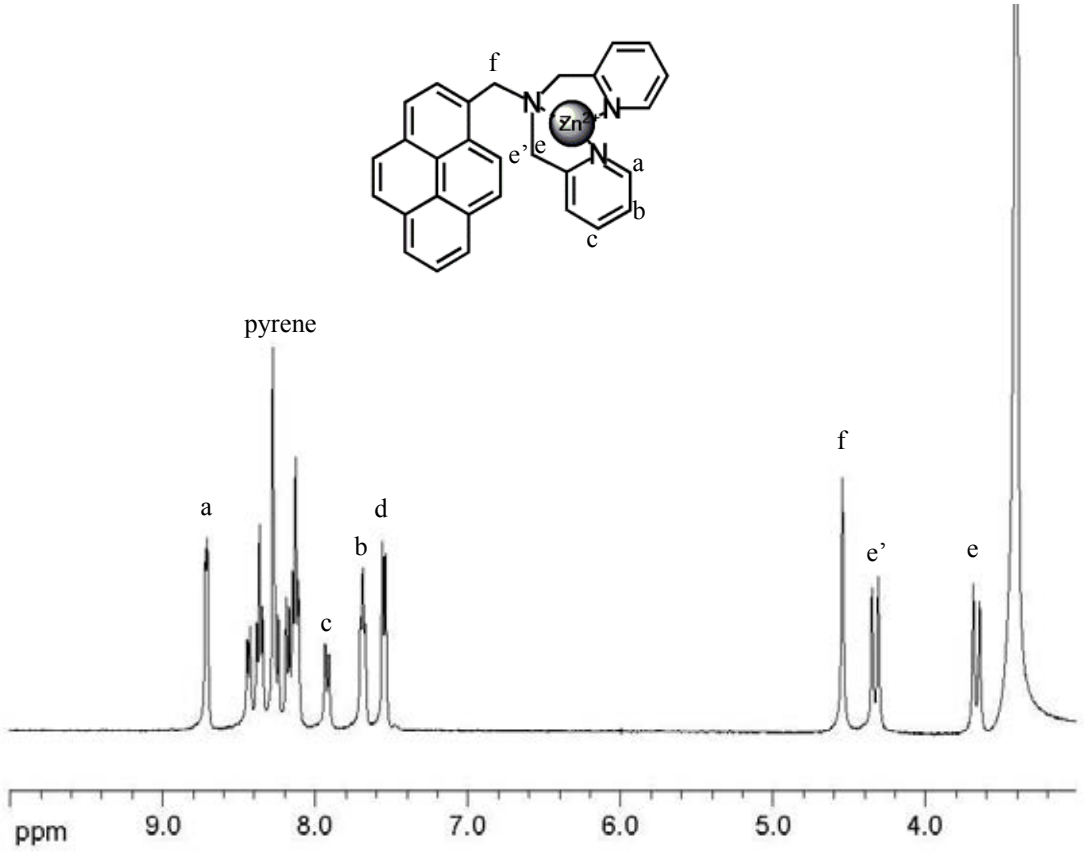

Figure 4.7 The ^{1}H-NMR spectrum of **L2•Zn** complex in DMSO-d_6 (400 MHz).

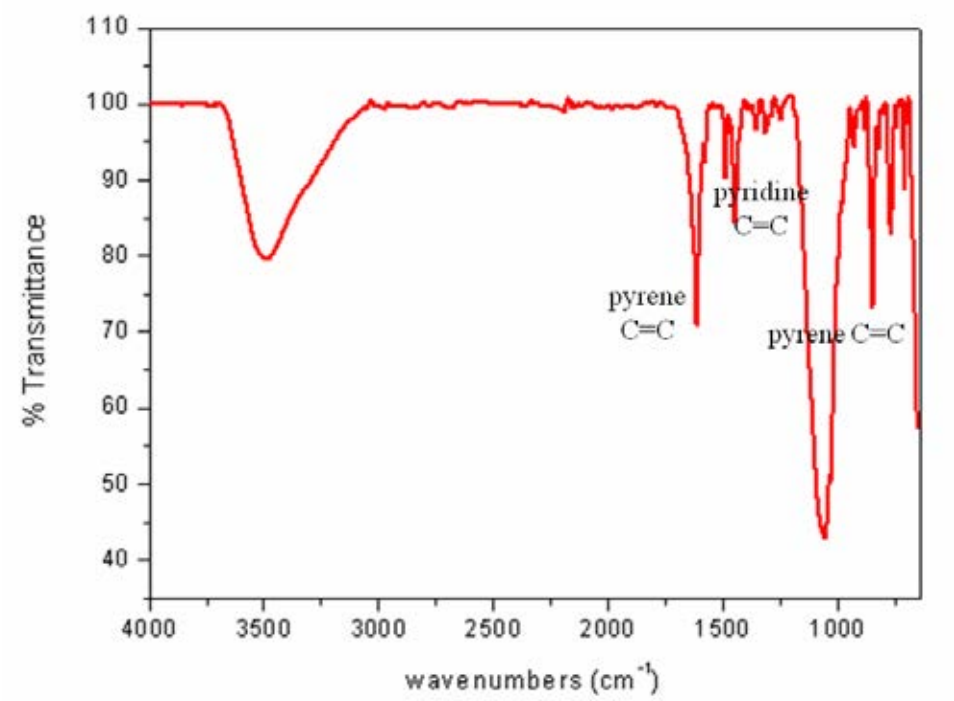

Figure 4.8 IR spectrum of **L2•Zn** complex.

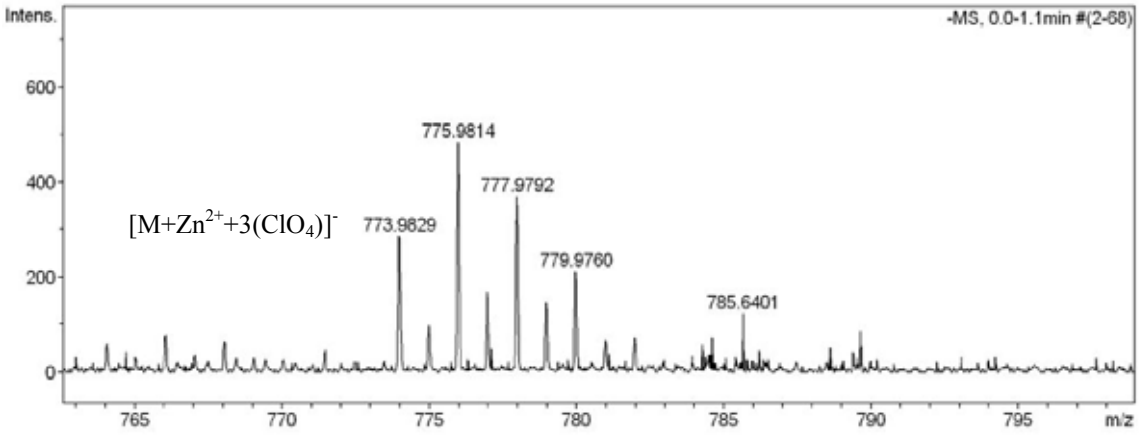

Figure 4.9 ESI-HRMS mass spectrum of **L2•Zn** complex

4.3 Determination of quantum yield of ligand **L1**[65-66]

The fluorescence quantum yield (Φ) gives the efficiency of the fluorescence process. It is defined as the ratio of the number of photons emitted to the number of photons absorbed. Quantum yield was obtained by relative basis with reference to a standard having known quantum yield. The integrated fluorescence spectra of sample were plotted versus absorbance at the excitation wavelength to obtain the gradients. The quinine sulfate in 1*N* H_2SO_4 was used as reference sample. (Φ =0.58 in 1*N* H_2SO_4) The gradients of the graphs are proportional to the quantum yield of the different samples. Absolute values are calculated using the standard samples which have the fixed and known fluorescence quantum yield values, according to the following equation:

$$\mathbf{Q_x = Q_{std}\left(\frac{Grad_x}{Grad_{std}}\right)\left(\frac{n_x^2}{n_{std}^2}\right)} \qquad \text{…..……(1)}$$

Q_x = quantum Yield of sample

Q_{std} = quantum Yield of standard

$Grad_x$ = gradient of sample

$Grad_{std}$ = gradient of standard

η_x = refractive index of solvent of sample

η_{std} = refractive index of solvent of standard

Plots of the integrated fluorescence intensity *vs* the absorbance of ligand **L1** in various solvents such as CH_3CN, $CHCl_3$ and THF were shown in Figure 4.10. The quantum yields obtained from the calculation following equation (1) were listed in the Table 4.2.

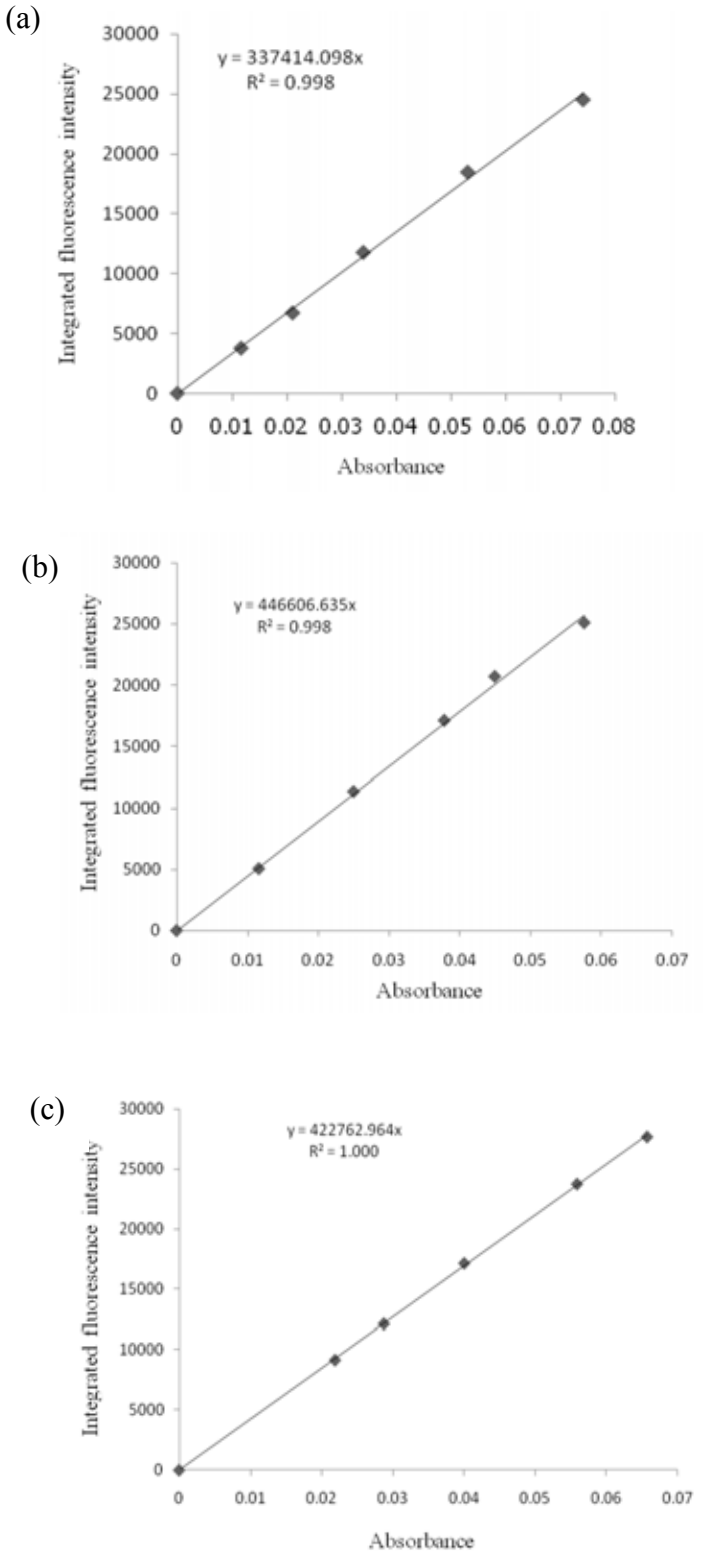

Figure 4.10 Linear plots of ligand **L1** in (a) CH_3CN (b) $CHCl_3$ and (c) THF.

Table 4.2 Quantum yields of **L1** in various solvents.

solvent	refractive index of solvent (η_x)	quantum yield		
		first	second	average
acetonitrile	1.3441	0.24	0.24	0.24
chloroform	1.4460	0.37	0.37	0.37
tetrahydrofuran	1.4072	0.33	0.33	0.33

4.4 The complexation studies of ligand L1

Sensor **L1** also contains the nitrogen donor atoms of the dipicolyl amine moieties, which capable to bind with transition metals such as Zn^{2+} and Cu^{2+} and BF_2-Curcumin moiety as fluorophore. Thus, we have studied the binding abilities of ligand **L1** toward transition metals by ^{1}H-NMR, UV-Vis and fluorescent techniques.

4.4.1 Zn^{2+} ion complexation studies by ^{1}H-NMR spectroscopy

The binding ability of complexation between sensor **L1** and Zn^{2+} ion were investigated by ^{1}H-NMR spectroscopy. To reduce the effect of ion pair, perchlorate should be used as counter anion. To evaluate the binding properties, sensor **L1** was titrated with zinc perchlorate monohydrate as shown in Figure 4.11. ^{1}H-NMR spectra were found that the chemical shift of the characteristic pyridine protons (NC*H*) at 8.58 ppm was significantly affected upon zinc complex. After adding 4 equiv. of Zn^{2+}, the signal of aromatic protons of NC*H* showed a downfield shift from 8.57 ppm to 8.68 ppm. Presumably, lone pair electrons of N atoms bound to Zn^{2+} ions resulting in

decrease of electron density. Furthermore, the changes in remaining aromatic protons of ligand were significantly observed. These protons displayed the downfield shift from 7.72-7.26 ppm to 8.289-7.46 ppm, while the protons at conjugate system of curcumin part remained unchanged. It was implied that zinc complex did not affect to the curcumin part. Interestingly, the obvious change of the singlet peak of methylene protons (C*H*$_2$) at 4.90 ppm was monitored. The change of these protons demonstrated the splitting of singlet peak into two broad peaks corresponding to the complexation of ligand and Zn^{2+}. [67] Deeply considering ^{1}H-NMR spectra, no changes of all assignments were observed after adding more than 2 equiv. of Zn^{2+}. This suggested that the complexation of **L1** and Zn^{2+} was completed at 2 equiv. of Zn^{2+}. The chemical shifts of sensor **L1** and their induced chemical shifts upon the formation of complexes with various equivalent of Zn^{2+} were listed in Table 4.3.

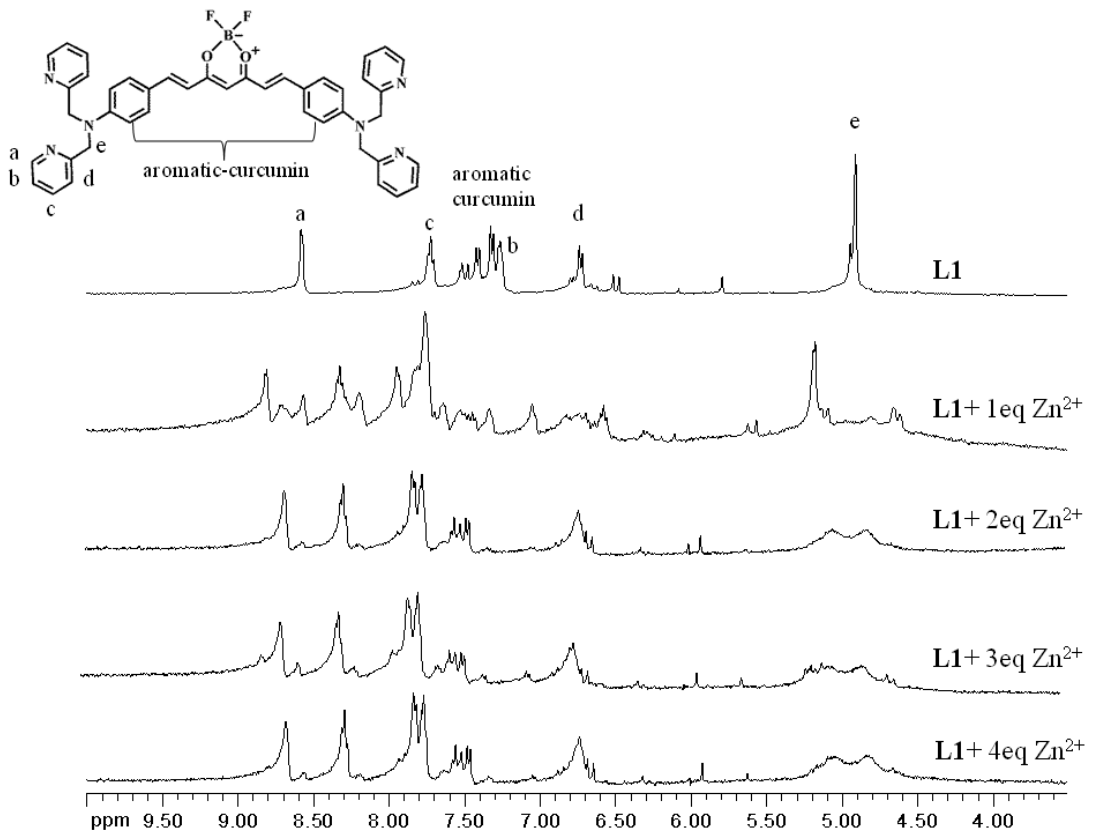

Figure 4.11 The ^{1}H-NMR titration spectra of sensor **L1** with Zn^{2+} ion in CD_3CN (400 MHz).

Table 4.3 ^{1}H-NMR chemical shift (ppm) for sensor **L1** with Zn^{2+} ion in CD_3CN (400 MHz).

^{1}H-NMR in species	NC*H*	aromatic proton of remain pyridine	CH_2
L1	8.57	7.72-6.47	4.90
0.1 eq	8.57	7.74-6.47	4.91
0.2 eq	8.59	7.78-6.47	4.93
0.3 eq	8.61	7.83-6.47	4.95
0.4 eq	8.64	ND	4.99
0.5 eq	8.67	ND	5.03
0.6 eq	8.69	8.17-6.63	5.06
0.7 eq	8.74	8.19-6.68	5.10
0.8 eq	8.74	8.56-6.63	5.15
0.9 eq	8.77	8.54-6.59	5.17
1.0 eq	8.79	ND	5.16
1.2 eq	8.80	8.70-6.55	5.17
1.4 eq	8.80	8.66-6.55	5.17
1.6 eq	8.81	8.67-6.74	5.17
1.8 eq	ND	ND	*
2.0 eq	ND	8.65-6.74	*
2.5 eq	8.67	8.29-6.73	*
3.0 eq	8.67	8.29-6.68	*
3.5 eq	8.68	8.29-6.68	*
4.0 eq	8.68	8.29-6.68	*
5.0 eq	8.67	8.29-6.68	*

* disappearance of peak

ND = not determined

All spectra were recorded on Variance 400 MHz nuclear resonance spectrometers.

4.4.2 Cations Zn^{2+} and Cu^{2+} complexation studies by UV-Vis and fluorescence spectrophotometry

Ligand **L1** posses three nitrogen atom of dipicolyl amine moieties as binding sites for Zn^{2+} and Cu^{2+} ion and BF_2-curcumin is expected to be an excellent fluorophore for cation sensing. The maximum absorption and emission band of ligand **L1** displayed at 488 nm and 587 nm, respectively (spectra illustrated in Figure 4.12).

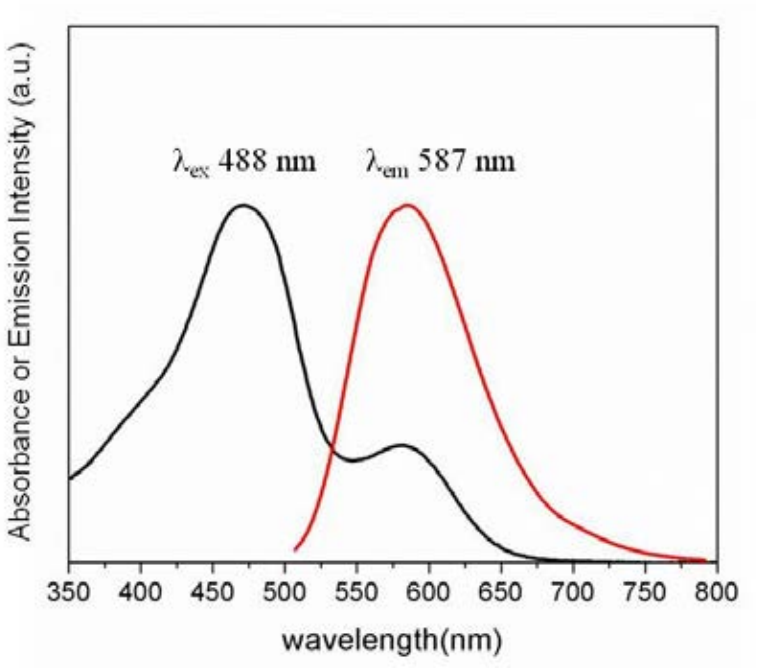

Figure 4.12 The absorption and the emission spectra of **L1** in acetonitrile.

4.4.2.1 Cations Zn^{2+} complexation studies by UV-Vis and fluorescence spectrophotometry

The complexation abilities of ligand **L1** with Zn^{2+} ion have been investigated using the absorption titrations. The Absorption spectra of ligand **L1** (in Figure 4.13) was changed upon a gradual increase of Zn^{2+} solution. All experiments of absorption titrations were carried out in acetonitrile. The UV-Vis spectra of unbound **L1** showed

the absorption band at 472 nm and 581 nm corresponding to the BF_2-Cur part defined as an acceptor group. The characteristic peak of dipicolyl amine moieties as donor groups displayed a small absorption band at 258 nm. Upon the gradual addition of Zn^{2+} ion to a solution of **L1**, the absorption bands of **L1** at 472 and 581 nm were progressively decreased while a new band at 421 nm was developed. In addition, the absorption band at 258 nm of dpa part was decreased with a concomitant of a small blue shift. It was indicative of the occurrence of zinc complexed to **L1** at dipicolyl amine parts.[68] The blue shift of absorption band at 472 nm and 581nm upon the addition of Zn^{2+} ion can be explained that the electron acceptor ability of the difluoroboron unit was reduced since the lone pair electron on N atom of dpa unit was employed to bind with Zn^{2+} resulting in the suppression of electron delocalization through the conjugate system to the BF_2-Cur part. [69] Additionally, the visually color change from orange to yellow was markedly observed upon binding with Zn^{2+} (Figure 4.13 inset).

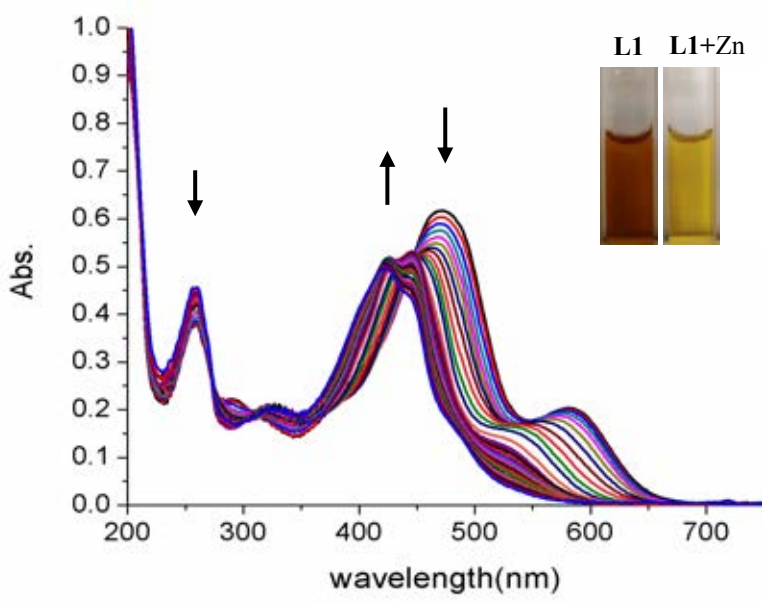

Figure 4.13 The absorption spectra changes of **L1** (1.80×10^{-5} M) upon the addition of Zn^{2+} (3.60×10^{-4} M), (inset) the color change of **L1** and **L1**+Zn^{2+} in acetronitrile.

Moreover, the cation complexation ability of ligand **L1** with Zn^{2+} ion was also investigated by the fluorometric titrations in acetonitrile. The fluorescence response of unbound **L1** appeared the characteristic emission band at 587 nm corresponding to fluorophore BF_2-curcumin. Upon the addition of Zn^{2+} ion, the fluorescence intensity was gradually quenched along with a small bathochromic shift from 587 nm to 615 nm (as shown in Figure 4.4). The change in the fluorescence spectrum has been attributed to the complexation of Zn^{2+} and **L1**.[32] We proposed that a small bathochromic shift for the complexation of **L1**⊂Zn^{2+} was occurred by the substantial suppression of NLCT (spin-allowed amine-to-ligand charge-transfer) character in their emissive states.[70]

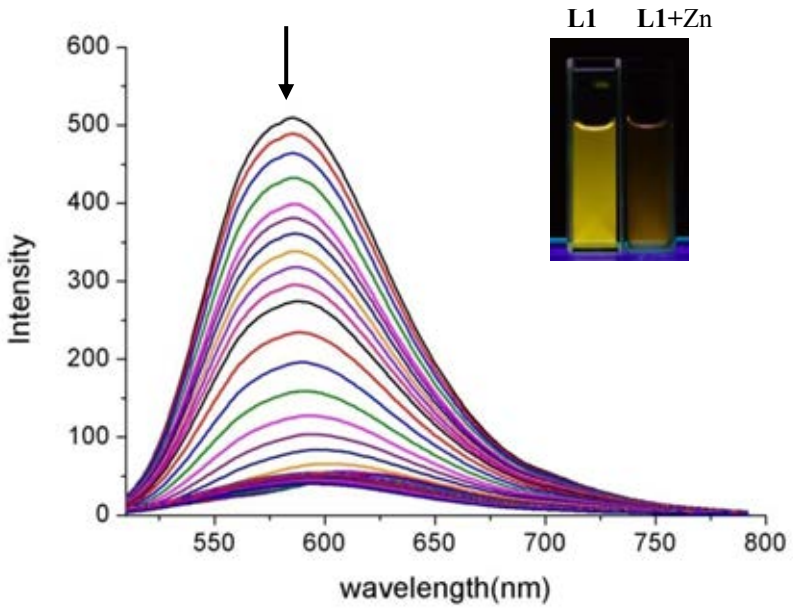

Figure 4.14 The fluorescence spectrum of **L1** ($5x10^{-6}$ M) in acetonitrile upon the addition of Zn^{2+} ($2.00x10^{-4}$ M), (inset) the color changes of **L1** and **L1**+Zn^{2+} in acetronitrile upon the exposure under UV lamp at 365 nm.

The Job's plot analysis was evaluated to determine the binding mode of **L1** and Zn^{2+} using fluorescence technique. A Job's plot showing a maximum point at 0.67 mole fraction indicates that the stoichiometry of host and guest is 1:2 complexes as shown in Figure 4.15.

The fluorimetric titration was performed at least twice and the binding constant of **L1**⊂Zn^{2+} determined by SPECFIT32 program was collected in Table 4.4. The log *K* value of **L1**⊂2Zn complex was found to be 8.25.

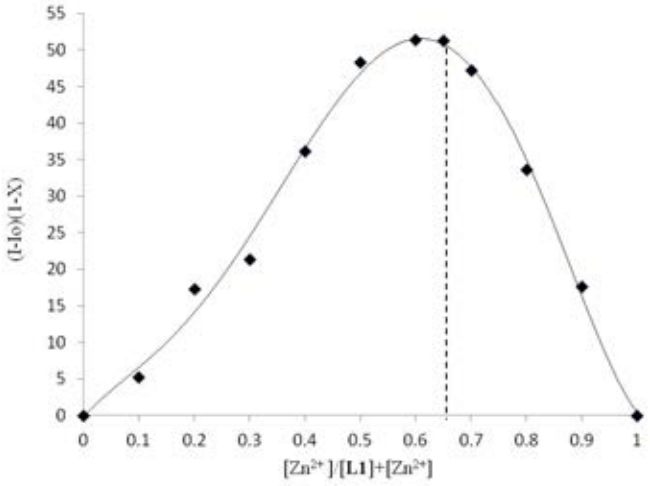

Figure 4.15 Job's plot of the complexation between **L1** and Zn^{2+} was measured by fluorescence spectrophotometry

Table 4.4 The binding constants of ligand **L1** towards Zn^{2+}

first		second		average	
log *K*	SD	log *K*	SD	log *K*	SD
8.26	± 0.1057	8.25	± 0.1372	8.255	± 0.1214

The detection limit of Zn^{2+} ion for **L1** was calculated as following the equation of

$$LOD = 3SD/S$$

where SD is the standard deviation of the blank and S is a slope of calibration curve.

According to the data from table 4.5 and Figure 4.16, the detection limit of Zn^{2+} by **L1** was 5.52×10^{-8} M or 3.60 ppb in acetonitrile.

Table 4.5 Fluorescence intensity data of free **L1** at 588 nm for repetition 10 times and its standard deviation

free L2•Zn	**I_F at 587 nm**
1	326.2759
2	321.4394
3	317.2442
4	316.1473
5	317.0889
6	314.0702
7	313.536
8	313.5498
9	310.0667
10	309.7274
SD	5.035566
3SD	15.1067

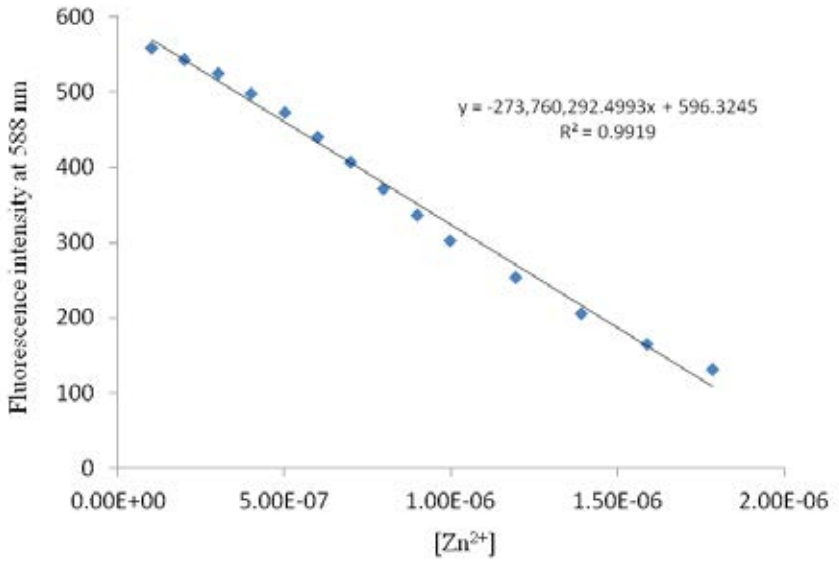

Figure 4.16 Plot of fluorescence intensity of **L1**⊂2Zn^{2+} complex at 588 nm versus concentration of Zn^{2+}.

In order to further test the interference for other common metal ions on the determination of Zn^{2+}, a competition experiment was performed. The fluorescent probe **L1** in the presence of Zn^{2+} was added by exam of other metal ions. The concentration of **L1** was fixed at 5.0×10^{-6} M in acetonitrile. The fluorescence intensity of **L1** was significantly quenched upon the addition of 10 equiv of Zn^{2+}. Upon the addition of 100 equiv. of various metal ions including Co^{2+}, Ni^{2+} and Cu^{2+}, the fluorescence quenching was remarkably observed. The case of Ag^{+} did not induce the fluorescence change of **L1**⊂2Zn^{2+} and Cd^{2+} showed a small fluorescence quenching. The relative error of a competition experiment was listed in Table 4.6. We found that the influence of other transition metals toward the Zn^{2+} sensing of **L1** showed the relative error less than ±10% indicating that **L1** has an excellent selectivity for Zn^{2+}.

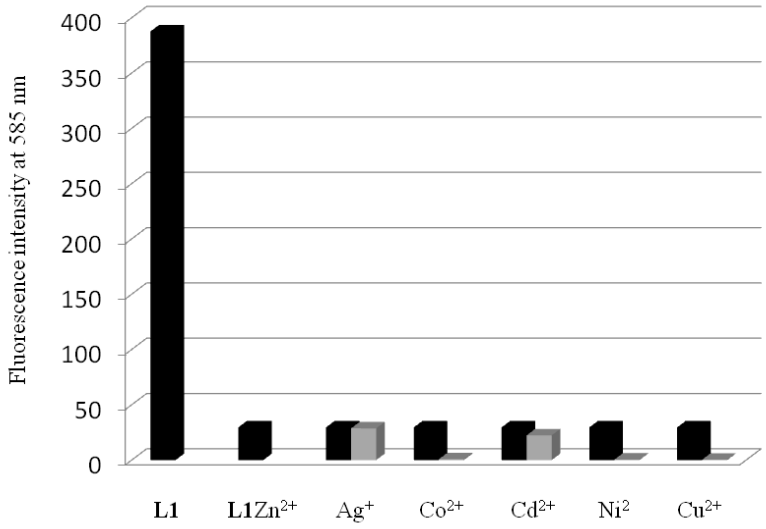

Figure 4.17 Fluorescence intensity changes of **L1** (5.0×10^{-6} M) in the presence of 10 equiv of Zn^{2+} (back bar) followed by 100 equiv of other cations (gray bar).

Table 4.6 Interference of several metal ions to the fluorescence response of **L1** with Zn^{2+} (4.76×10^{-5} mol/L)

Interference	Concentration (mol/L)	Fluorescence ($\triangle F=F-F_o$)	Relative error (%), ($\triangle F/F_0)\times100$
Ag^{+}	4.76×10^{-3}	0.84472	-0.24
Co^{2+}	4.76×10^{-3}	-28.7489	-8.03
Cd^{2+}	4.76×10^{-3}	-7.16991	-2.00
Ni^{2+}	4.76×10^{-3}	-29.0731	-8.18
Cu^{2+}	4.76×10^{-3}	-29.1245	-8.13

4.4.2.2 Cations Cu^{2+} complexation studies by UV-Vis and fluorescence spectrophotometry

The UV-Vis titration spectra of **L1** toward Cu^{2+} ion were carried out in acetonitrile. Figure 4.18 displayed the absorption change of **L1** with a gradual increase amount of Cu^{2+} solution. The UV-Vis spectra of unbound **L1** showed the absorption band at 472 nm and 581 nm. Upon the addition of Cu^{2+} ion to a solution of **L1**, the absorption band at 472 and 581 nm decreased gradually and a new band at 421 nm was appeared. Furthermore, the absorption band at 258 nm corresponding to dpa part was progressively developed along with a small blue shift. It suggested that the Cu^{2+} was complexed to **L1** at dipicolyl amine parts. It is noteworthy that the absorption peak *ca.*315 nm is a characteristic peak of Cu^{2+} ion observing from the gradual increase of this peak upon the increment of Cu^{2+}.

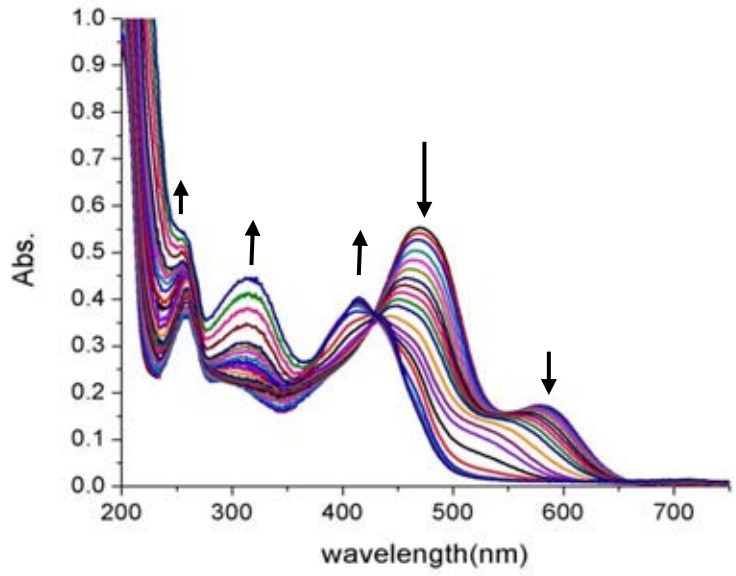

Figure 4.18 The absorption spectral changes of **L1** ($2.00x10^{-5}$ M) upon the addition of increasing amounts Cu^{2+} ($1.00x10^{-3}$ M)

Considering, the fluorescence responses of **L1** to Cu^{2+} ion by fluorometric titration in acetonitrile exhibited in Figure 4.19. The characteristic emission band of **L1** appeared at 587 nm. After adding the solution of Cu^{2+} ion, the fluorescence

spectra showed a strongly fluorescent quenching at 587 nm with a concomitant of the small blue shift corresponding to the binding of the copper ion to receptor. The fluorescence quenching behavior underwent a PET mechanism which was described that the electron configuration of Cu^{2+} as d^9 was stabilized by obtaining the electron at excited state of ligand.[71] Consequently, the excited electron could not transfer to ground state resulting in quenching the fluorescent intensity.

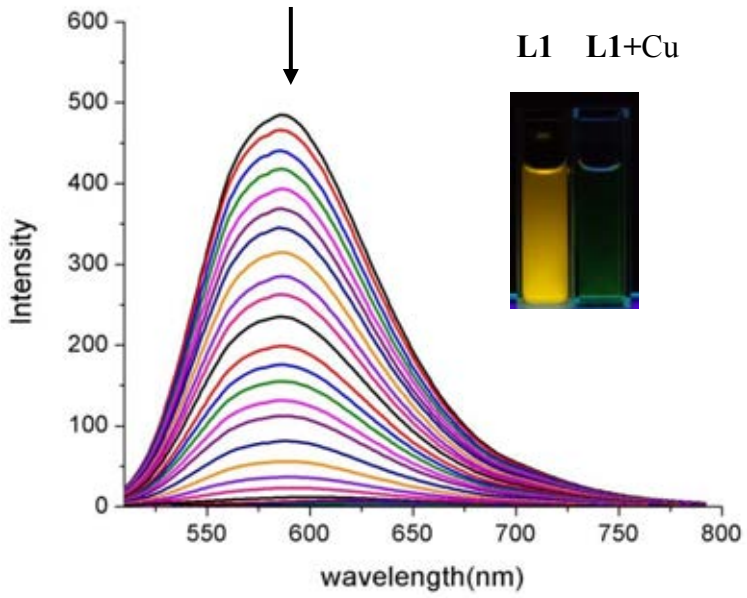

Figure 4.19 The fluorescence spectrum of **L1** ($5x10^{-6}$ M) in acetonitrile upon addition of increasing amounts of Cu^{2+} ($2.00x10^{-4}$ M), (inset) the color change between **L1** and **L1**+Cu^{2+} in acetronitrile under UV lamp at 365 nm.

The Job's plot analysis for the stoichiometry of **L1** and Cu^{2+} showed the maximum point at 0.67 mole fraction suggesting a 1:2 binding mode (Figure 4.20). The fluorimetric titration was performed at least twice and the binding constant of **L1** with Cu^{2+} determined by SPECFIT32 program was recorded in Table 4.7. The log *K* value of **L1•2Cu** complex was found to be 10.52.

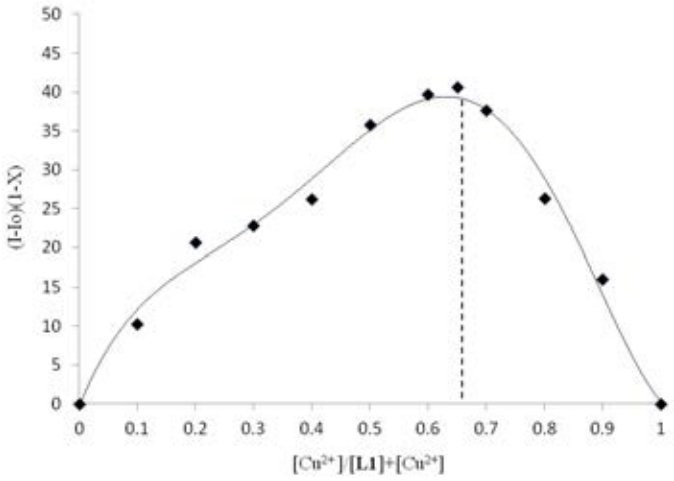

Figure 4.20 Job's plot of the complexation between **L1** and Cu^{2+} was measured by fluorescence spectrophotometry.

Table 4.7 The binding constants of ligand **L1** towards Cu^{2+}

first		second		average	
log *K*	SD	log *K*	SD	log *K*	SD
10.53	± 0.04271	10.51	± 0.03016	10.52	± 0.03643

Fluorescence detection limit of Cu^{2+} for **L1** calculated on the basis of 3SD/slope was found to be 1.24×10^{-7} M or 7.90 ppb. (Figure 4.21)

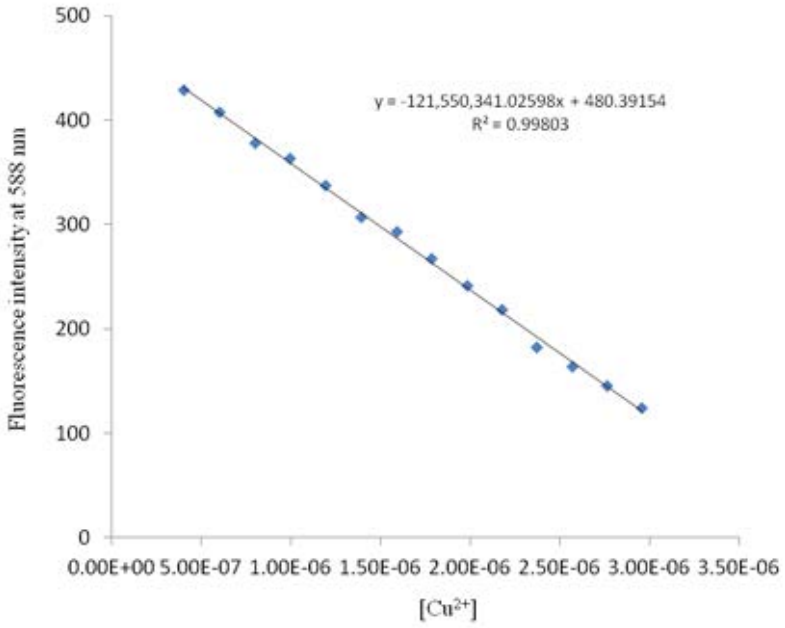

Figure 4.21 Plot of fluorescence intensity of **L1**·2Cu^{2+} complex at 588 nm versus concentration of Cu^{2+}.

The interference of other cations toward Cu^{2+} sensing for **L1** was examined using fluorescence technique (shown in Figure 4.22.). The fluorescence spectra showed no significant change for all other metal ions. The relative errors of a competition of transition metals were collected in Table 4.8. Thus, **L1** posses a high selectivity for Cu^{2+} over Zn^{2+} ion.

The relative errors of a competition of the transition metal toward Cu^{2+} detection are less than ±10%. Considering, the influence of other metal ions toward Cu^{2+}sensing for **L1** showed % relative error less than that of other metal ions toward Zn^{2+}sensing. This implied that **L1** preferred to bind Cu^{2+} over Zn^{2+} which agreed with the binding constant results.

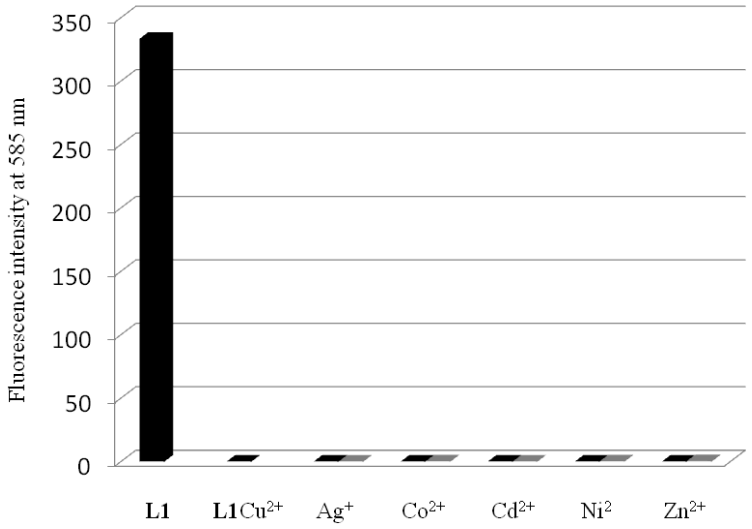

Figure 4.22 Fluorescence intensity changes profile of **L1** (5.0×10^{-6} M) in the presence of 10 equiv of Cu^{2+} (black bar) followed by 100 equiv of other cations (gray bar).

Table 4.8 Interference of several metal ions to the fluorescence response of **L1** with Cu^{2+} (4.76×10^{-5} mol/L)

Interference	Concentration (mol/L)	Fluorescence ($\triangle F=F-F_o$)	Relative error (%), ($\triangle F/F_0$)×100
Ag^{+}	4.76×10^{-3}	0.0202	0.01
Co^{2+}	4.76×10^{-3}	0.2539	0.08
Cd^{2+}	4.76×10^{-3}	0.0220	0.01
Ni^{2+}	4.76×10^{-3}	0.2521	0.07
Zn^{2+}	4.76×10^{-3}	0.4366	0.13

4.5 The complexation study of L1•2Zn with nucleotide in aqueous solution

In order to study the binding ability with nucleotide, we used **L1•2Zn** complex is a sensor for detection of nucleotide in aqueous solution. Figure 4.23 showed the fluorescence change of **L1•2Zn** upon the addition of ATP in HEPES buffer (0.01 M, pH 7.4) and water. The result showed that after adding the solution of ATP in HEPES buffer, the fluorescence spectrum of **L1•2Zn** complex was turned to free ligand **L1** which displayed the characteristic emission band at 587 nm corresponding of free **L1**. It is indicated that Zn^{2+} ion was removed from **L1** in the water. To gain more information results, the addition of water into the solution of **L1•2Zn** complex gave the identical fluorescence response with the free ligand **L1**. The removal of Zn^{2+} ion from **L1** was occurred in water because the lone pair electron of nitrogen atoms at *para* substituted position of benzene ring would delocalize into the conjugate system of BF_2-Cur part and subsequent to suppress the binding ability of Zn^{2+} with the N atom adjacent to aromatic ring based curcumine derivatives . Therefore, the binding affinity between Zn^{2+} and two N atoms based pyridine part is very poor. The purposed binding mechanism of **L1** with Zn^{2+} ion was demonstrated in Figure 4.24.

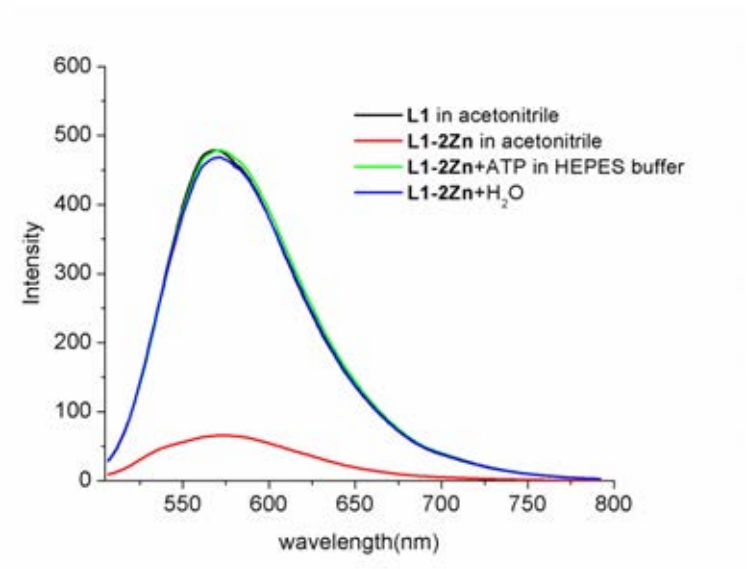

Figure 4.23 The fluorescence spectral changes of **L1** and **L1•2Zn** upon the addition of ATP in HEPES buffer and H_2O.

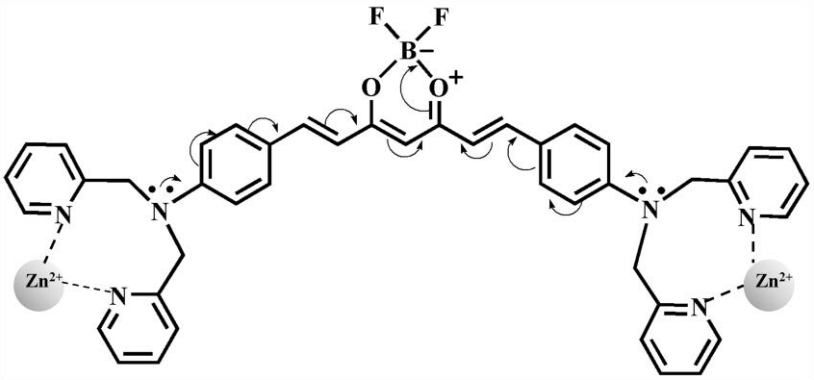

Figure 4.24 The proposed binding mode of **L1** with Zn^{2+} ion.

However, the use of **L1•2Zn** for nucleotide sensing in aqueous media cannot be studied as a result of Zn^{2+} removal from **L1** in water. Therefore, the **L1•2Zn** complex cannot be applied to nucleotide-sensing purpose in aqueous.

4.6 The complexation studies of ligand L2•Zn by fluorescence spectrophotometry

Ligand **L2** containing three nitrogen atom of dipicolyl amine moiety is favorable to chelate Zn^{2+} ion. This sensor has a pyrene unit as a fluorophore. Therefore, it is an interest of studying the effect of anions toward the binding abilities of **L2•Zn** complex. Considering, types of nucleotide anion with a different charge and structure might influent on the binding properties. Consequently, we paid attention on studying the binding properties of **L2•Zn** toward various nucleotide anions such as PPi, ATP, ADP, AMP, UTP, UDP, UMP, GDP, GMP and CMP in two conditions of media.

The sensor **L2•Zn** was synthesized for binding to various nucleotides by using electrostatic interactions based on metal-ligand coordination. The maximum absorption band of **L2•Zn** complex displayed 3 bands at 315, 330 and 347 nm. The characteristic emission band of sensor **L2•Zn** appeared at 360–450 nm which was assigned to the pyrene monomer emission as shown in Figure 4.25.

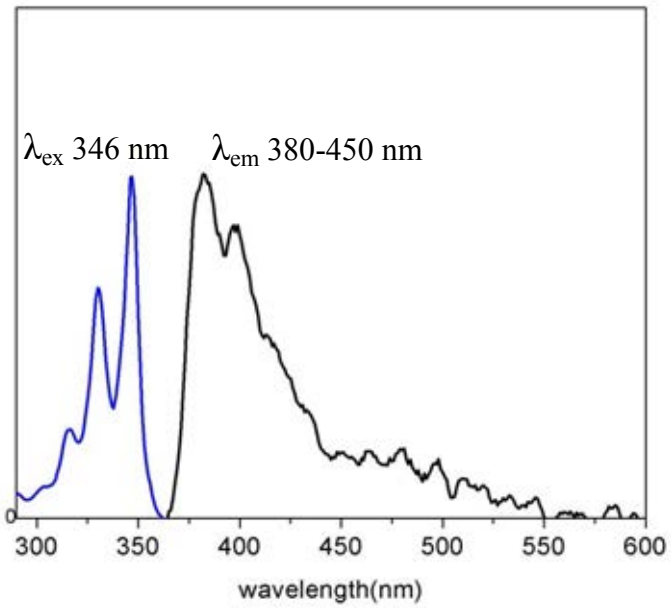

Figure 4.25 The absorption and the emission spectra of **L2•Zn** in aqueous solution (DMSO:HEPES buffer 0.01M, pH 7.4, 1:99 v/v).

The sensing ability of **L2•Zn** with nucleotides was investigated by fluorescence spectrophotometry in aqueous solution with 2 different solvent systems of in 1:99 and 90:10 v/v DMSO:HEPES buffer (10 mM, pH 7.4).

4.6.1 The complexation studies of sensor L2•Zn in 1:99 v/v DMSO:HEPES buffer (10 mM, pH 7.4) by fluorescence spectrophotometry

Generally, most biological applications are relevant in aqueous media. Hence, the sensing ability of **L2•Zn** with nucleotides was investigated by fluorescence spectrophotometry in aqueous solution of DMSO:HEPES buffer (10 mM, pH 7.4 with 1:99 v/v).

Figure 4.26 exhibited the effect of nucleotide anions on the fluorescence spectra of sensor **L2•Zn** in an aqueous solution of DMSO:HEPES buffer (10 mM, pH 7.4 with 1:99 v/v). The characteristic emission band of sensor **L2•Zn** appeared at 360–450 nm which was assigned to the pyrene monomer emission. Upon the addition of various nucleotide anions, PPi showed an obvious fluorescence enhancement of monomer emission. A slight fluorescence enhancement was observed upon the

addition of ATP and ADP, while other nucleotides show slight change in their spectra. These results suggested that sensor **L2•Zn** has a higher sensitivity for PPi over other nucleotides in the order of PPi > ATP > ADP.

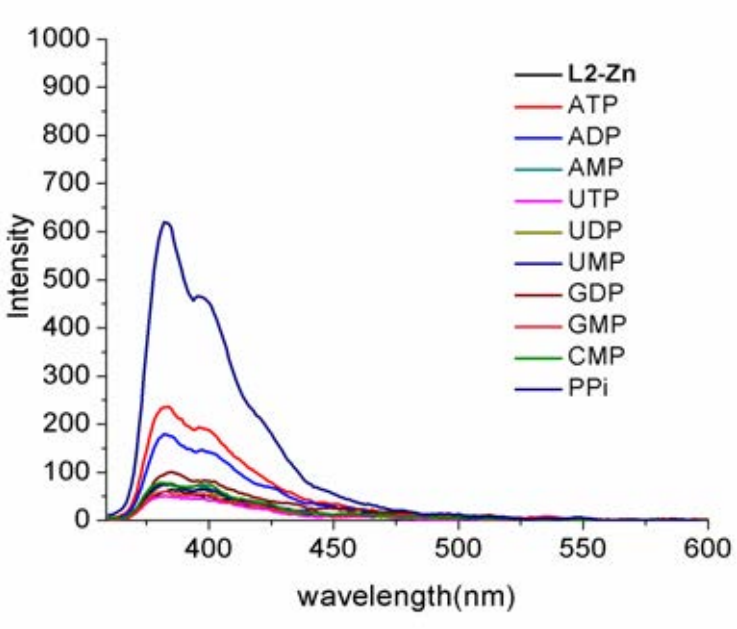

Figure 4.26 Fluorescence emission spectra of **L2•Zn** ($1x10^{-5}$ M) in DMSO:HEPES buffer (0.01M, pH 7.4) (1:99 v/v) in the presence of various nucleotides (10 equiv). Excitation wavelength is 346 nm.

The fluorescence titration of **L2•Zn** with PPi in aqueous solution was illustrated in Figure 4.27. Upon the gradual addition of PPi solution into the solution of **L2•Zn** complex**,** the fluorescence intensity at ca. 380-450 nm assigned to monomer pyrene progressively increased. The fluorescence enhancement of **L2•Zn** can be described that PPi promoted the strong complex of the Zn^{2+} coordination with nitrogen atoms of dpa moiety. Addition of PPi presumably produced its electrostatic and coordination assistance to form **L2•Zn**-PPi complex. Hence, this binding mode can prohibit the electron transfer from nitrogen donor atom of dpa part to pyrene, resulting in the fluorescence enhancement.[72]

The fluorimetric titration was performed 2 times and the binding constants obtained by SPECFIT32 program were recorded in Table 4.9. The log *K* value of

L2•Zn complexed with PPi was 10.22 ± 0.03. In the case of ATP and ADP, their log *K* values cannot be determined. The Job's plot analysis for the binding mode of **L2•Zn** and PPi showed the maximum point at approximately 0.30 mole fraction suggesting a 2:1 stoichiometry illustrated in Figure 4.28. The selectivity of **L2•Zn** for PPi over ATP can be explained on the basis of the structural anion and the charge density of phosphate unit. The total negative charge density of phosphate unit based PPi is much higher than that of phosphate unit based ATP.[73, 74]

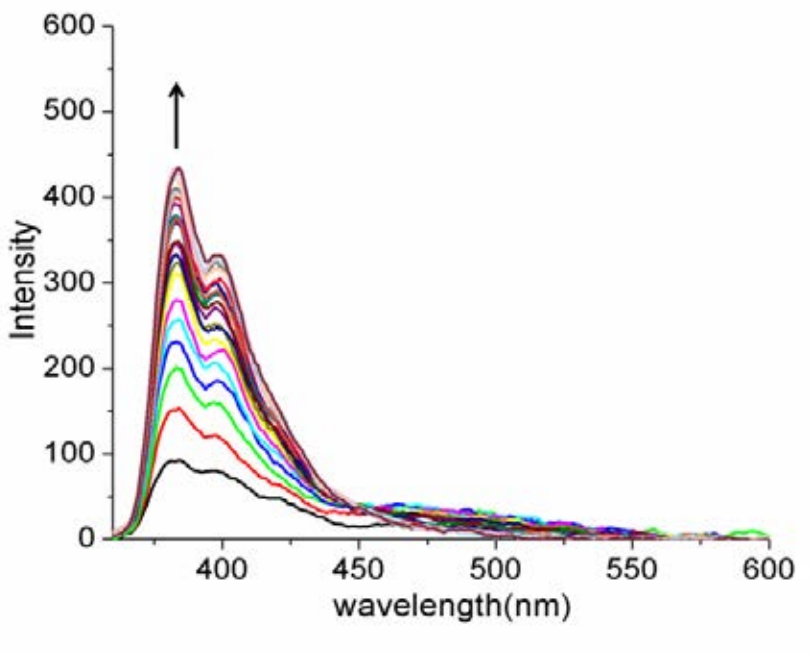

Figure 4.27 Fluorescence titration of **L2•Zn** ($1x10^{-5}$ M) upon addition of PPi in DMSO:HEPES buffer (0.01M, pH 7.4) (1:99 v/v).

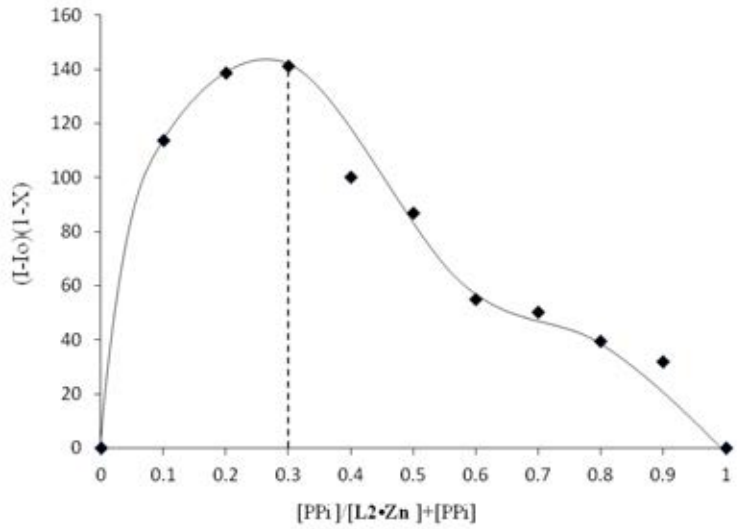

Figure 4.28 Job's plot of the complexation between **L2•Zn** and PPi was measured by fluorescence spectrophotometry.

Table 4.9 The binding constants of ligand **L2•Zn** towards PPi

first		second		average	
log *K*	SD	log *K*	SD	log *K*	SD
10.22	± 0.03481	10.22	± 0.03724	10.22	± 0.03602

Furthermore, to develop the PPi sensing application of **L2•Zn** on solid support, the word "PPi" was prepared by the solution of **L2•Zn** on the filter paper using paintbrush and then dipped in PPi solution. Upon exposure to the UV irradiation at 365 nm, the word "PPi" exhibited a tremendous brighter luminescence as shown in Figure 4.29.

(a) (b)

Figure 4.29 Image patterns of **L2•Zn** dipped with PPi solution on a filter paper (a) in the visible light and (b) under UV irradiation at 365 nm.

The detection limit of **L2•Zn** for minimum detection of PPi using the fluorescence technique was found to be 8.90×10^{-8} M. The fluorescence intensity of **L2•Zn** and standard deviation were recorded in Table 4.10. Figure 4.30 showed the calibration curve of **L2•Zn** with increasing amount of PPi in aqueous solution.

Table 4.10 Fluorescence intensity data of free **L2•Zn** at 379 nm for repetition 10 times and its standard deviation in DMSO:HEPES (1:99 v/v)

free L2•Zn	**I_F at 587 nm**
1	51.28407
2	52.27292
3	52.49924
4	54.77846
5	51.11066
6	50.49717
7	52.37495
8	50.46529
9	53.2473
10	53.41538
SD	1.385723
3SD	4.157169

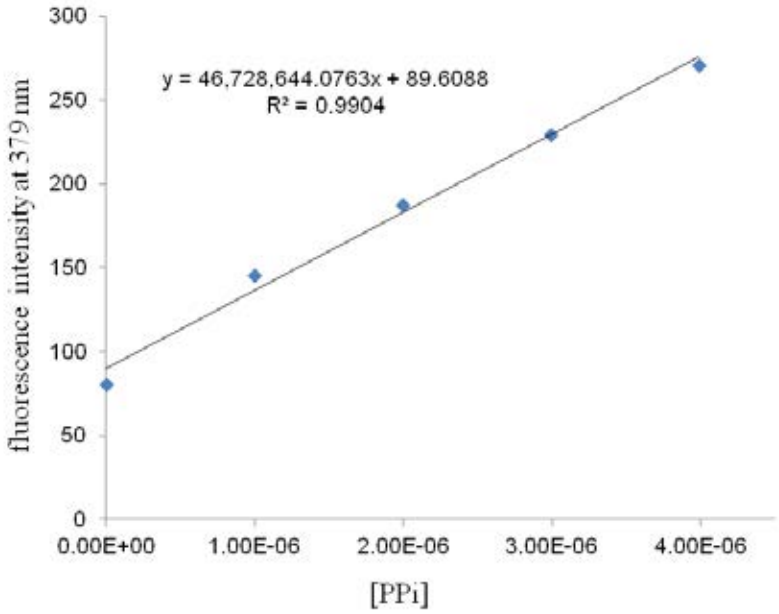

Figure 4.30 Plot of fluorescence intensity of **L2·Zn** with PPi complex at 379 nm versus concentration of PPi.

4.6.2 The complexation studies of sensor L2•Zn in 90:10 v/v DMSO:HEPES buffer (10 mM, pH 7.4) by fluorescence spectrophotometry

Actually, most of anion sensors function in organic solvent because the solvation energy is relatively small and the electrostatic interactions operate effectively. Hence, we also investigated the binding properties of **L2•Zn** and nucleotides in organic solvent (90% of DMSO in H_2O). Figure 4.31 showed the fluorescence changes of **L2•Zn** upon the addition of various analytes such as UTP, ATP, UDP, ADP, GDP, UMP, AMP, GMP, CMP and PPi in DMSO:HEPES (0.01 M, pH 7.4, 90:10 v/v). Upon the addition of nucleoside triphosphate such as UTP and ATP, the observation of the strong fluorescence enhancement of **L2•Zn** at 383 nm indicated a high affinity towards UTP and ATP. For nucleoside diphosphates (ADP, UDP, GDP), the emission band was slightly changed, while nucleoside monophosphate (AMP, GMP, CMP, UMP) did not induce any fluorescence changes of **L2•Zn**. In contrast, PPi induced a small fluorescence quenching at 383 nm.

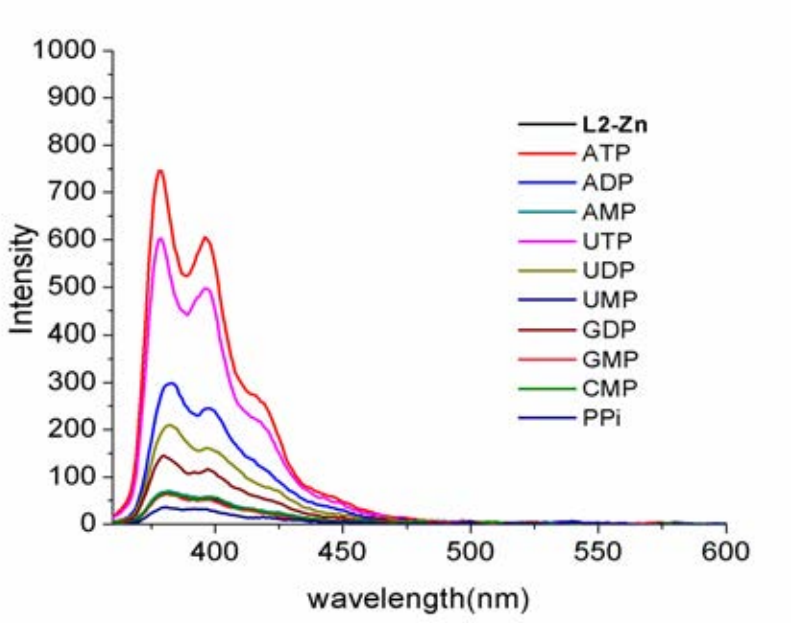

Figure 4.31 Fluorescence emission spectra of **L2•Zn** ($1x10^{-5}$ M) in DMSO:HEPES buffer (0.01M, pH 7.4) (90:10 v/v) in the presence of various nucleotides (10 equiv). Excitation wavelength is 346 nm.

Figure 4.32 exhibited the relative fluorescence emission responses of **L2•Zn** in increasing the concentration of various nucleotide anions including ATP, UTP, ADP and GDP. This study showed a small fluorescence changes in ADP and UDP and the significant changes in the case of ATP and UTP. Unfortunately, the binding constants of the complexation between **L2•Zn** and various nucleotides such as ATP, UTP, UDP and ADP cannot be determined by analysis of the emission spectra. However, the preliminary results from fluorescence titration showed the selectivity of **L2•Zn** in the order of ATP, UTP > ADP, UDP. The binding properties of **L2•Zn** with various number of phosphate species based nucleotides can be ascribed under the fluorescence changes. It can be implied that electrostatic interaction is an important factor to effective metal-ligand coordination. The different binding mode may be attributed by various numbers of anionic charges of the phosphate species based nucleotide. Thus, the polyanionic species would preferably form with the cationic Zn^{2+} clelated compound over the monoionic species. [75]

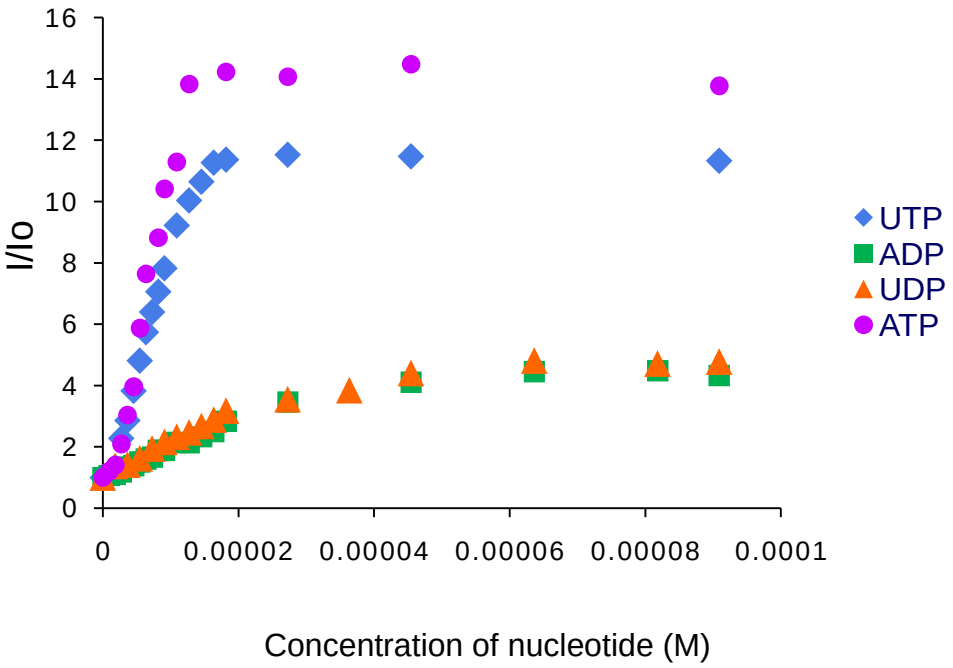

Figure 4.32 Relative fluorescence emission response of **L2·Zn** ($1x10^{-5}$ M) to the anion concentration in DMSO:HEPES (90:10 v/v) (0.01M, pH 7.4).

The detection limits of **L2•Zn** with ATP, UTP, ADP and UDP were calculated similarly to in aqueous solution by 3SD/slope. The fluorescence intensity of **L2•Zn** and standard deviation in 90% DMSO were recorded in Table 4.11. Figure 4.33 demonstrated the fluorescence titration plot of **L2•Zn** with increasing amount of nucleotides in 90%DMSO. The detection limits of **L2•Zn** for minimum detection of ATP, UTP, ADP and UDP were $1.12x10^{-7}$, $1.11x10^{-7}$, $9.66x10^{-7}$ and $1.03x10^{-6}$ M, respectively. (as listed in Table 4.12)

Table 4.11 Fluorescence intensity data of free **L2•Zn** at 379 nm for repetition 10 times and its standard deviation in DMSO-HEPES (90:10 v/v)

free L2•Zn	**I_F at 587 nm**
1	52.3404808
2	52.43090439
3	52.02252579
4	53.87373352
5	56.43795013
6	52.24953842
7	58.77352142
8	53.03754044
9	54.33998108
10	58.33358765
SD	2.566540144
3SD	7.699620431

(a)

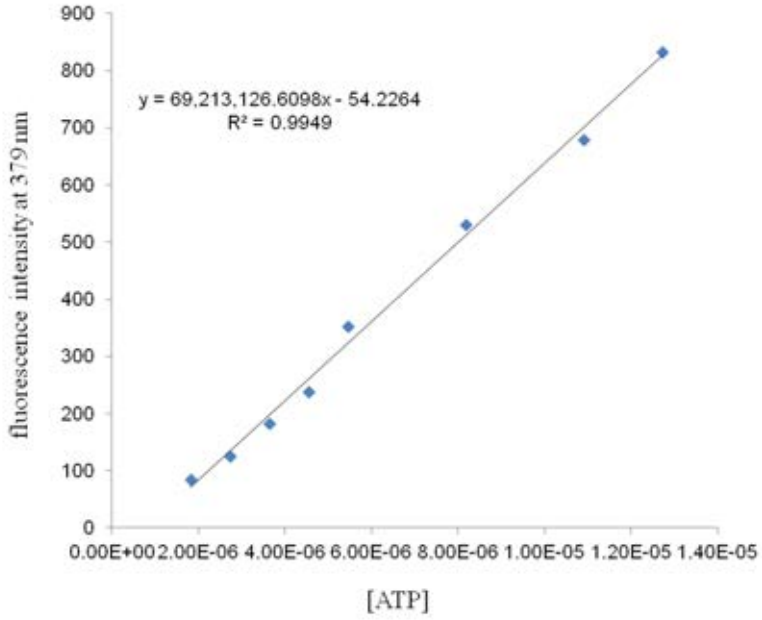
y = 69,213,126.6098x - 54.2264
R² = 0.9949
fluorescence intensity at 379 nm
[ATP]
0
100
200
300
400
500
600
700
800
900
0.00E+00
2.00E-06
4.00E-06
6.00E-06
8.00E-06
1.00E-05
1.20E-05
1.40E-05

(b)

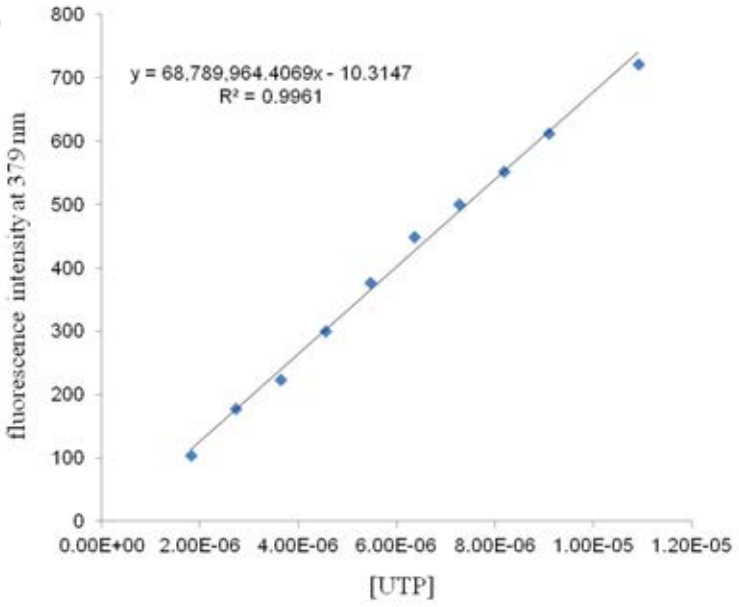
y = 68,789,964.4069x - 10.3147
R² = 0.9961
fluorescence intensity at 379 nm
[UTP]
0
100
200
300
400
500
600
700
800
0.00E+00
2.00E-06
4.00E-06
6.00E-06
8.00E-06
1.00E-05
1.20E-05

(c)

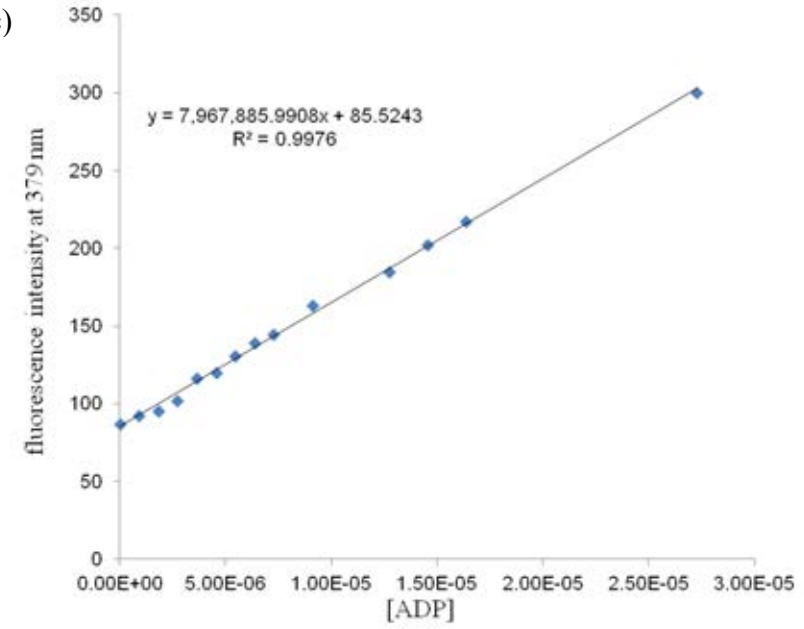

(d)

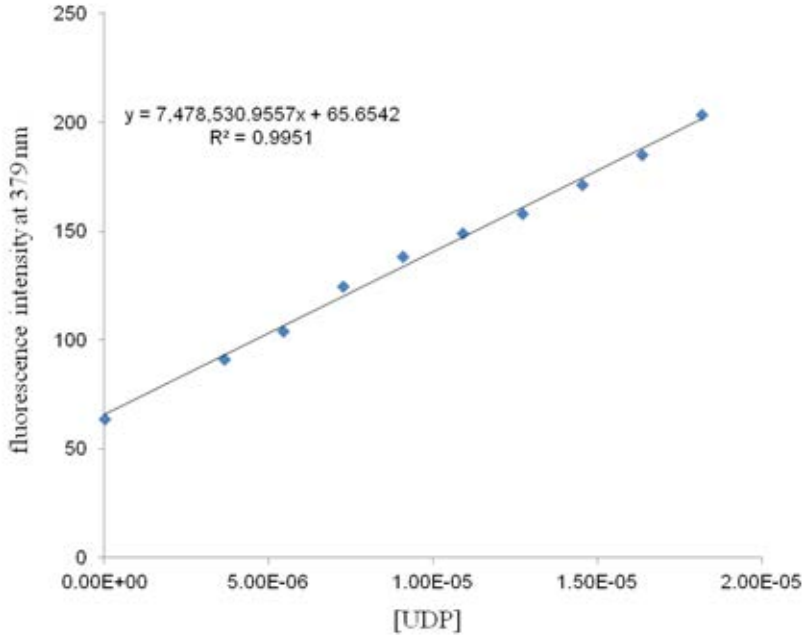

Figure 4.33 Plot of fluorescence intensity of **L2·Zn** with (a) ATP (b) UTP (c) ADP and (d) UDP complex at 397 nm versus concentration of nucleotides.

Table 4.12 Detection limit of **L2•Zn** toward ATP, UTP, ADP and UDP at 379 nm in DMSO:HEPES (90:10 v/v)

nucleotides	LOD (M)
ATP	$1.12x10^{-7}$
UTP	$1.11x10^{-7}$
ADP	$9.66x10^{-7}$
UDP	$1.03x10^{-6}$

4.6.3 Study on the binding mode of L2•Zn and nucleotides using the computational method and NMR spectroscopy

The structural optimizations of PPi/(**L2•Zn**)$_2$, ATP/(**L2•Zn**)$_2$ complexes and their components were carried out using density functional theory (DFT) at the B3LYP/LANL2DZ level of theory. All computations were performed using GAUSSIAN 03 program.[76]The optimized structures of PPi and ATP complexes were illustrated in Figure 4.34[77-79]. Upon complexation of **L2•Zn** with PPi and ATP, the strong bonds between cationic Zn^{2+} ion and oxygen atom of PPi and ATP occurred. The interactions of PPi/(**L2•Zn**)$_2$ and ATP/(**L2•Zn**)$_2$ complexes mainly stemmed from six and five hydrogen bonding interactions, respectively. Furthermore, the most stable form of PPi/(**L2•Zn**)$_2$ and ATP/(**L2•Zn**)$_2$ complexes cannot induce the eximer formation of pyrene moieties. This result is consistent with the results obtained by the fluorescence method.

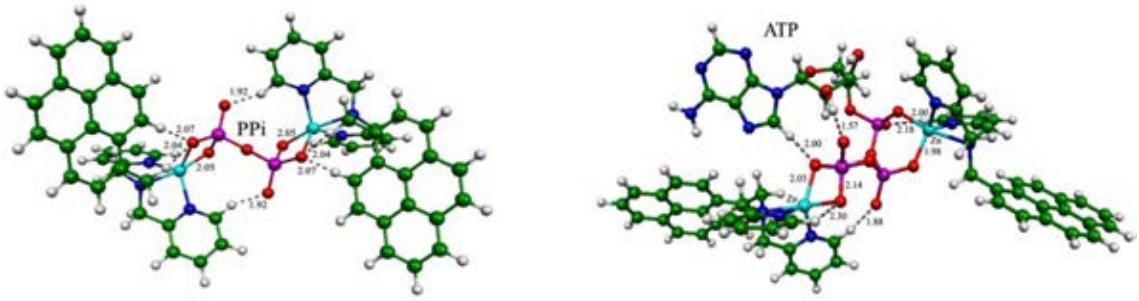

(a) (b)

Figure 4.34 The B3LYP/LANL2DZ optimized structures of (a) PPi/(**L2•Zn**)$_2$ and (b) ATP/(**L2•Zn**)$_2$ complexes. The bond lengths and bond distances are in Å.

The association energies of overall associations of **L2•Zn** complexed with ATP and PPi in the gas phase and aqueous phase, and free energy of their association in aqueous solution are collected in Table 4.13. The results showed that the formation of PPi/(**L2•Zn**)$_2$ was more stable than that of the ATP/(**L2•Zn**)$_2$, either in gas phase or aqueous phase. Therefore, the PPi/(**1•Zn**)$_2$ association is a more thermodynamically favourable pathway in aqueous solution.

Table 4.13 The association energies of overall associations of ATP complexed with **L2•Zn** and PPi complexed with **L2•Zn**, in gas phase and aqueous phase, and free energy of their association in aqueous solution.

Overall association	$\triangle E$ [a]		$\triangle G^{298}$ [a]
	In vacuo [b]	In aqueous [c]	In aqueous [c]
2 **L2•Zn** + ATP →ATP/(**L2•Zn**)$_2$	–922.16	–105.78	–90.73
2 **L2•Zn** + PPi → PPi/(**L2•Zn**)$_2$	–1,100.64	–115.82	–106.80

[a] In kcal/mol.

[b] Computed using the B3LYP/LANL2DZ method.

[c] Computed using the CPCM(UAKS)/B3LYP/LANL2DZ method.

In order to gain the support for the binding mode between **L2•Zn** and ATP, ^{1}H-NMR experiment and 2D NOESY of **L2•Zn** with ATP in the mix solvent of DMSO-d_6 and D_2O (7:1 v/v) were examined. ^{1}H NMR spectra of **L2•Zn** in the absence and presence of ATP were shown in Figure 4.35. Addition of 1 equiv of ATP to the solution of **L2•Zn** in DMSO-d_6 caused the downfield shifts of aromatic protons (H_1) of pyridine moieties around 0.12 ppm. In addition, a slightly downfield shift of imidazole proton (H_a) of adenine based ATP at 8.48 ppm was observed. It was indicative of the strong hydrogen bonding interactions between these corresponding protons and the phosphate groups of ATP. On the other hand, the remaining pyridine protons in Dpa part of **L2•Zn** including H_2 and H_4 underwent a large upfield shift, whereas H_3 proton showed a small upfield shift by 0.22, 0.26 and 0.068 ppm, respectively. The shifts of these protons revealed the geometry change due to ATP complexes [80]. Moreover, the significant shifts of CH_2 protons (H_5, H_6, H_7, H_8, H_9) demonstrated the perturbation of the aliphatic protons in Dpa part upon the complexation of ATP and **L2•Zn**. To gain more important information about the structure of the complex, 2D NMR NOESY was also investigated. From the NOESY spectrum of **L2•Zn** with ATP, the correlation peaks between adenosine protons based ATP and pyrene based **L2•Zn** have not been observed. The result suggested that the binding mode stemmed from the interactions of Zn^{2+} ion with the phosphate part of ATP without the influence of the adenosine part (Figure 4.36). The NOSEY data were consistent with the results from spectrophotometric and computation studies.

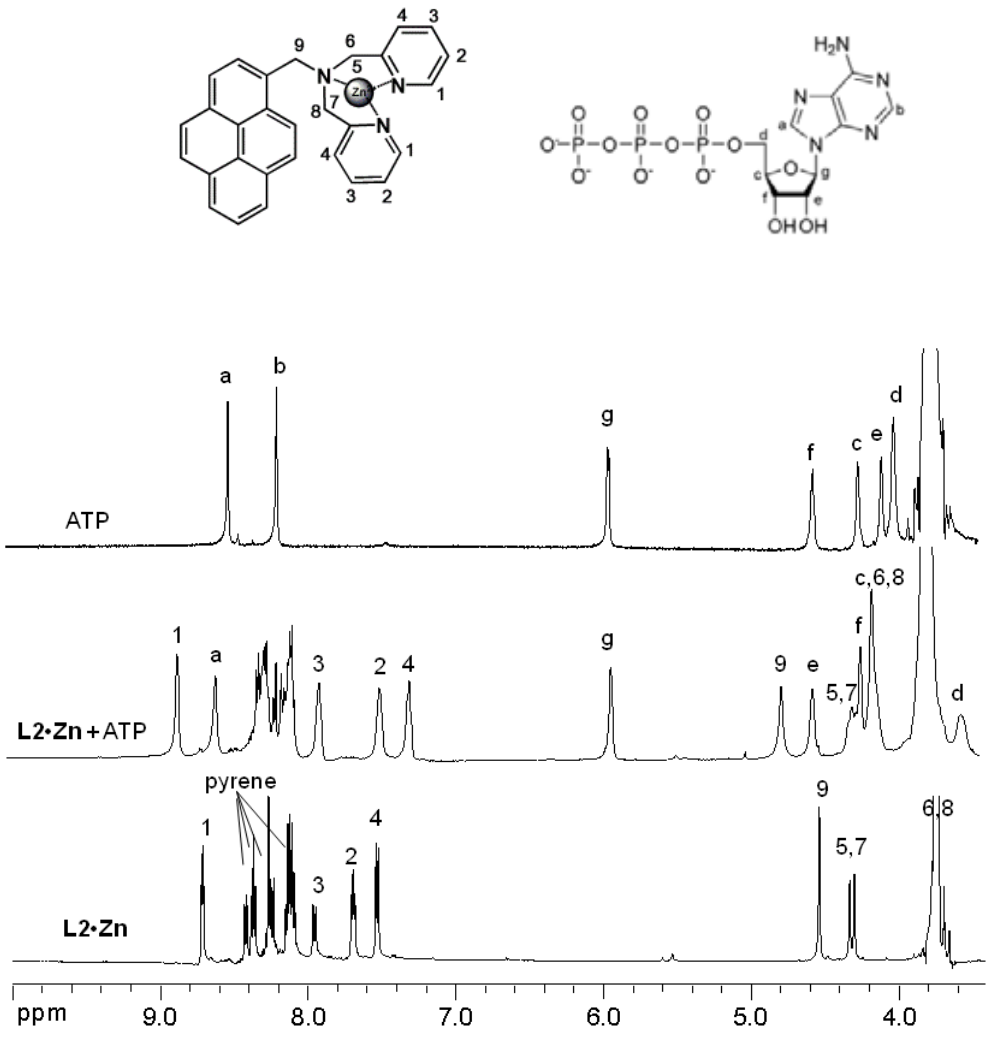

Figure 4.35 Partial ^{1}H NMR spectra of **L2•Zn**, **L2•Zn** + ATP (1 equiv) and ATP in DMSO-d_6 :D_2O (7:1 v/v)(500 MHz).

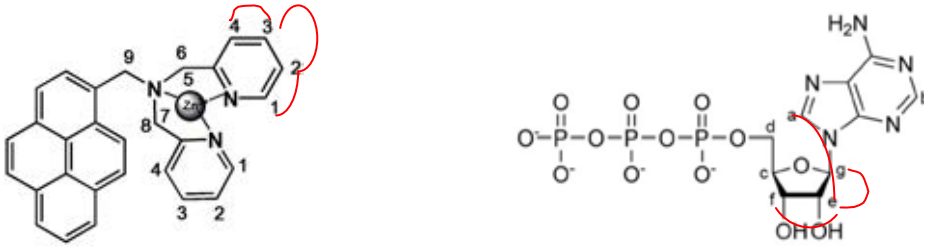

(a)

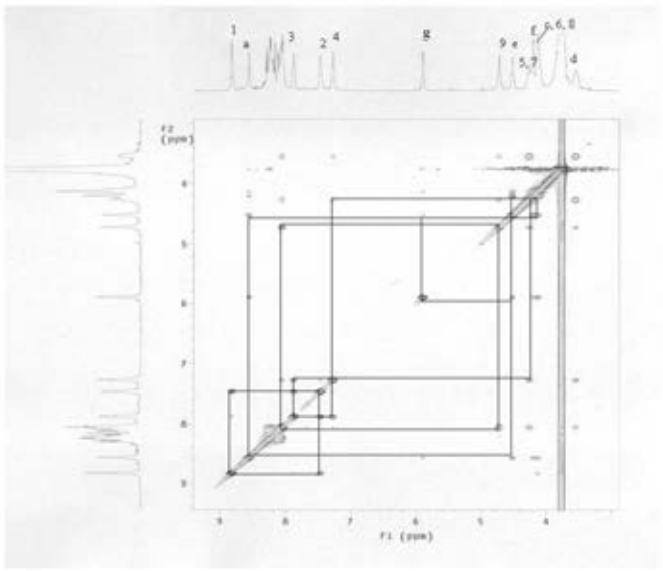

(b)

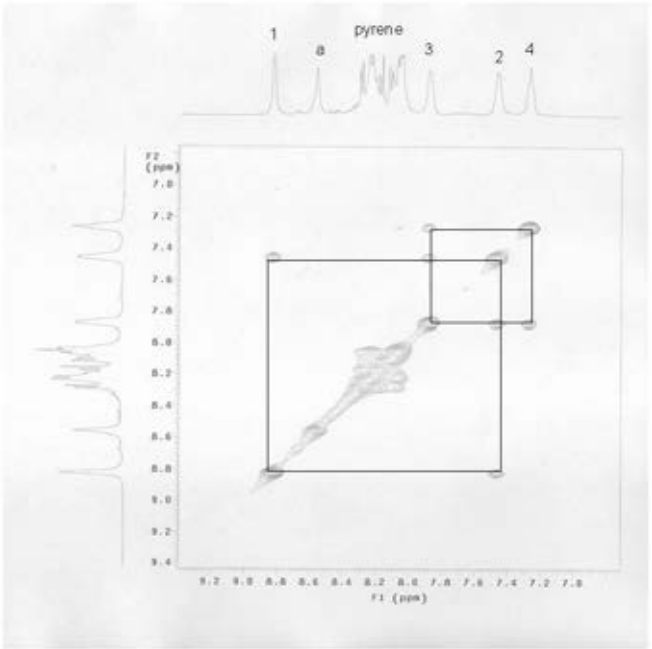

Figure 4.36 (a) Full 2D NOESY spectrum of **L2•Zn +ATP** (b) zoom-in on the range of aromatic of **L2•Zn +ATP** in DMSO-d_6:D_2O (7:1 v/v) (500 MHz).

4.6.4 Discrimination of nucleotides by Principal Component Analysis (PCA)

Considering the complex results from two solvent systems (1% and 90% DMSO in HEPES buffer), the binding affinity of **L2•Zn** and nucleotides showed the absolutely different recognition patterns of the fluorescence intensity changes (Figure 4.37). These results encouraged us to verify the discrimination of binding affinity between **L2•Zn** and nucleotides by examining the fluorescence responses of complexes obtained from the two solvent systems. PCA is used to demonstrate a combinatorial library of a single sensor in the two solvent systems. This approach allows the discrimination of 10 nucleotide anions.

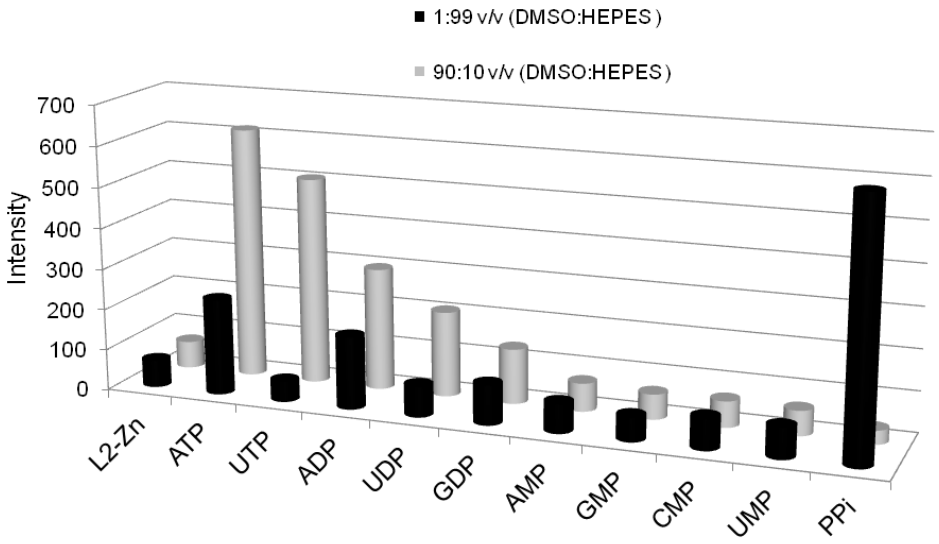

Figure 4.37 The comparison of the fluorescence intensity of **L2•Zn** toward various nucleotides at 383 nm in DMSO:HEPES (1:99 v/v) (black bar) and (90:10 v/v) (0.01M, pH 7.4) (gray bar).

Principal Component Analysis (PCA) is a non-supervised approach utilized to reduce the dimensionality of the data set into a new coordinate system called "Principal Components (PCs)". For each of five trials, the intensity values were

recorded for each of 10 nucleotides. To identify patterns in the data, a principal component (PC) axis is calculated to lie in the direction of maximum variance in the original data. The first component (PC1) always represents the greatest variance and the second greatest variance is projected to the second component (PC2) and so on. Only the scores are used to reveal clustering based on the similarity of analytes [81-85]. All data analysis using PCA with Non-linear Iterative Partials Least Squares (NIPALS) method [81]were performed in MATLAB version 7.11 (R2011a).

The PCA results for **L2•Zn** with various nucleotide anions in DMSO:HEPES (1:99v/v) shows 99.6% variance along PC1, while the vertical PC2 axis displays 0.1% variance (Figure 4.38a). It can classify only the cluster of PPi from other nucleotides. To quantify the classification performance, Linear Discriminant Analysis (LDA) with leave-one-out cross validation approach [81] was used to express the discrimination of the nucleotides. Cross-validated LDA shows 82% accurate classification for all 10 nucleotides. On the other hand, PCA score plot of 90% DMSO in HEPES buffer solution showed the horizontal PC1 axis with 99.1% of variance and illustrated 0.7% of variance along PC2 (Figure 4.38b). This PCA plot exhibited a different discrimination pattern from the mentioned system. In particular, the nucleoside triphosphates including ATP and UTP can be separated from the remaining nucleotides and LDA cross validation showed 74% correct classification in 50 cases.

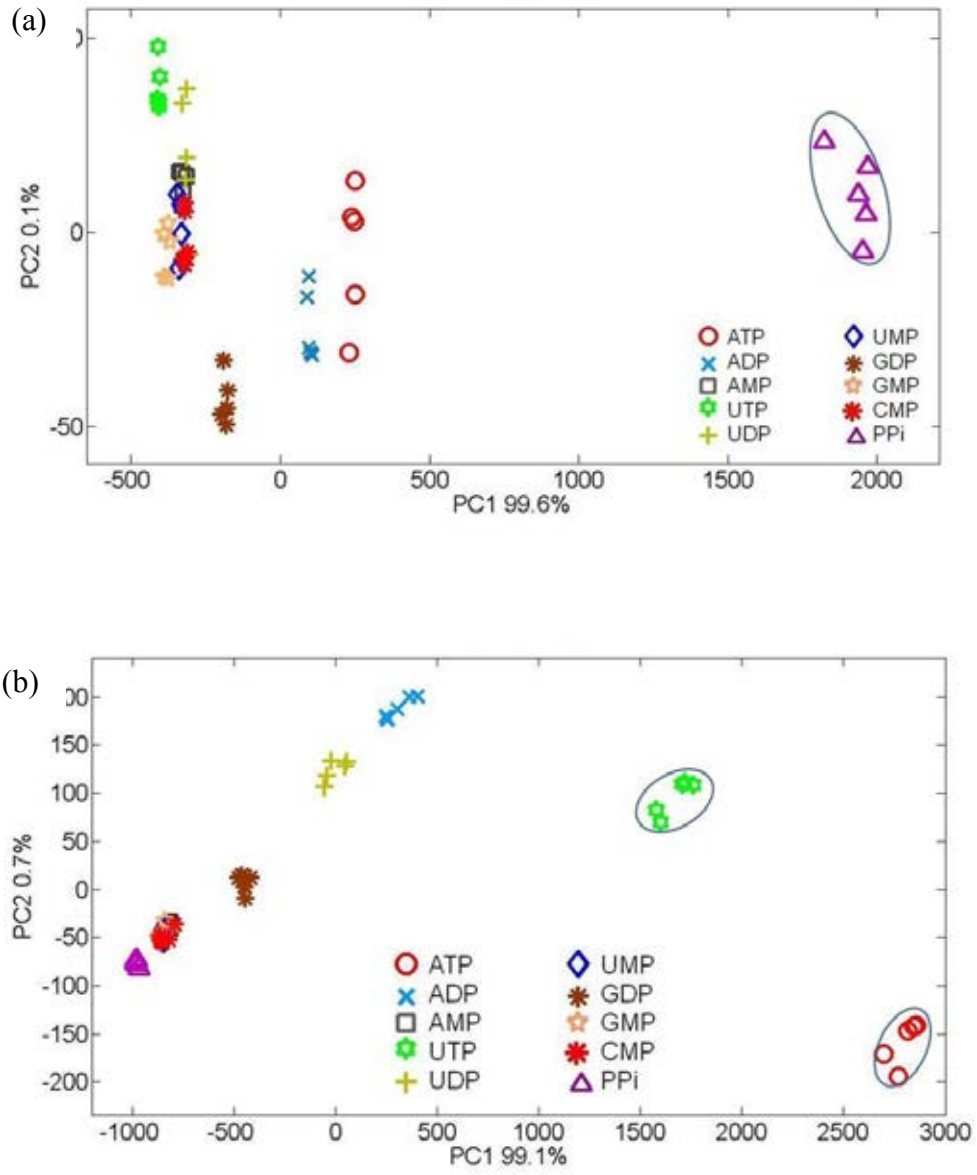

Figure 4.38 PCA score plot of two PCs describing ca. 100% of the total variance for all 10 nucleotides (5 trials each) of **L2•Zn** in (a) DMSO:HEPES (1:99v/v) (b) DMSO:HEPES (90:10v/v).

To improve a certain level of discrimination between 10 nucleotides, the recognition patterns obtained by fluorescent responses in the two solvent systems was combined and subsequently applied to PCA plots. A two dimensional score plot for the first two principal components (PC1 and PC2) representing nearly 100% of variance (as shown in Figure 4.39) exhibits an impressive discrimination with

clustering of the 10 nucleotides in the two solvent systems. The PCA score plot for this combinatorial data showed 76.3% of the variance along the PC1 and the PC2 axis displayed 23.0% of the variance. Clearly, the PCA plot is capable to classify the representative number of phosphate anions such as inorganic pyrophosphate (PPi), triphosphate anions (UTP and ATP), diphosphate anions (ADP, UDP, and GDP), and mono-phosphate anion (UMP, AMP, GMP and CMP). Deeply considering, the appearance of ATP cluster on the right can be separated from UTP cluster in the right upper of the PCA score plot. The case of ADP, GDP and UDP clusters appeared in the left upper close to monophosphate group, while the PPi cluster appeared in the left lower corner. This pattern shows a large differentiation between the similarity of analytes. [86]

Additionally, cross-validated LDA for class prediction illustrated a perfect discrimination of PPi, tri- and di- phosphate anions in 100% accuracy, with the exception of monophosphate anions (70% accuracy). However, cross-validated LDA showed 88% accuracy of overall prediction for 10 nucleotides which was a poor value. This may be caused by the unsuitable binding of **L2•Zn** toward the monophosphate.

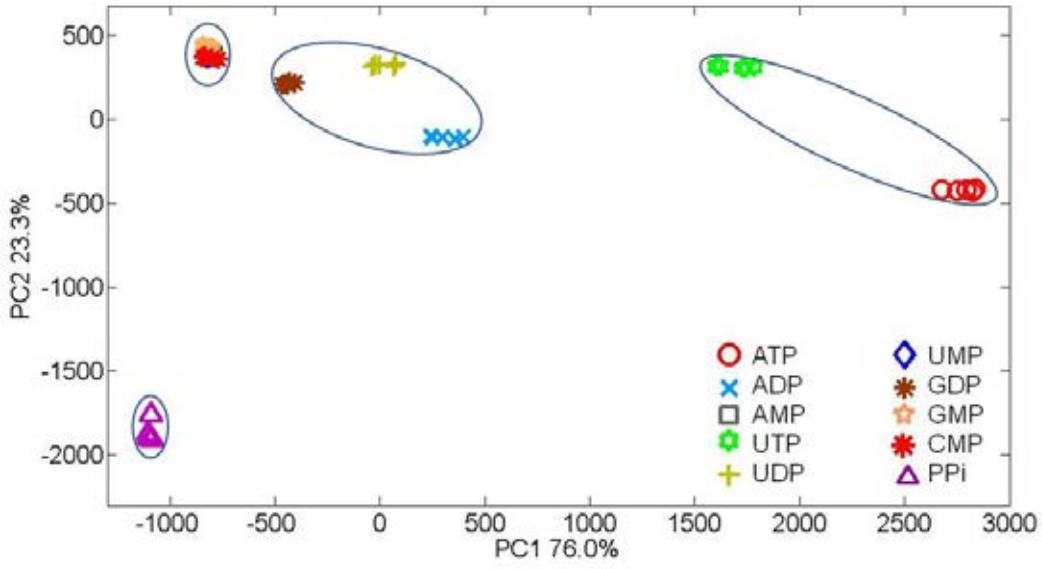

Figure 4.39 PCA score plot of two PCs describing ca. 100% of the total variance for all 10 nucleotides (5 trials each) of **L2•Zn** in mix between in DMSO:HEPES (1:99v/v) and DMSO:HEPES (90:10 v/v).

Interestingly, the PCA analysis can significantly separate between ATP, AMP and PPi. After a successful discrimination of ATP, AMP and PPi, we expected to extend the scope of our system to follow the amount of the PPi and ATP in the ATP hydrolysis which theoretically produces the AMP and PPi in the cellular system. In our hypothesis, the quantitative identification of the ratios of PPi and ATP using **L2•Zn** in both solvent systems were achieved by the different fluorescent responses illustrated by PCA score values.

As anticipated, each pattern of the PCA score plot generated by the sensor with the ratio between PPi and ATP in the range of 0:10 to 10:0 is reduced to a few score and plotted in the new space (PC space) as shown in Figure 4.40. The different recognition patterns of **L2•Zn** towards various nucleotides can be detectable upon the addition of 10 equivalents of analyte. This is a rationalization that the ATP hydrolysis studies were measured in the range of 0:10 to 10:0 for PPi and ATP ratios. The PCA score plot of a single sensor in aqueous system shows the linear relationship of PC1 and PC2 axes while that of the sensor in DMSO solution showed non-linearity. The PCA method shows the high cross reactivity to discriminate the ratio of PPi/ATP in particular of the aqueous system.

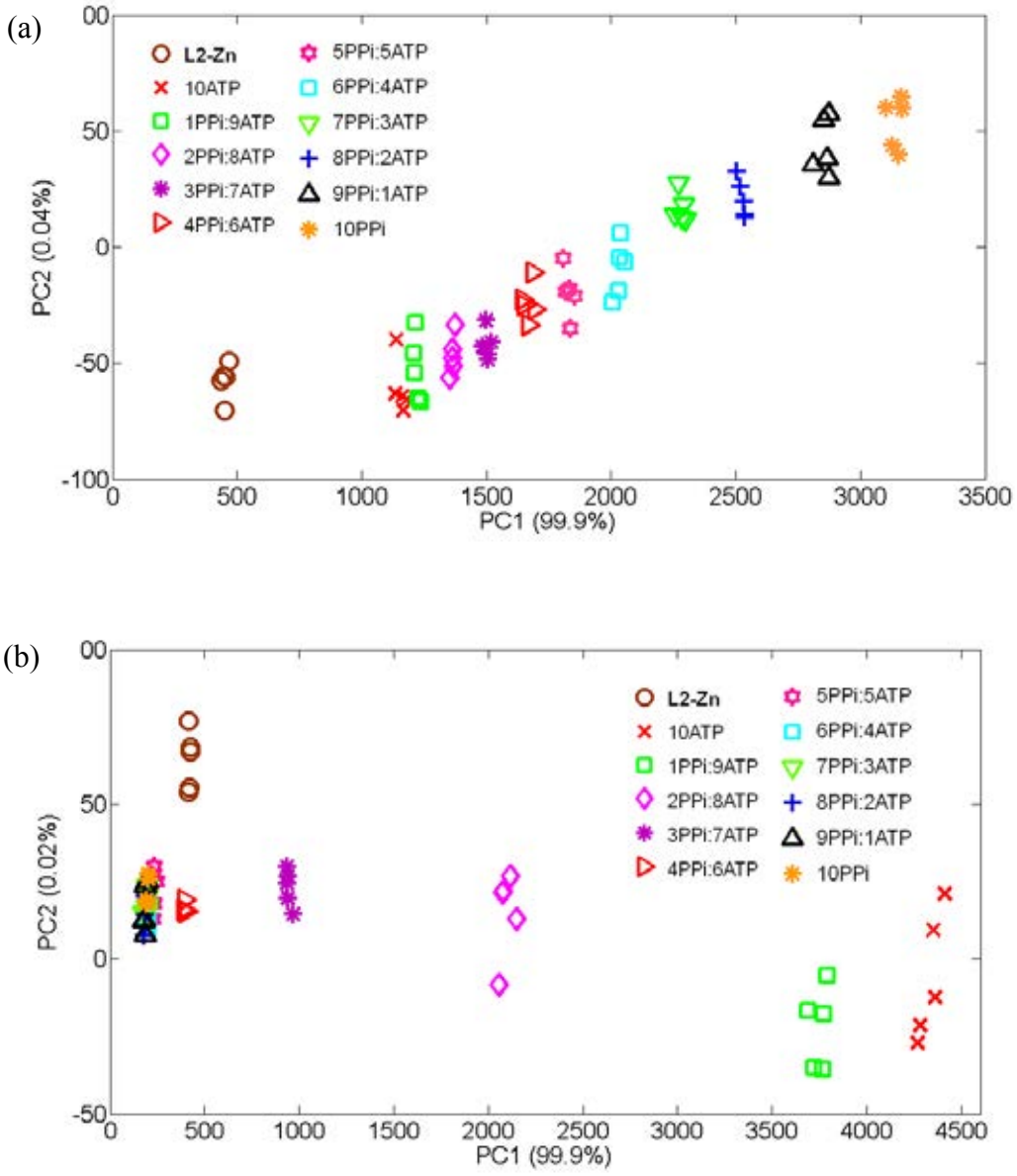

Figure 4.40 PCA score plot of the ratio variation between PPi and ATP PCs describing ca. 100% of the total variance. PCA score plot shows clustering for all 11 samples (5 trials each) in (a) DMSO:HEPES (1:99v/v) (b) DMSO:HEPES (90:10 v/v).

In our effort to evaluate the fluorescence responses from both solvent systems, the plot between the ratios of fluorescence intensity of the sensor in HEPES system and in DMSO (I_H/I_D) against the ratio of PPi and ATP (in the range of 0:10 to 10:0)

was constructed. It exhibited the calibration curve with R^2 of 0.9848 as shown in Figure 4.41. This result can be used for qualitative prediction of the ration PPi and ATP with the detection limit of 2:8 ratios.

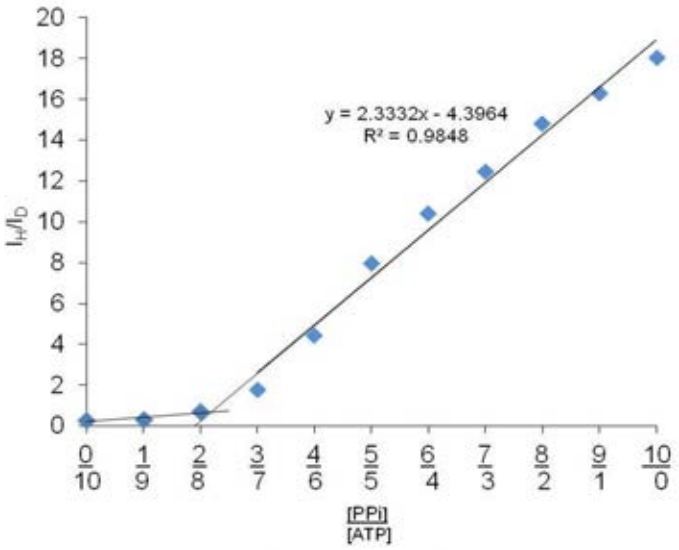

Figure 4.41 Plot between mole ratio of PPi/ATP against the ratios of fluorescence intensity of the sensor in HEPES system and in DMSO.

CHAPTER V

CONCLUSION

A new fluorescence sensor for Zn^{2+} and Cu^{2+} ions based on BF_2-Cur and dipicolyl amine have been successfully synthesized and its binding ability toward Zn^{2+} and Cu^{2+} ion was examined by UV-Vis and fluorescence techniques. The sensor demonstrates the blue-shifted absorption band from 472 nm to 421 nm after adding both Zn^{2+} and Cu^{2+} ions in acetonitrile. For fluorescence technique, the appearance of the emission band of free ligand **L1** showed at 587 nm. Upon the addition of Zn^{2+} and Cu^{2+} ion, the fluorescence quenching was observed. The log *K* values of sensor **L1** with Zn^{2+} and Cu^{2+} ion are 8.25 and 10.52, respectively. Moreover, the low detection limits of Zn^{2+} and Cu^{2+} ions for sensor **L1** are 3.60 and 7.90 ppb, respectively. In this research we focused on the detection of nucleotide in aqueous solution. Thus, we used **L1•2Zn** complex is a sensor for detection of nucleotide in aqueous solution. Unfortunately, **L1•2Zn** complex cannot be used for nucleotide detection since Zn^{2+} ion was removed from **L1** in the water. Therefore, we have demonstrated the design of optical signal transduction pyrene bearing dpa-Zn^{2+} center as **L2•Zn** complex. It performed the selective fluorescent chemosensor for PPi over other anions in an aqueous solution. The Job's plot analysis for the binding mode of **L2•Zn** and PPi suggests a 2:1 stoichiometry and the log *K* value of **L2•Zn** complexed with PPi was 10.22 ± 0.03. On the other hand, the sensor is more favorable for UTP, ATP than PPi in DMSO solution. The complexation structure of **L2•Zn** and ATP was studied by ^{1}H-NMR spectroscopy and computational method. The complexed results showed the promising binding mode relied on anion-cation recognition of phosphate unit and Zn^{2+} without the interactions between the adenosine based ATP and the pyrene moiety. Interestingly, sensor **L2•Zn** exhibited the highly different recognition patterns toward nucleotides in different solvent systems such as aqueous and DMSO. Consequently, we applied the beneficial PCA method by the combinatorial data of fluorescent intensity obtained from a single sensor in two solvent systems to discriminate 10 phosphate anions. A two dimensional score plot for the first two

principal components (PC1 and PC2) representing nearly 100% of variance illustrated an impressive discrimination with clustering of the 10 nucleotides in the two solvent systems. Additionally, cross-validated LDA showed 88% accuracy of overall prediction for 10 nucleotides. Furthermore, the use of PCA was applied for ATP hydrolysis by using the combination of fluorescent responsive data from both solvent systems. The prediction of the ratio between PPi and ATP showed the detection limit of 2:8 ratios. This approach presented here highlighted the benefits of further use of one simple fluorescence sensor with different solvent system for sensing application of a variety of analytes in real-time analysis in the medical diagnosis.

Suggestion for future works:

1. Attempt to recrystallize the ligand **L1**, **L2•Zn** and their complexes with various ionic guests to gain the structure of synthetic receptor and its complexation in solid state.
2. The possibility of using ligand **L1** and **L2•Zn** as a molecular device should be explored.

CHAPTER VI

ANTHRAQUINONE IMIDAZOLE-BASED SENSORS FOR DETECTION OF NUCLEOTIDES

6.1 Design concept

The recognition of biological anion such as nucleotides is currently of major interest. The design and synthesis of molecular sensor that capable to detect nucleotide depends on their properties such as charge, size, pH, solvation and geometry. Considering, the general structure of nucleotide is composed of nucleobase (nitrogenous base), a five carbon sugar and phosphate groups. The boronic acid functional group is known to form reversible covalent linkages with diols, α-hydroxy acids and some α-amino acids. [87] And it is well known that oxygen and nitrogen donor atom can bind to Zn^{2+} ion using their lone pair electron. [88-90]

Therefore, we designed and synthesized the molecular sensor based on an anthraquinone imidazole and the boronic acid. Actually, the boronic acid is a binding site for diol sugar part in nucleotide. Moreover, anthraquinone imidazole does not only act as a binding site for Zn^{2+} ion but also acts as a signaling unit. The synthetic pathway is shown in Scheme 6.1.

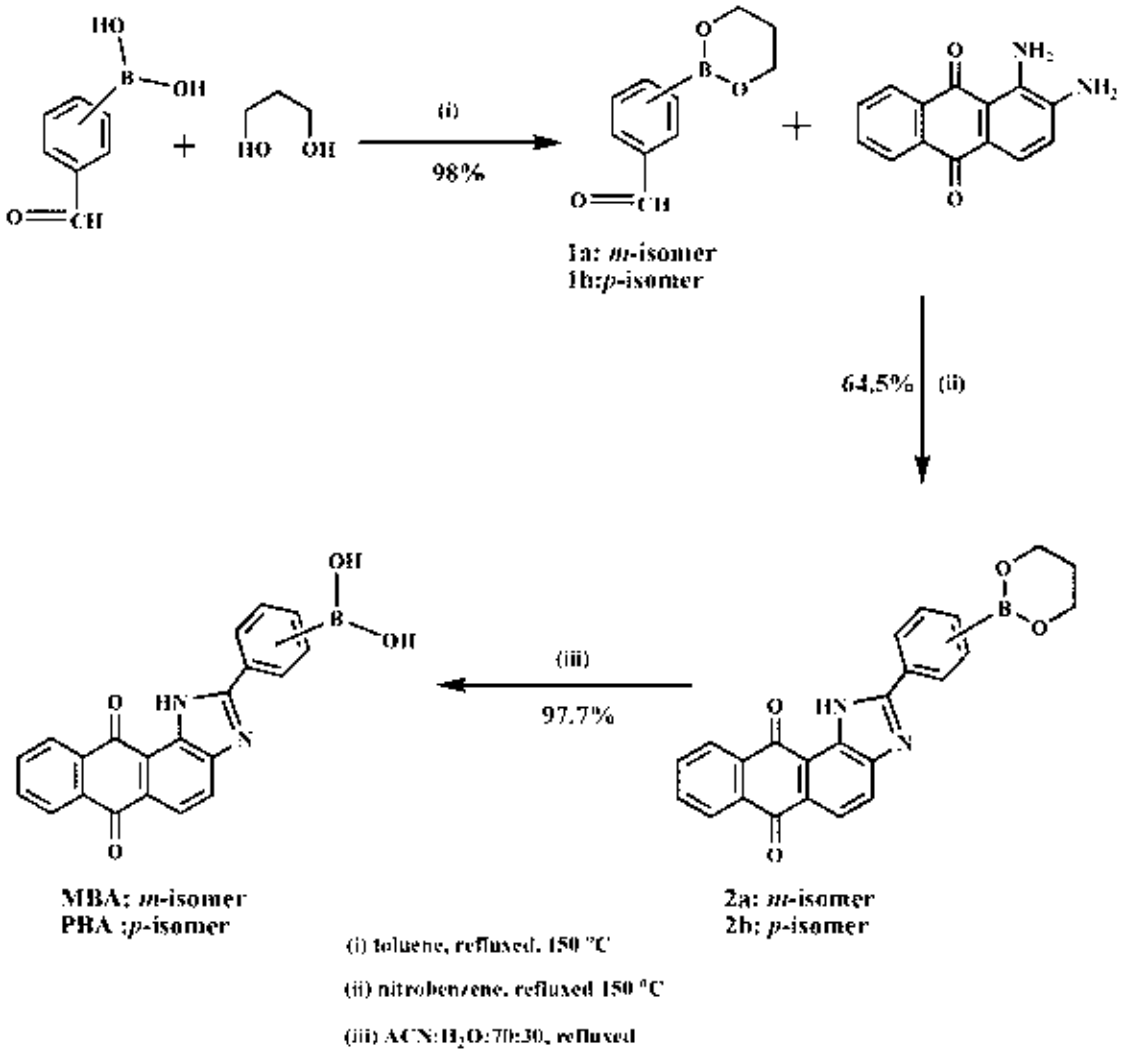

Scheme 6.1 Synthetic pathway of **MBA** and **PBA**

6.2 Synthesis and characterization of molecular sensors based on anthraquinone imidazole (MBA and PBA)

6.2.1 Preparation of compounds 1a and 1b

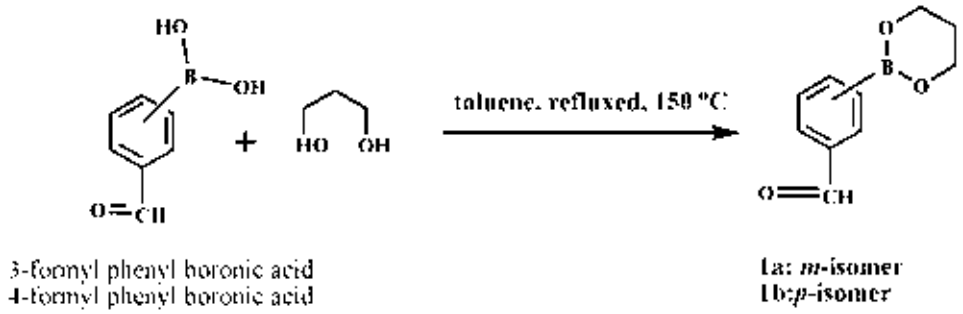

In a 250 mL round bottom flask equipped with a magnetic bar, 3- or 4-phenyl boronic acid (1.21 g, 8 mmol), 1,3 propanediol (0.60 g, 8 mmol) and 100 mL toluene were refluxed at 105°C by using Dean-stark under nitrogen atmosphere for 12 h. The solvent of the reaction mixture was removed to dryness under the reduced pressure. The product yielded as white oil (1.51 g, 98%).

Characterization data for 1a

^{1}H-NMR spectrum (400 MHz, $CDCl_3$): δ (in ppm)

δ 10.05 (s, 1H, ArCO*H*), 8.26 (s, 1H, Ar*H*), 8.02 (d, *J* = 4.6 Hz, 1H, Ar*H*), 7.94 (d, *J* = 8Hz, 1H, Ar*H*), 7.50 (t, *J* = 7.6 Hz, 1H, Ar*H*), 4.19 (t, *J* = 5.6 Hz, 4H, OCH_2CH_2CH_2O), 2.08 (t, *J* = 5.6 Hz, 2H, OCH_2CH_2CH_2O)

Characterization data for 1b

^{1}H-NMR spectrum (400 MHz, d_6-DMSO): δ (in ppm)

δ 10.08 (s, 1H, ArCO*H*), 7.84 (s, 4H, Ar*H*), 4.11 (t, *J* = 5.2 Hz, 4H, OCH_2CH_2CH_2O), 2.00 (t, *J* = 5.2 Hz, 2H, OCH_2CH_2CH_2O)

6.2.2 Preparation of compounds 2a and 2b

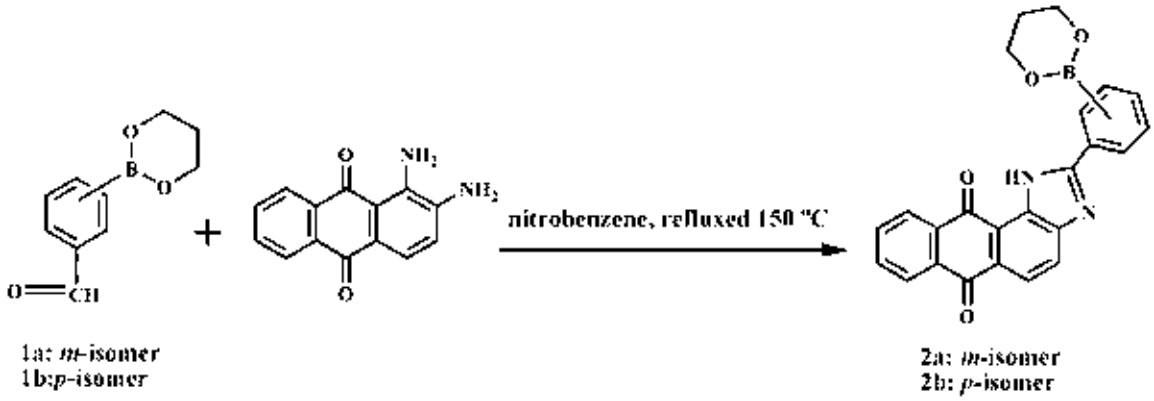

In a 250 mL two-neck round bottom flask equipped with a magnetic bar, 1,2 diamino anthaquinone (1.51 g, 6 mmol) and 70 mL nitrobenzene were stirred for 30 mins under N_2 atmosphere. Then, the white oil of **1** (1.21 g, 6 mmol) in 50 mL nitrobenzene was slowly added into the reaction mixture. The reaction was heated at 100 ºC for 1 h and then heated at 150 ºC for 12 h by using Dean-stark. After the reaction completed, the mixture was cooled down. The desired product was purified by precipitation with hexane to give the yellow solid (1.58 g, 64.5%).

Characterization data for 2a

^{1}H-NMR spectrum (400 MHz, $CDCl_3$): δ (in ppm)

δ 11.36 (s, 1H, N*H*), 8.46 (s, 1H, Ar*H*), 8.36-8.23 (m, 4H, Ar*H*), 8.14 (d, *J* = 8.4Hz, 1H, Ar*H*) 7.95 (d, *J* = 7.6 Hz, 1H, Ar*H*), 7.82-7.80 (m, 2H, Ar*H*), 7.55 (t, *J* = 7.6 Hz, 1H, Ar*H*), 4.23 (t, *J* = 5.6 Hz, 4H, $OCH_2CH_2CH_2O$), 2.11 (t, *J* = 5.2 Hz, 2H, $OCH_2CH_2CH_2O$)

Characterization data for 2b

^{1}H-NMR spectrum (400 MHz, $CDCl_3$): δ (in ppm)

δ 11.36 (s, 1H, N*H*), 8.37-8.24 (m, 3H, Ar*H*), 8.16 (d, *J* = 8.0 Hz, 3H, Ar*H*), 7.99 (d, *J* = 7.6Hz, 2H, Ar*H*), 7.82 (d, *J* = 4.0 Hz, 2H, Ar*H*), 4.23 (t, *J* = 5.6 Hz, 4H, $OCH_2CH_2CH_2O$), 2.11 (t, *J* = 5.2 Hz, 2H, $OCH_2CH_2CH_2O$)

6.2.3 Preparation of compounds MBA and PBA

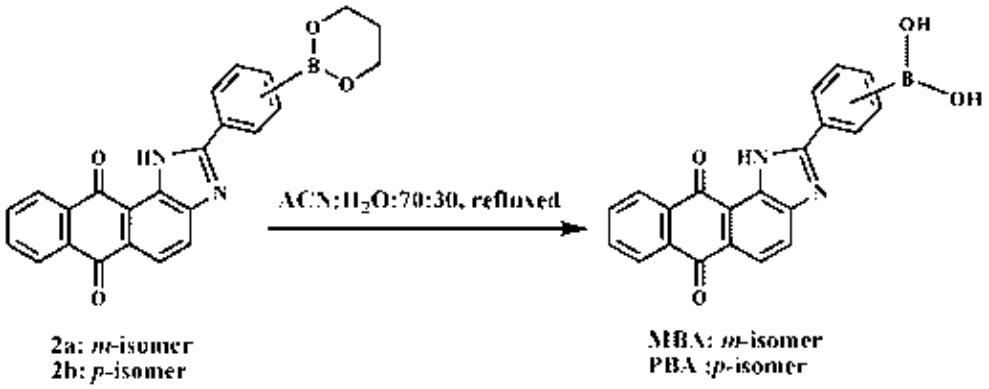

In a 100 mL two-neck round bottom flask equipped with a magnetic bar, compound **2** (0.20 g, 0.05 mmol) and 50 mL of 70% acetonitrile in water were refluxed at 150 ºC by using Dean-stark under N_2 atmosphere for 12 h. Then the product was precipitated into the reaction. After the reaction completed, the precipitate was filterred and washed with diethyl ether. The desired product was obtained in the yellow solid (0.19 g, 97.7%).

Characterization data for MBA

^{1}H-NMR spectrum (400 MHz, d_6-DMSO): δ (in ppm)

δ 13.05 (s, 1H, N*H*), 8.78 (s, 1H, Ar*H*), 8.43 (d, *J* = 7.2 Hz, 1H, Ar*H*), 8.28 (s, 2H, O*H*), 8.22-8.07 (m, 4H, Ar*H*), 7.96-7.92 (m, 3H, Ar*H*), 7.54 (t, *J* = 7.6 Hz, 1H, Ar*H*)

Characterization data for PBA

^{1}H-NMR spectrum (400 MHz, d_6-DMSO): δ (in ppm)

δ 13.21 (s, 1H, N*H*), 8.42 (d, *J* = 7.6 Hz, 2H, Ar*H*), 8.27-8.22 (m, 3H, Ar*H*), 8.18-8.10 (m, 2H, Ar*H*), 7.99-7.94 (m, 3H, Ar*H*)

The synthesis of boronic imidazole based anthraquinone was accompanied by the condensation reaction in various conditions. The synthetic pathway was started with protecting the boronic acid part by condensation reaction between formyl phenyl boronic acid and 1,3 propanediol. The ^{1}H-NMR spectrum of compound **1** showed the characteristic peaks of formyl phenyl group as a singlet of the aldehyde proton (ArCO*H*) at 10.05 ppm and the aromatic protons (Ar*H*) from 8.26 to 7.50 ppm. Additionally, two triplets of methylene protons of propane moiety were found at 4.19 and 2.08 ppm. The 1,2 diamino anthaquinone was reacted with compound **1** by condensation reaction in nitrobenzene. The desired product was obtained by precipitation in hexane to gain 64.5% yield as the yellow solid of compound **2**. The ^{1}H-NMR data of the compound **2** displayed the absence of the singlet peak of aldehyde proton at 10.05 ppm. Moreover, a singlet of N*H* proton of imidazole moiety was found at 11.36 ppm and the aromatic protons of anthraquinone were found at 8.36-7.95 ppm. The hydrolysis of compound **2** was carried out by refluxing in 70% acetonitrile in water to afford the deprotected compound as the yellow solid in 97.7% yield. The ^{1}H-NMR spectrum depicted in Figure 6.1 displayed the disappearance of aliphatic protons of the protecting group at 4.23 and 2.11 ppm corresponding to the deprotecting boronic imidazole based anthraquinone.

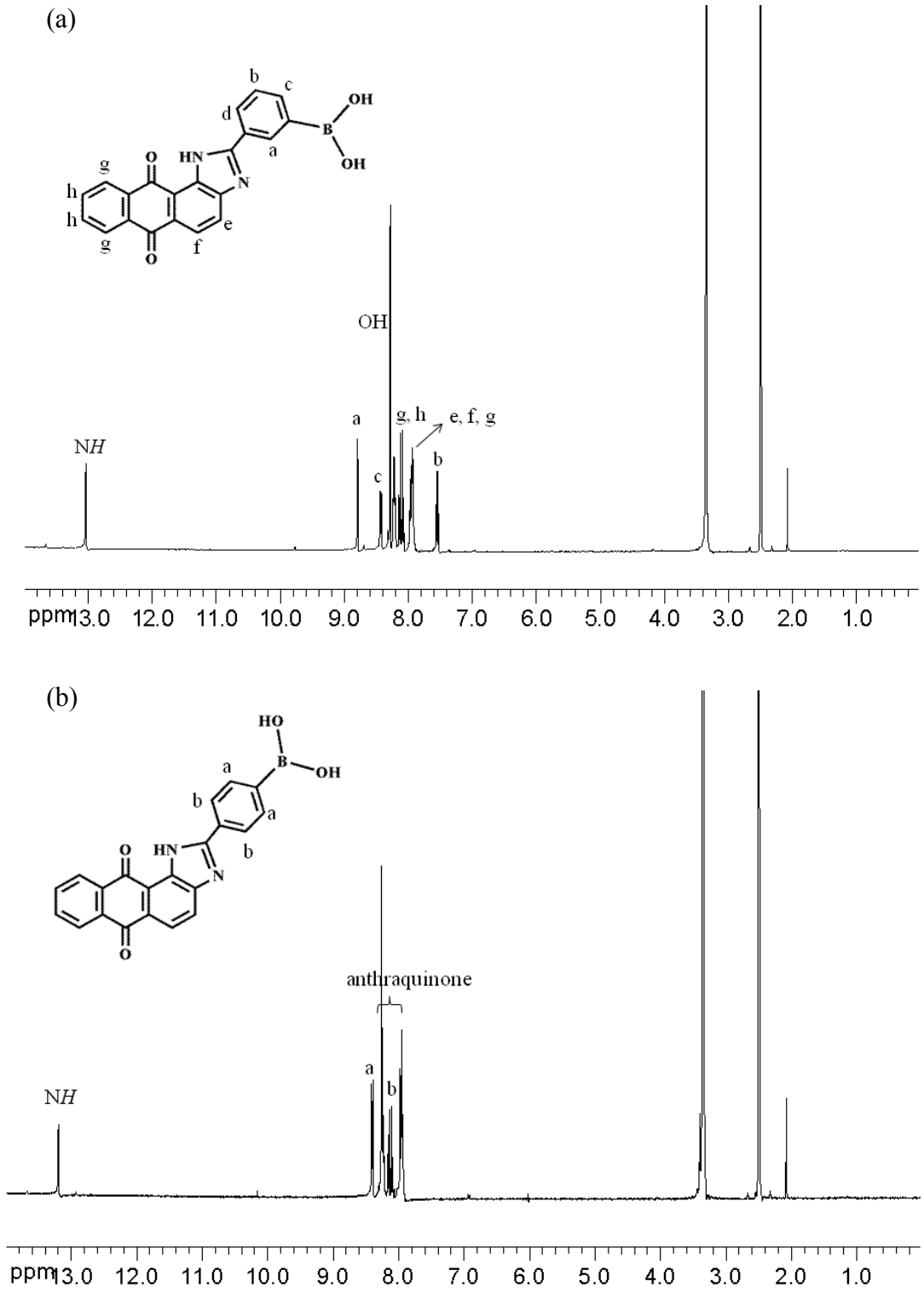

Figure 6.1 ^{1}H-NMR spectra of (a) **MBA** and (b) **PBA** in d_6-DMSO (400 MHz).

6.3 Complexation studies of molecular sensor MBA and PBA toward various nucleotides by UV-Vis spectrophotometry

To evaluate the potential of ligand **MBA** and **PBA** with nucleotides, the binding properties were investigated by UV-Vis techniques. Ligand **MBA** and **PBA** consist of nitrogen and oxygen atoms at imidazole ring and anthraquinone unit, respectively, which was expected to bind with Zn^{2+} ion. [91] In our hypothesis, the anthraquinone-Zn(II) chelate moiety has the vacant site to bind phosphate part based nucleotide and boronic acid site for diol of nucleotide as shown in Figure 6.2. Moreover, we would like to study the influence of boronic acid position toward the binding properties. Therefore, the binding affinity of **MBA** and **PBA** containing the boronic acid at *para*- and *meta*-position, respectively, were also examined by UV-Vis techniques.

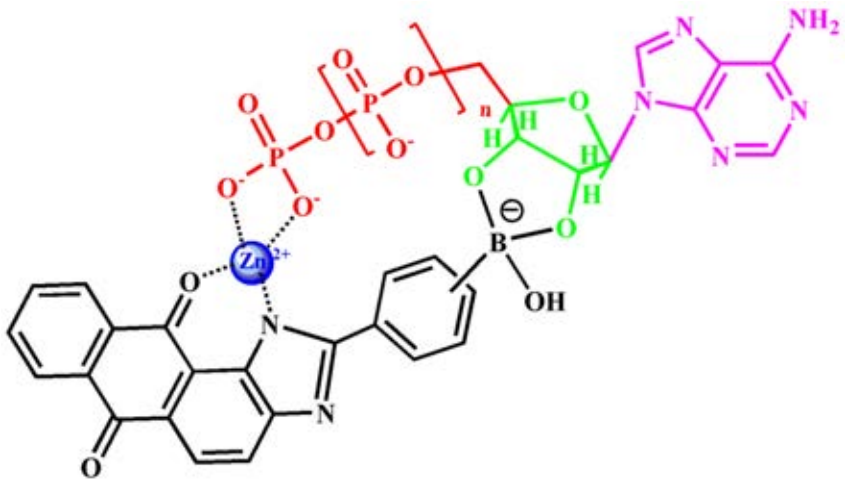

Figure 6.2 The proposed structure mode of **Ligand**⊂Zn^{2+} to nucleotide.

Absorption spectrum of ligand **MBA** and **PBA** (6.0×10^{-5} M) were recorded from 200-700 nm at ambient temperature. The maximum absorption band of ligand **MBA** displayed at 396 nm in ethanol. Meanwhile, 50% ethanol in water (HEPES buffer 0.05M,

pH 8), the maximum absorption band at 404 nm was observed. This result implied that the solution at pH 8.0 is able to induce the deprotonation process of N*H* proton. Preliminary, we have studied the complexation of **MBA** and **PBA** with Zn^{2+} ion in 50 % EtOH in water (HEPES buffer 0.05M, pH 8.0, 1:1v/v) by UV-Vis spectrophotometry. Upon the addition of Zn^{2+} (0-9 equiv) into **MBA**, the absorption band at 404 nm progressively decreased with a concomitant of a small bathochromic shift to 409 nm illustrated in Figure 6.3a. Possibly, these changes stemmed from the interaction between Zn^{2+} and anthraquinone moiety. [92-93] On the other hand, the addition of Zn^{2+} into **PBA** exhibited a slight increase of the absorption band at 404 nm as shown in Figure 6.3b. It suggested that Zn^{2+} ion cannot bind with anthraquinone moiety of **PBA**. Possibly, this sensor posses only two atom donors of nitrogen and oxygen atoms for binding with Zn^{2+} ion. Therefore, the interaction between **PBA** and Zn^{2+} is highly poor.

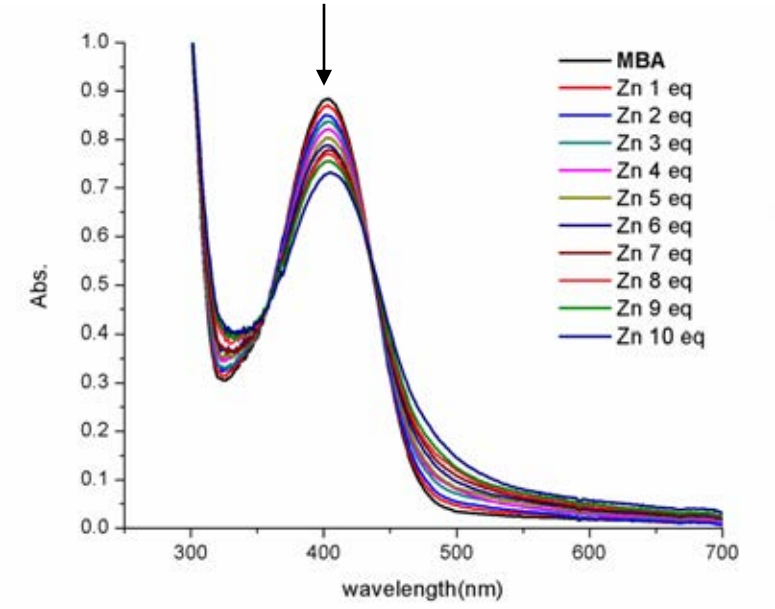

Figure 6.3a Absorption spectra of **MBA** ($6.00x10^{-5}$ M) toward Zn(II) ion in EtOH:H_2O (HEPES 0.05 M , pH 8.0, 1:1 v/v).

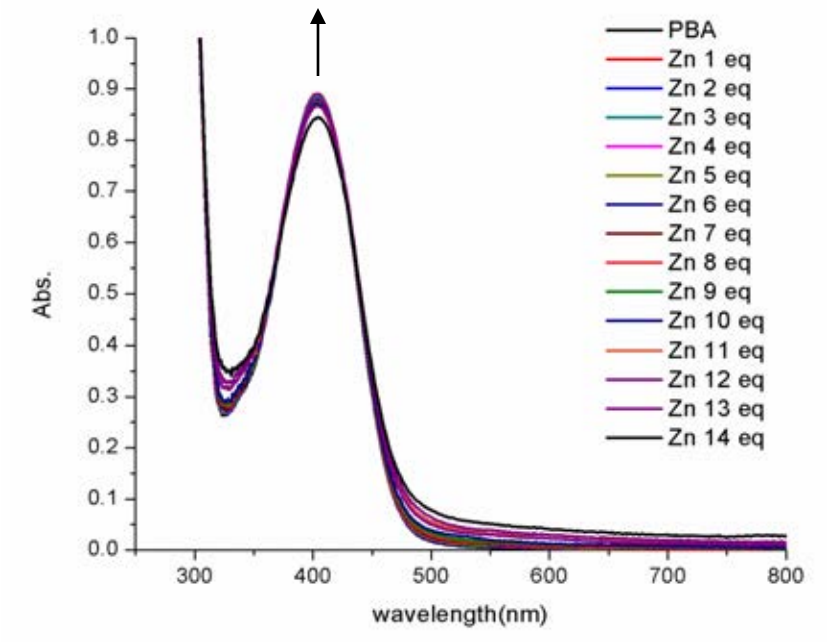

Figure 6.3b Absorption spectra of **PBA** ($6.00x10^{-5}$ M) toward Zn(II) ion in EtOH:H_2O (HEPES 0.05 M , pH 8.0, 1:1 v/v).

In expectation, Zn^{2+} chelated **MBA** can coordinate with phosphates anion based ATP. Thus we have focused on studying the binding properties of **MBA**⊂Zn^{2+} toward ATP by UV-Vis techniques.

The maximum absorption band of **MBA**⊂Zn^{2+} displayed the characteristic peak at 404 nm. Upon addition of the ATP to **MBA**⊂Zn^{2+}, the absorption band at 404 nm was slightly increased and then, the absorption band was turned similarly to the characteristic absorption band of **MBA**. It can be explained that **MBA**⊂Zn^{2+} cannot bind to nucleotide. Presumably, Zn^{2+} was released from **MBA**⊂Zn^{2+} by the addition of nucleotide.

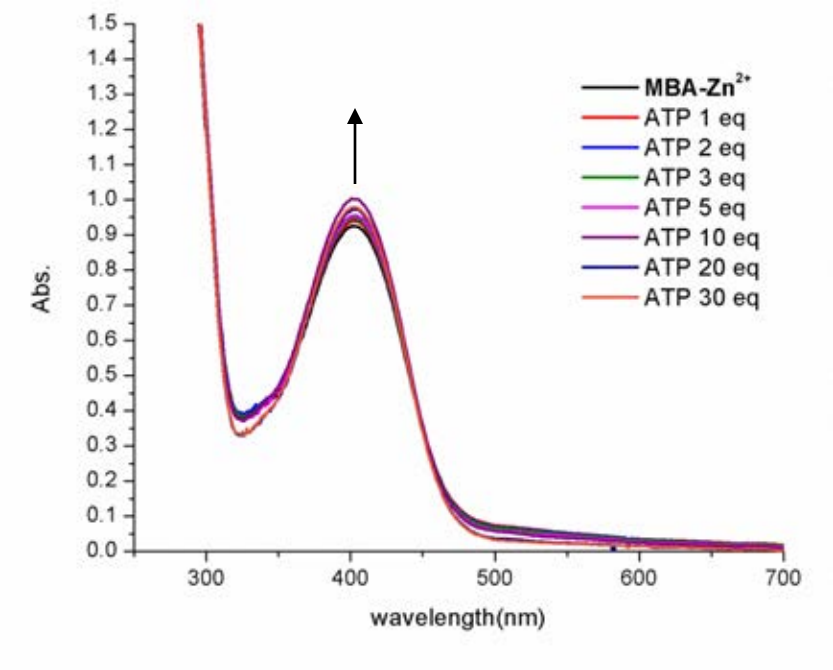

Figure 6.4 Absorption spectra of **MBA**⊂Zn^{2+} ($6.00x10^{-5}$ M ligand and 8 equivalent of Zn^{2+}) upon addition of increasing amounts of ATP in EtOH:H_2O (HEPES 0.05 M , pH 8.0, 1:1 v/v).

To gain more the informative support of **MBA**⊂Zn^{2+} toward ATP, ^{1}H-NMR experiment in the mix solvent of DMSO-d_6 and D_2O (7:1 v/v) was examined. ^{1}H-NMR spectra exhibited the chemical shit of the characteristic protons of **MBA** from 8.70 to 7.52 ppm as shown in Figure 6.5. After addition of 5 equiv. of Zn^{2+} ion and ATP, the signal of protons remained unchanged. This result suggested that **MBA**⊂Zn^{2+} cannot bind to ATP. The ^{1}H-NMR data were consistent with the results from UV-Vis experiment. Therefore, **MBA** cannot be used as a sensor for nucleotides.

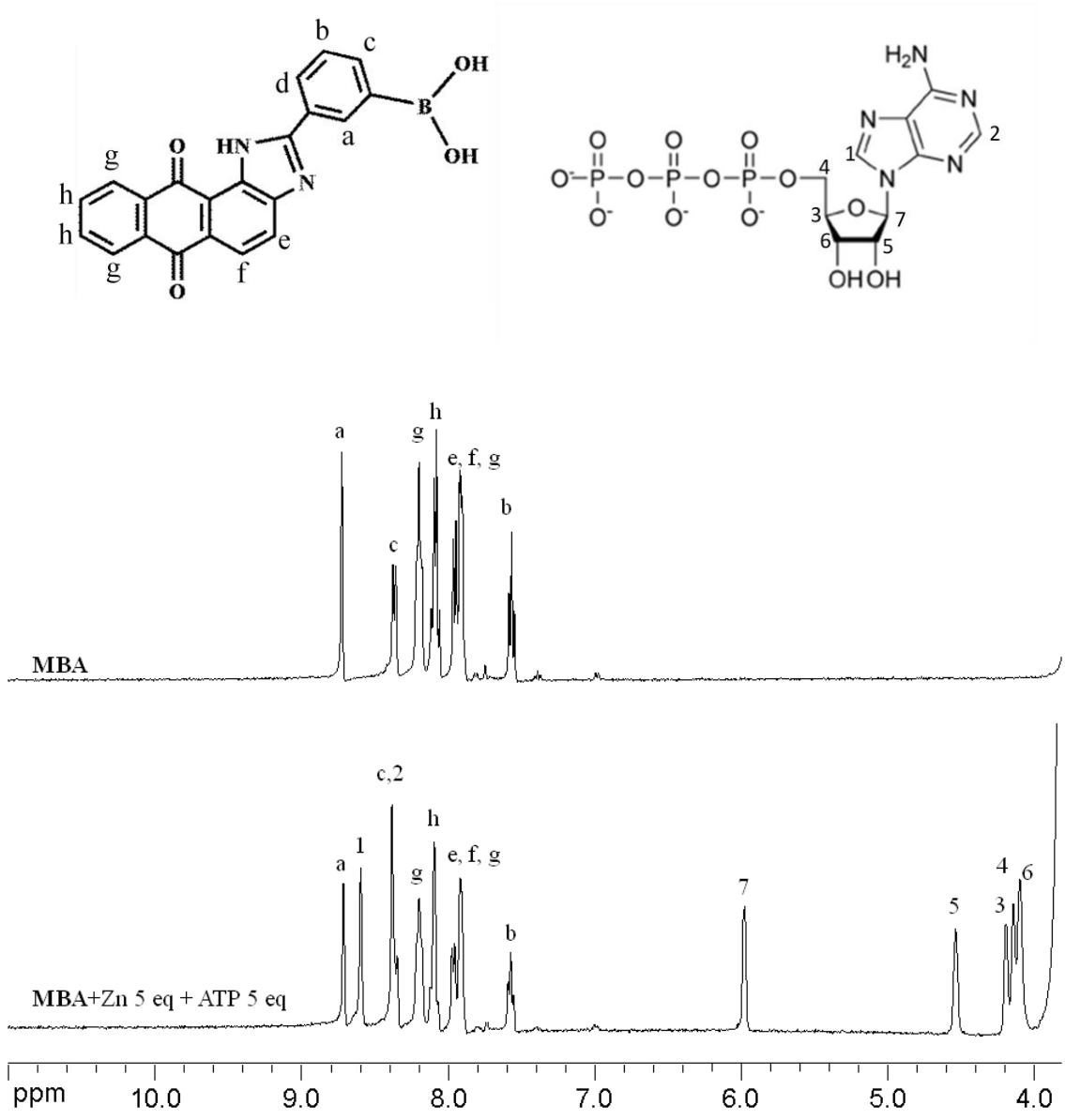

Figure 6.5 Partial ^{1}H-NMR spectra of **MBA** and **MBA⊂**Zn +ATP (5 equiv.) in DMSO-d_6:D_2O (7:1 v/v) (400 MHz).

REFERENCES

[1] Suksai, C. and Tuntulani, T. Chromogenic Anion Sensors. Chem. Soc. Rev. 32 (2003): 192-202.

[2] Berg, J.M., and Shi, Y. The galvanization of biology: A growing appreciation for the roles of zinc. Science 271 (1996): 1081-1085.

[3] Bush, A. Metals and neuroscience. Curr. Opin. Chem. Biol. 4 (2000): 184-191.

[4] Noy, D., Solomonov, I., Sinkevih, O., Arad, T., Kjaer, K., and Sagi, I. Zinc amyloid beta interactions on a millisecond time-scale stabilize non-fibrillar Alzheimer-related species. J. Am. Chem. Soc. 130 (2008): 1376-1383.

[5] Kornberg, A. DNA replication. J. Biol. Chem. 263 (1988): 1-4.

[6] Shen, X., Mizuguchi, G., Hamiche, A., and Wu, C. A chromatin remodelling complex involved in transcription and DNA processing. Nature 406 (2000): 541-544.

[7] Burnstock, G. Pathophysiology and therapeutic potential of purinergic signaling. Pharmacol Rev. 58 (2006): 58-86.

[8] Jang, Y.J., Jun, E.J., Kim, Y.S., Kim, J.S., and Yoon, J. Highly effective fluorescent and colorimetric sensors for pyrophosphate over $H_2PO_4^-$ in 100% aqueous solution. J. Org. Chem. 70 (2005): 9603-9606.

[9] Lehn, J.M. Supramolecular Chemistry: Concepts and Perspectives. Weinheim: VCH , 1995.

[10] Lehn, J.M. Organic Chemistry: Its Language and Its State of the Art. in Kisakurek, M. V. (Ed.) Proceeding of the Centenary of the Geneva Conference Weinheim: VCH, 1993.

[11] Vogtle, F. Supramolecular Chemistry: An introduction. Chichesters: John Wiley& Sons, 1991.

[12] Paul, D., Gale, P.A., and Smith, D.K. Supramolecular chemistry. Oxford: Oxford university press, 1999.

[13] Bargossi, C., Fiorini, M.C., Montalti, M., Prodi, L., and Zaccheroni, N. Recent developments in transition metal ion detection by luminescent chemosensors. Coord. Chem. Rev. 208 (2000): 17-32.

[14] Löhr, H-G., and Vögtle, F. Chromo-and fluoroionophores a new class of dye reagents. Acc. Chem. Res. 18 (1985): 65-72.

[15] Ataman, D., and Akkaya, E.U. Selective chromogenic respone via regioselective binding of cations: a novel approach in chemosensor design. Tetrahedron Lett. 43 (2002): 3981-3983.

[16] Wu, F., Hu, M., Wu, Y., Tan, X., Zhao, Y., and Ji, Z. Fluoride-seletive colorimetric sensor based on thiourea binding site and anthraquinone receptor. spectrochimica acta part A 65 (2006): 633-637.

[17] Valeur, B., and Leray, I. Design principles of fluorescent molecular sensors for cation recognition. Coord. Chem. Rev. 205 (2000): 3-40.

[18] Jiang, P., and Guo, Z. Fluorescent detection of zinc biological system: recent development on the design of chemosensors and biosensors. Coord. Chem. Rev. 248 (2004): 205-229.

[19] Bren,V.A. Fluorescent and photochromic chemosensors. Russ. Chem. Res. 70 (2001): 1017-1036.

[20] McCarrick, M., Wu, B., Harris, S.J., Diamond, D., Barrett, G., and McKervey, M. A. Novel chromogenic ligands for lithium and sodium based on calix[4]arene tetraesters. J. Chem. Soc. Chem. Commun. (1992): 1287-1289.

[21] McCarrick, M., Wu, B., Harris, S.J., Diamond, D., Barrett, G., and McKervey, M.A. Chromogenic ligands for lithium based on calix[4]arene tetraesters bearing nitrophenol residues. J. Chem. Soc. Perkin. Trans.2 (1993): 1963-1968.

[22] Valeur, B. Determination of the stoichiometry of a complex by the method of continuous variations (Job's method). Molecular Fluorescence Principles and Applications Weinheim: Wiley-VCH, 2002.

[23] Miller, J.N. and Miller. J.C. Statistic and chemometric for analytical chemistry Harow: Prentice Hall, 2000.

[24] Fery-Forgues, S., Le Bris, M-T., Guetté, J-P., and Valeur, B. Ion-responsive fluorescent compounds. 1. Effect of cation binding on photophysical properties of a benzoxazinone derivative linked to monoaza-15-crown-5. J. Phys. Chem. 92 (1988): 6233-6237.

[25] Bouson, J., and Valeur, B. Ion-responsive fluorescent compounds. 2. cation- steered intramolecular charge transfer in a crowned merocyanine. J. Phys. Chem. 93 (1988): 3871-3876.

[26] Bouson, J., Pouget, J., and Valeur, B. Ion-responsive fluorescent compounds. 4. Effect of cation binding on the photophysical properties of a coumarin linked to monoaza- and diaza-crown ethers. J. Phys. Chem. 97 (1993): 4552-4557.

[27] Brereton, R.G. Chemometrics Data Analysis for the Laboratory and Chemical Plant England: John Wiley&Sons, 2003.

[28] Walkup, G.K., Burdette, S.C., Lippard, S.J., and Tsien, R.Y. A new cell-permeable fluorescent probe for Zn^{2+} J. Am. Chem. Soc. 122 (2000): 5644-5645.

[29] Zhang, Y., Guo, X., Si, W., Jia, L., and Qian, X. Ratiometric and Water-Soluble Fluorescent Zinc Sensor of Carboxamidoquinoline with an Alkoxyethylamino Chain as Receptor. Org. Lett. 10 (2008): 473-476.

[30] Hirano, T., Kikuchi, K., Urano, Y., Higuchi, T., and Nagano, T. Highly zinc-selective fluorescent sensor molecules suitable for biological applications. J. Am. Chem. Soc. 122 (2000): 12399-12400.

[31] Maruyama, S., Kikuchi, K., Hirano, T., Urano, Y., and Nagano, T. A Novel, Cell-Permeable, Fluorescent Probe for Ratiometric Imaging of Zinc Ion. J. Am. Chem. Soc. 124 (2002): 10650-10651.

[32] Xu, Z., Qian, X., Cui, J., and Zhang, R. Exploiting the deprotonation mechanism for the design of ratiometric and colorimetric Zn^{2+} fluorescent chemosensor with a large red-shift in emission. Tetrahedron 62 (2006): 10117–10122.

[33] Wang, H., Gan, Q., Wang, X., Xue, L., Liu, S., and Jiang, H. A Water-soluble, small molecular fluorescent sensor with femtomolar sensitivity for zinc ion. Org. Lett. 9 (2007): 4995-4998.

[34] Atilgan, S., Ozdemir, T., and Akkaya, E.U. A Sensitive and Selective Ratiometric Near IR Fluorescent Probe for Zinc Ions Based on the Distyryl-Bodipy Fluorophore. Org. Lett. 10 (2008): 4065-4067.

[35] Cho, H.K., Lee, D.H., and Hong, J.I. A fluorescent pyrophosphate sensor via excimer formation in water. Chem. Commun. (2005): 1690–1692.

[36] Lee, H.N., et al. Simple but Effective Way to Sense Pyrophosphate and Inorganic

Phosphate by Fluorescence Changes. Org. Lett. 9 (2007): 243-246.

[37] Shao, N., Wang, H., Gao, X., Yang, R. H., and Chan, W. Spiropyran-Based Fluorescent Anion Probe and Its Application for Urinary Pyrophosphate Detection. Anal. Chem. 82 (2010): 4628–4636.

[38] Zhang, J.F., et. al. Pyrophosphate-Selective Fluorescent Chemosensor Based on 1,8-Naphthalimide-DPA-Zn(II) Complex and Its Application for Cell Imaging. Org. Lett. 13 (2011): 5294-5297.

[39] Xu, Z., et. al. Unique Sandwich Stacking of Pyrene-Adenine-Pyrene for Selective and Ratiometric Fluorescent Sensing of ATP at Physiological pH. J. Am. Chem. Soc. 131 (2009): 15528–15533.

[40] Neelakandan, P.P., Hariharan, M., and Ramaiah, D. Synthesis of a Novel Cyclic Donor-Acceptor Conjugate for Selective Recognition of ATP. Org. Lett. 7 (2005): 5765-5768.

[41] Nakano, S., Mashima, T., Matsugami, A., Inoue, M., Katahira, M., and Morii, T. Structural Aspects for the Recognition of ATP by Ribonucleopeptide Receptors. J. Am. Chem. Soc. 133 (2011): 4567–4579.

[42] Schneider, S. E., O'Neil, S.N., and Anslyn, E.V. Coupling Rational Design with Libraries Leads to the Production of an ATP Selective Chemosensor. J. Am. Chem. Soc. 122 (2000): 542-543.

[43] Ojida, A., Park, S.K., Mito-oka, Y., and Hamachi, I. Efficient fluorescent ATP sensing based on coordination chemistry under aqueous neutral conditions. Tetrahedron Lett. 43 (2002): 6193–6195.

[44] Moro, A.J., Cywinski, P.J., Korstena, S., and Mohr, G.J. An ATP fluorescent chemosensor based on a Zn(II)-complexed dipicolylamine receptor coupled with a naphthalimide chromophore. Chem. Commun. 46 (2010): 1085–1087.

[45] Kurishita, Y., Kohira, T., Ojida, A., and Hamachi, I. Rational Design of FRET-Based Ratiometric Chemosensors for in Vitro and in Cell Fluorescence Analyses of Nucleoside Polyphosphates J. Am. Chem. Soc. 132 (2010): 13290–13299.

[46] Singh, N., and Jang, D.O. A selective ATP chromogenic sensor for use in an indicator displacement assay. Tetrahedron Letter. 52 (2011): 5094–5097.

[47] Feng, L., Musto, C.J., Kemling, J.W., Lim, H.S., Zhong, W., and Suslick, K.S. Colorimetric Sensor Array for Determination and Identification of Toxic Industrial Gases. Anal. Chem. 82 (2010): 9433-9440.

[48] Musto, C.J., and Suslick, K.S. Differential Sensing of Sugars by Colorimetric Arrays. Curr. Opin. Chem. Biol. 14 (2010): 758-766.

[49] Baumes, L.A., Buaki, M., Jolly, J., Corma, A., and Garcia, H. Fluorometric detection and discrimination of α-amino acids based on tricyclic basic dyes and cucurbiturils supramolecular assembly Tetrahedron Lett. 52 (2011): 1418-1421.

[50] McCleskey, S.C., Griffin, M.J., Schneider, S.E., McDevitt, J.T., and Anslyn, E.V. Differential Receptors Create Patterns Diagnostic for ATP and GTP. J. Am. Chem. Soc. 125 (2003): 1114-1115.

[51] Folmer-Andersen, J.F., Kitamura, M., and Anslyn, E.V. Pattern-Based Discrimination of Enantiomeric and Structurally Similar Amino Acids: An Optical Mimic of the Mammalian Taste Response. J. Am. Chem. Soc. 128 (2006): 5652-5653.

[52] Schiller, A., Vilozny, B., Wessling, R.A., and Singaram, B. Recognition of phospho sugars and nucleotides with an array of boronic acid appended bipyridinium salts. Anal. Chimica Acta 627 (2008): 203–211.

[53] Hewage, H.S., and Anslyn, E.V. Pattern-Based Recognition of Thiols and Metals Using a Single Squaraine Indicator. J. Am. Chem. Soc. 131 (2009): 13099–13106.

[54] Lin, H., and Suslick, K.S. A Colorimetric Sensor Array for Detection of Triacetone Triperoxide Vapor. J. Am. Chem. Soc. 132 (2010): 15519–15521.

[55] O'Neil, E.J., and Smith, B.D. Anion recognition using dimetallic coordination complexes. Coord. Chem. Rev. 250 (2006): 3068-3080.

[56] Mizukami, S., Nagano, T., Urano, Y., Yasuteru, U., Odani, A., and Kikuchi, K. A Fluorescent Anion Sensor That Works in Neutral Aqueous Solution for Bioanalytical Application. J. Am. Chem. Soc.124 (2002): 3920-3925.

[57] Kim, S.K., Lee, D.H., Hong, J.I., and Yoon, J. Chemosensors for Pyrophosphate. Acc. Chem. Res. 42 (2009): 23-31.

[58] Chen, W.H., Xing, Y., and Pang, Y. A Highly Selective Pyrophosphate Sensor Based on ESIPT Turn-On in Water. Org. Lett. 13 (2011): 1362-1365.

[59] Ghosh, A., et. al. Colorimetric Sensor for Triphosphates and Their Application as a Viable Staining Agent for Prokaryotes and Eukaryotes. Anal. Chem. 80 (2008): 5312–5319.

[60] Lee, J.H., Park, J., Lah, M.S., Chin, J., and Hong, J.H. High-Affinity Pyrophosphate Receptor by a Synergistic Effect between Metal Coordination and Hydrogen Bonding in Water. Org. Lett. 9 (2007): 3729-3731.

[61] Lee, H.G., et. al. Zinc selective chemosensor based on pyridyl-amide fluorescence. Tetrahedron 67 (2011): 8073-8078.

[62] Ran, C. et. al. Design, Synthesis, and Testing of Difluoroboron-Derivatized Curcumins as Near-Infrared Probes for In Vivo Detection of Amyloid-Beta Deposits. J. Am. Chem. Soc. 131 (2009):.15257-15261.

[63] Peng, X., et. al. A Selective Fluorescent Sensor for Imaging Cd^{2+} in Living Cells. J. Am. Chem. Soc. 129 (2007): 1500-1501.

[64] Ran, C., et. al Design, Synthesis, and Testing of Difluoroboron-Derivatized Curcumins as Near-Infrared Probes for in Vivo Detection of Amyloid-β Deposits. J. Am. Chem. Soc. 131 (2009): 15257-15261.

[65] Melhuish, W.H. Quantum Efficients of Fluorescence of Organic Substances: Effect of Solvent and Concentration of the Fluorescent Solute. J. Chem. Phy. 65 (1961): 229-235.

[66] Dawson, W.R., and Winsor, M.W. Fluorescence yields of aromatic compounds. J. Phy. Chem. 72 (1968): 3251-3260.

[67] Xu, Y., and Pang, Y. Zinc binding-induced near-IR emission from excited-state intramolecular proton transfer of a bis(benzoxazole) derivative. Chem. Commun. 46 (2010): 4070-4072.

[68] Taki, M., Watanabe, Y., and Yamamoto, Y. Development of ratiometric fluorescent probe for zinc ion based on indole fluorophore. Tetrahedron Lett. 50 (2009): 1345-1347.

[69] Ojida, A., Takashima, I., Kohira, T., Nonaka, H., and Hamachi, I. Turn-On Fluorescence Sensing of Nucleoside Polyphosphates Using a Xanthene-Based Zn(II) Complex Chemosensor. J. Am. Chem. Soc. 130 (2008): 12095-12101.

[70] Lee, P.K., Law, W.H.T., Liu, H.W., and Lo, K.K.W. Luminescent Cyclometalated Iridium(III) Polypyridine Di-2-picolylamine Complexes: Synthesis, Photophysics, Electrochemistry, Cation Binding, Cellular Internalization, and Cytotoxic Activity. Inorg. Chem. 50 (2011): 8570-8579.

[71] Arunkumar, E., Ajayaghosh, A., and Daub, J. Selective Calcium Ion Sensing with a Bichromophoric Squaraine Foldamer. J. Am. Chem. Soc. 127 (2005): 3156-3164.

[72] Chen, X., Jou, M.J., and Yoon, J. An "*Off-On*" Type UTP/UDP Selective Fluorescent Probe and Its Application to Monitor Glycosylation Process. Org. Lett. 11 (2009): 2181-2184.

[73] Lee, D. H., Kim, S.Y., and Hong, J.I. A Fluorescent Pyrophosphate Sensor with High Selectivity over ATP in Water. Angew. Chem. Int. Ed. 43 (2004): 4777-4780.

[74] Lee, H. N., et. al. Pyrophosphate-Selective Fluorescent Chemosensor at Physiological pH: Formation of a Unique Excimer upon Addition of Pyrophosphate. J. Am. Chem. Soc. 129 (2007): 3828-3829.

[75] Jose, D. A., Mishra, S., Ghosh, A., Shrivastav, A., Mishra, S. K.; and Das, A. Colorimetric Sensor for ATP in Aqueous Solution. Org. Lett. 9 (2007): 1979-1982.

[76] Frisch, M.J., et. al. Gaussian 03, Revision D.02. Gaussian.,Wallingford, 2004.

[77] Hay, P.J., and Wadt, W.R. Ab initio effective core potentials for molecular calculations. Potentials for the transition metal atoms Sc to Hg. J. Chem. Phys. 82 (1985): 270-283.

[78] Wadt, W.R., and Hay, P.J. Ab initio effective core potentials for molecular calculations. Potentials for main group elements Na to Bi. J. Chem. Phys. 82 (1985): 284-298.

[79] Hay, P.J., and Wadt, W.R. Ab initio effective core potentials for molecular calculations. Potentials for K to Au including the outermost core orbitals. J. Chem. Phys. 82 (1985): 299-310.

[80] Ahmed, N., Shirinfar, B., and. Geronimoand, K.I. Fluorescent Imidazolium-Based Cyclophane for Detection of Guanosine-5'-triphosphate and I^- in Aqueous Solution of Physiological pH, Org. Lett. 13 (2011): 5476–5479.

[81] Brereton, R. G. Chemometrics for Pattern Recognition., West Sussex, United Kingdom:Wiley, 2009.

[82] Jurs, P.C., Bakken, G.A., and McClelland, H.E. Computational Methods for the Analysis of Chemical Sensor Array Data from Volatile Analytes. Chem. Rev. 100 (2000): 2649-2678.

[83] Carey, W P., Beebe, K.R., Kowalski, B.R., Illman, D.L., and Hirschfeld, T. Selection of adsorbates for chemical sensor arrays by pattern recognition. Anal. Chem. 58 (1986): 149-153.

[84] Zhang, C., and Suslick, K.S. Colorimetric Sensor Array for Soft Drink Analysis. J. Agric.Food. Chem. 55 (2007): 237-242.

[85] Wright, A.T., Anslyn, E.V., and McDevitt, J.T. A Differential Array of Metalated Synthetic Receptors for the Analysis of Tripeptide Mixtures. J. Am. Chem. Soc. 127 (2005): 17405-17411.

[86] Palacios, M.A., Wang, Z., Montes, A.V., Zyryanov, G.V., and Jr, A. Rational Design of a Minimal Size Sensor Array for Metal Ion Detection. J. Am. Chem. Soc. 130 (2008): 10307-10314.

[87] Zhu, L. and Anslyn, E.V. Facile quantification of enantiomeric excess and concentration with indicator-displacement assays: an example in the analyses of α-hydroxyacids. J. Am. Chem. Soc. 126 (2004): 3676-3677.

[88] Kampman, B., Lian, Y., Klikel, K.L., Vecchi, P.A., Quiring, H.L., Soh, C.C., and Syes, A.G. Luminescence and Structural Comparisons of Strong-Acid Sensor Molecules. 2. J. Org. Chem. 67 (2002): 3878-3883.

[89] Kumar, S.P., and Kaur, S. Photoactive chemosensors. Part 1: A 9,10-anthraquinone and 2-aminothiophenol based Cu(II) selective chemosensor. Tetrahedron Lett. 43 (2002): 1097-1099.

[90] Kadarkaraisamy, M., and Sykes A.G. Luminescence Detection of Transition and Heavy Metals by Inversion of Excited States: Synthesis, Spectroscopy, and X-ray Crystallography of Ca, Mn, Pb, and Zn Complexes of 1,8-Anthraquinone-18-Crown-5. Inorg. Chem. 45 (2006): 779-789.

[91] Batista, R.M.F., Oliveira, E., Costa, S.P.G., Lodeiro, C., and. Raposo, M.M.M. Synthesis and Ion Sensing Properties of New Colorimetric and Fluorimetric Chemosensors Based on Bithienyl-Imidazo-Anthraquinone Chromophores. Org. Lett. 9 (2007): 3201-3204.

[92] Hanaoka, K., Kikuchi, K., Kojima, H., Urano, Y., and Nagano, T. Development of a Zinc Ion-Selective Luminescent Lanthanide Chemosensor for Biological Applications. J. Am. Chem. Soc. 126 (2004): 1247012476.

[93] Hanaoka, K., Kikuchi, K., Kojima, H., Urano, Y., and Nagano, T. Selective Detection of Zinc Ions with Novel Luminescent Lanthanide Probes. Angew. Chem., Int. Ed. 42 (2003): 2996-2999.

APPENDIX

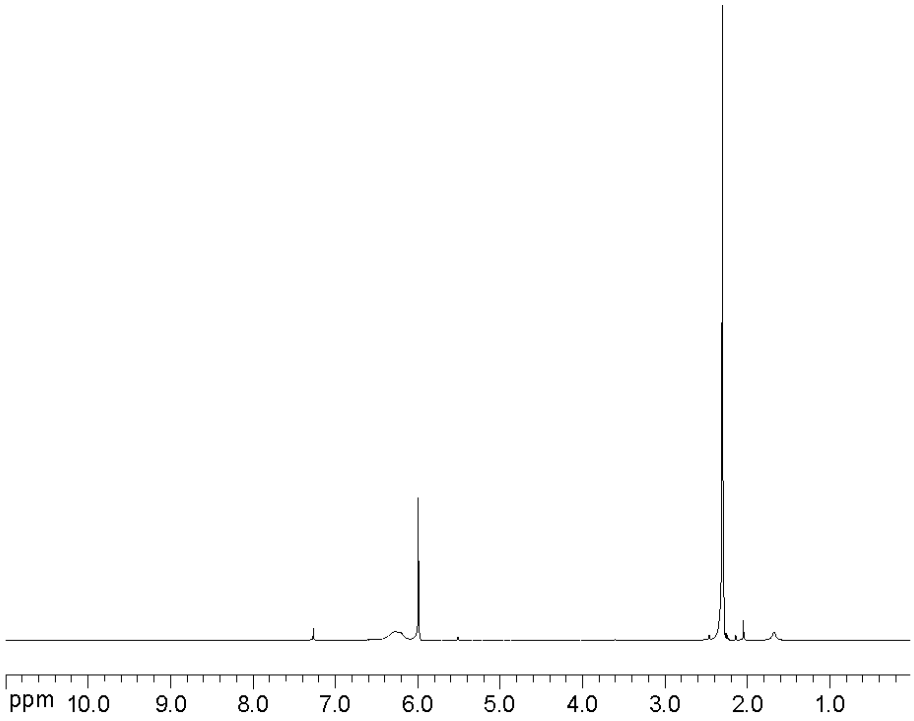

Figure A1 ^{1}H-NMR spectrum of **1** in $CDCl_3$ (400 MHz).

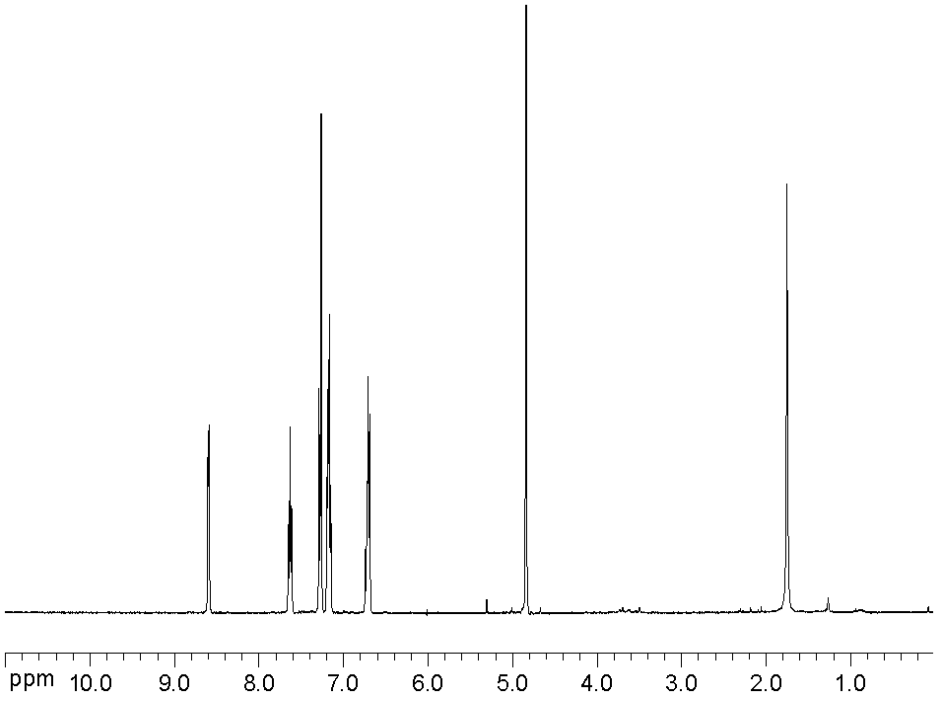

Figure A2 ^{1}H-NMR spectrum of **2** in $CDCl_3$ (400 MHz).

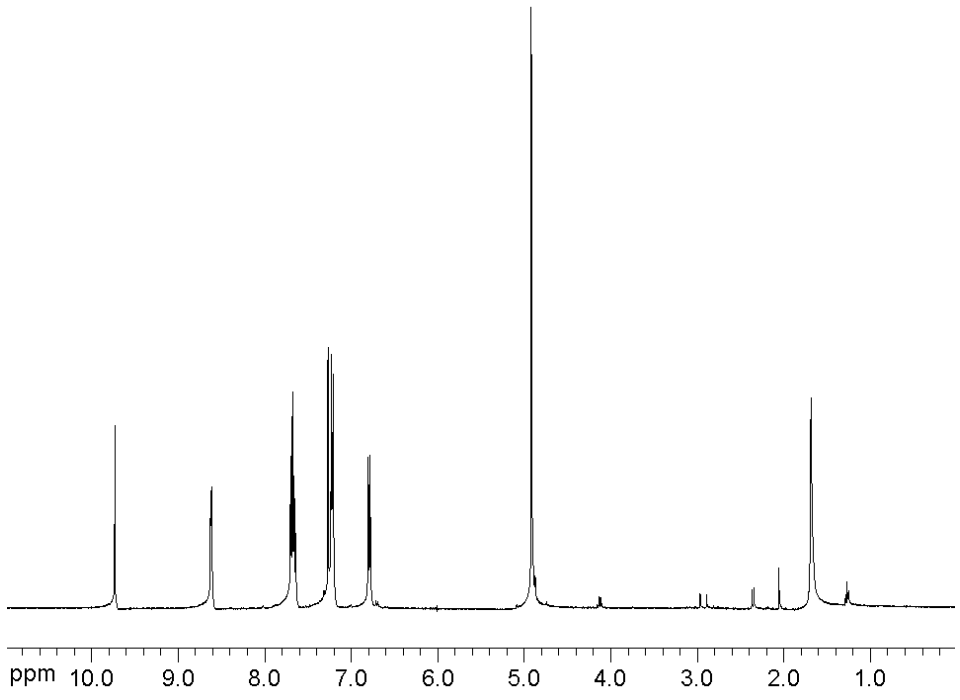

Figure A3 ^{1}H-NMR spectrum of **3** in $CDCl_3$ (400 MHz).

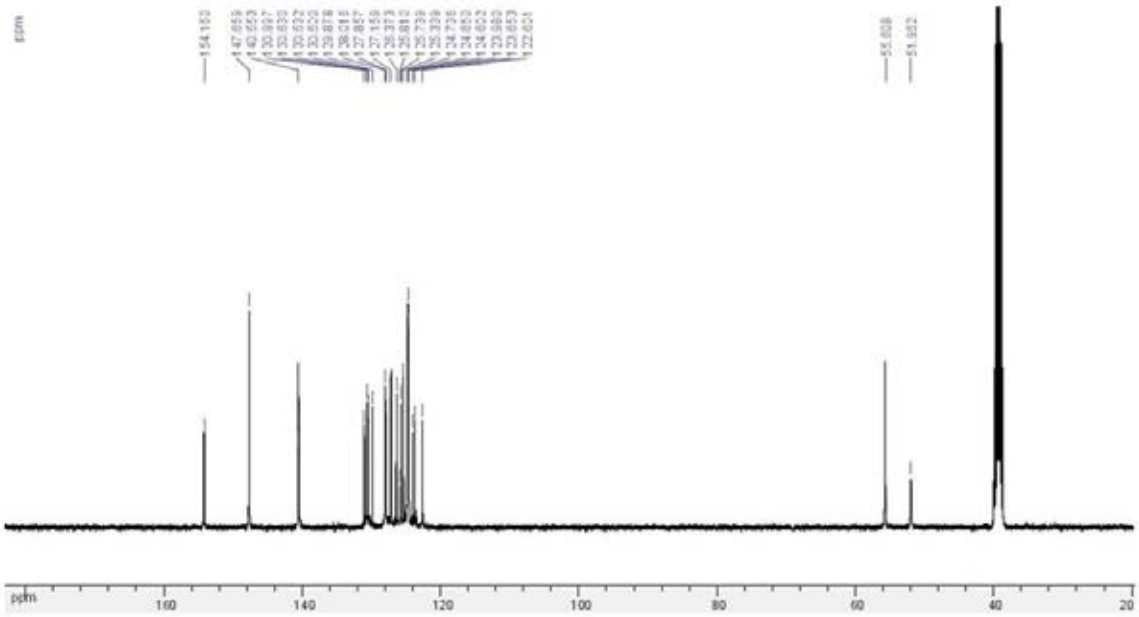

Figure A4 ^{13}C-NMR spectrum of **L2•Zn** in DMSO-d_6 (400 MHz).

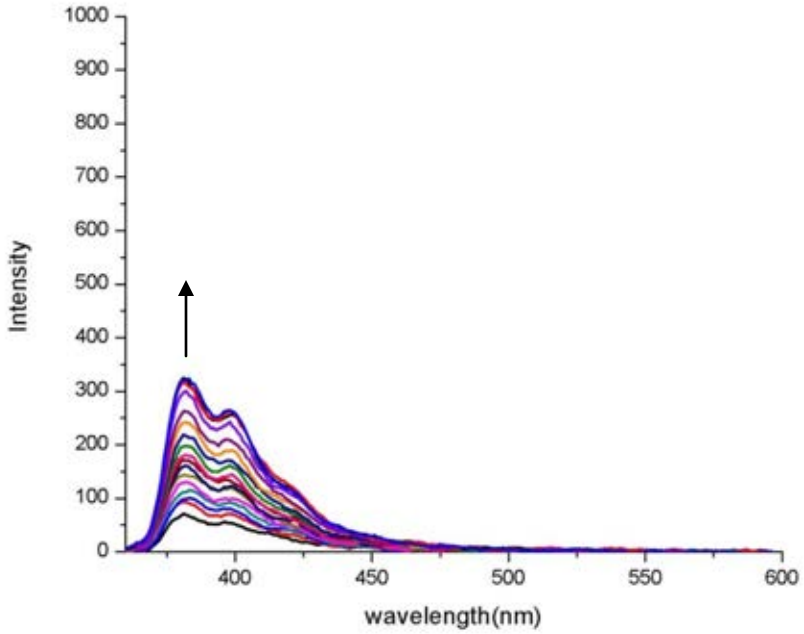

Figure A5 Fluorescence titration of **L2•Zn** ($1x10^{-5}$ M) upon addition of UDP in DMSO:HEPES buffer (0.01M, pH 7.4) (90:10 v/v).

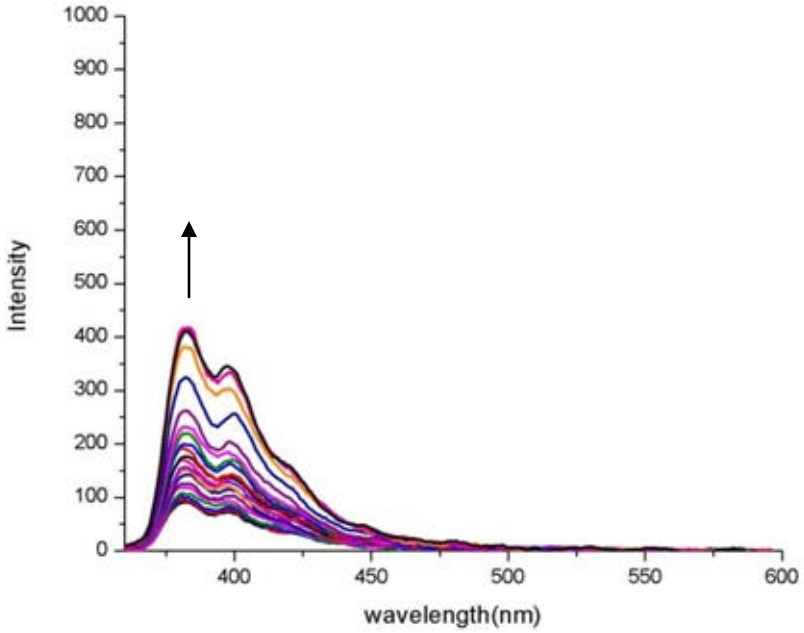

Figure A6 Fluorescence titration of **L2•Zn** ($1x10^{-5}$ M) upon addition of ADP in DMSO:HEPES buffer (0.01M, pH 7.4) (90:10 v/v).

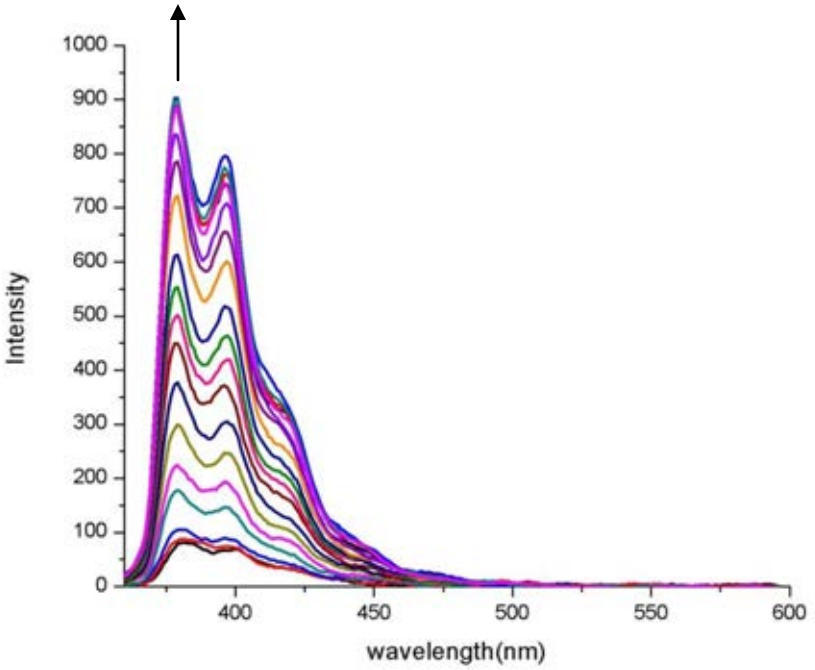

Figure A7 Fluorescence titration of **L2•Zn** ($1x10^{-5}$ M) upon addition of UTP in DMSO:HEPES buffer (0.01M, pH 7.4) (90:10 v/v).

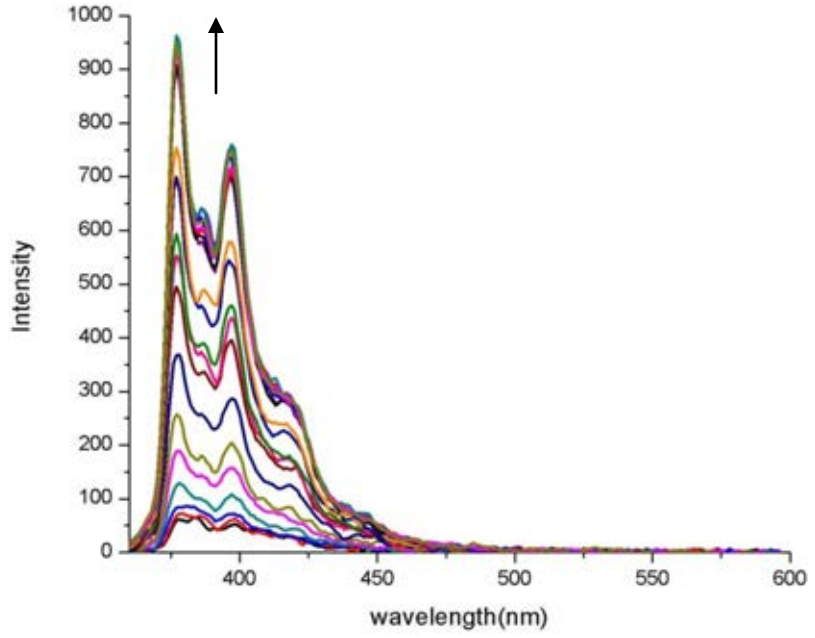

Figure A8 Fluorescence titration of **L2•Zn** ($1x10^{-5}$ M) upon addition of ATP in DMSO:HEPES buffer (0.01M, pH 7.4) (90:10 v/v).

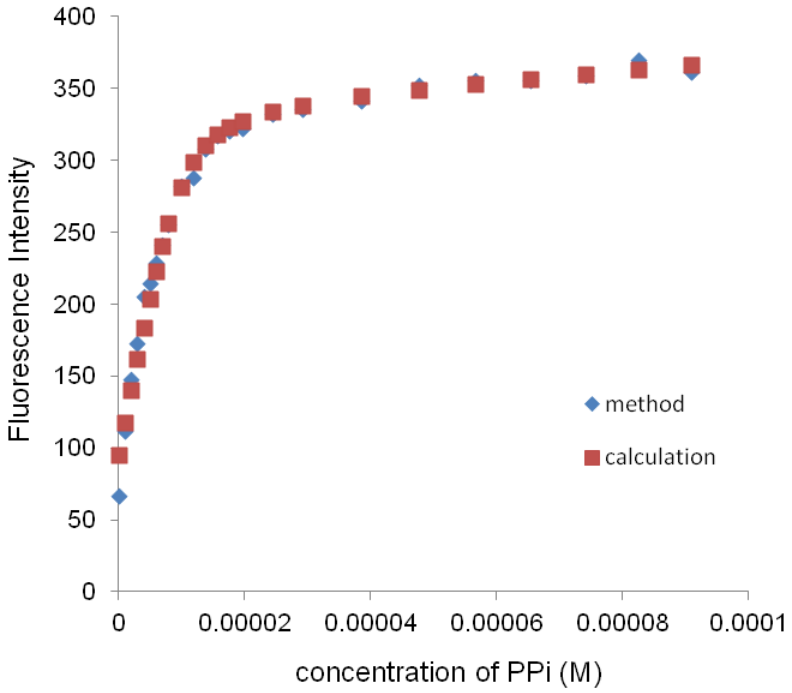

Figure A9 Fitting curve of fluorescence titration of **L2•Zn** ($1x10^{-5}$ M) upon addition of PPi in DMSO:HEPES buffer (0.01M, pH 7.4) (99:1 v/v).

VITA

Miss Sornkrit Marbumrung was born on May 3, 1980 in Nakhonratchasima, Thailand. She received her Bachelor's degree of Science in Chemistry from Kasetsart University in 2004. Since 2005, she has been a graduate student at the Department of Chemistry, Chulalongkorn University and become a member of Supramolecular Chemistry Research Unit under the supervision of Assistant Professor Dr. Boosayarat Tomapatanaget and Associate Professor Dr. Thawatchai Tuntulani. She finished her Master's degree of Science in the academic year 2006. In 2007, she has been a Ph.D. Candidate in Inorganic Chemistry under the supervision of Assistant Professor Dr. Boosayarat Tomapatanaget and Dr. Gamolwan Tumcharern.

Grants:

2008-2011	Thailand Graduate Institute of Science and Technology (TGIST)
2011	The 90th Anniversary of Chulalongkorn University Fund (Ratchadaphisek Somphot Endowment Fund)

Proceeding:

Synthesis of Molecule Based on Difluoroboroncurcumin (BF_2-Cur) and Dipicolyl Amine as a Sensor for Zinc and Nucleotide, ***Oral presentation*** in 7^{th} International Symposium on Advanced Materials in Asia-Pacific, 30 September-1 October 2010, Ishikawa High-Tech Exchange Center, Ishikawa, Japan